

Integrating Salinity of Flowback Fluid and Flow Data for Fracture Characterization and
Production Forecast in Unconventional Reservoirs

by

Ganxing Zhang

A thesis submitted in partial fulfillment of the requirements for the degree of

Doctor of Philosophy

in

PETROLEUM ENGINEERING

Department of Civil and Environmental Engineering
University of Alberta

© Ganxing Zhang, 2024

Abstract

The complexity inherent in hydraulic fracturing for oil and gas reservoirs demands sophisticated analytical tools for optimal performance and sustainability. The research presented in this study adopts a multi-faceted approach that synergistically combines flow-geochemical models for fracture characterization.

In the initial phase of the research, a coupled flow-geochemical model using commercial simulation software is developed. This model emphasizes the intricate interactions between key components such as oil, original formation water, injected water, and rocks. The model is validated through coreflood experimental data. It provides valuable insights into the complex mechanisms affecting oil recovery during water injection processes with varying salinity. For instance, the model reveals that while ion exchange plays a critical role in high-salinity water flooding, mineral dissolution/precipitation reactions are more dominant in low-salinity scenarios.

Then, the coupled flow-geochemical model is extended to a hydraulically fractured horizontal well model. The modelling results are analyzed to explore the temporal changes in the salinity of flowback fluid and production time. The simulation results are then used to train a set of regression models using Response Surface Modelling (RSM) to predict gas rate and total salinity as a function time for a variety of primary and secondary fracture properties and configurations. Validation exercises demonstrate its robust predictive capabilities, with R² values consistently above 0.95, confirming the model's reliability and applicability.

In the next phase, the regression models are integrated into an optimization workflow: Genetic Algorithm (RSM-GA) for fracture characterization. Its novelty lies in the integration of salinity in the analysis. The methodology's versatility is assessed across different reservoir and well

configurations, including both homogeneous and heterogeneous contexts. It examines the application in different scenarios such as uniform and non-uniform secondary fracture scenarios, heterogeneous fracture patterns, and advanced multi-stage horizontal well frameworks.

Finally, it is found that incorporating fracture parameters estimated from both salinity and rate data, even in the case of multi-stage horizontal wells with non-uniform primary fracture length and spacing or heterogeneous secondary fracture distributions, results in a more accurate representation of the reservoir's behaviour and production history match.

Preface

This thesis is an original work by Ganxing Zhang. Parts of the research project have been previously published or are ready for submission to the journal.

A version of Chapter 3 has been published as Zhang, G., & Leung, J. Y. (2023). Design of injected water salinity for enhanced oil recovery applications in sandstone reservoirs using coupled flow-geochemical simulation. *Geoenergy Science and Engineering*, 224, 211614. I was responsible for the data collection, model construction, analysis, and manuscript composition. Leung, J. Y. was the supervisory author involved in concept formation and manuscript composition.

A version of Chapter 4 has been published as Zhang, G., & Leung, J. Y. (2022, October). Numerical simulation of geochemical effects on flowback analysis and enhanced oil recovery strategies. In *Unconventional Resources Technology Conference, 20–22 June 2022* (pp. 1638-1655). I was responsible for the data collection, model construction, analysis, and manuscript composition. Leung, J. Y. was the supervisory author involved in concept formation and manuscript composition.

A version of Chapter 5 will be submitted for publication as Zhang, G., & Leung, J. Y. Integrating Salinity of Flowback Fluid and Flow Data for Fracture Characterization in Unconventional Reservoirs. I was responsible for the data collection, model construction, analysis, and manuscript composition. Leung, J. Y. was the supervisory author involved in concept formation and manuscript composition.

Chapter 1 summarizes the research background, problem statement, research objectives, and thesis structure. Chapter 2 summarizes the foundation upon which this study builds. Chapter 6

summarizes the conclusions reached in this thesis as well as the recommendations for future research. Chapters 1, 2 and 6 have never been published elsewhere.

Dedication

I would like to dedicate this work to

my beautiful, caring, and loving wife, Ruizhi Meng, for her love, kindness, patience, and endless supports.

my parents and parents in law and my older sister for their unconditional love, encouragements, and ultimate supports.

Acknowledgements

First of all, I would like to express my sincere gratitude to my supervisor, Dr. Juliana Leung, for giving me the opportunity to work on this thesis work under her guidance. Juliana was a tremendous mentor for me. It is her excellent teaching, enlightening guidance, continuous support and encouragement that helped me throughout the course of my Ph.D. study and finish this thesis. This thesis would not have been possible without their guidance.

I would also like to thank my supervisory committee members, Dr. Huazhou Li, Dr. Japan Trivedi, Dr. Sohrab Zendehboudi, and Dr. Bo Zhang for their guidance through this work. The discussion, ideas, and feedback have been absolutely invaluable.

I would like to thank all my colleagues in Dr. Leung's research group for providing an enjoyable research environment and all the inspiring discussions.

My gratitude also goes to China Scholarship Council (CSC) (No. 201908140120) and the Natural Sciences and Engineering Research Council of Canada (NSERC) (No. 2017-05779) for the financial support. I would also like to thank the Computer Modelling Group Ltd. (CMG), Golder Associates Ltd. and MathWorks® for providing the academic licenses for GEM, FracMan® and MATLAB R2022a, respectively.

Finally, I am truly grateful to my family, for their great love, endless support and encouragement.

Table of Contents

Abstract.....	ii
Preface.....	iv
Dedication.....	vi
Acknowledgements.....	vii
List of Tables	xii
List of Figures.....	xiv
List of Symbols.....	xviii
Chapter 1: Introduction.....	1
1.1 Background	1
1.2 Problem Statement	2
1.3 Research Objective.....	3
1.4 Thesis Outline	3
Chapter 2: Literature Review.....	5
2.1 Unconventional Reservoirs	5
2.2 Fracturing Process.....	6
2.3 Fracturing Fluid.....	6
2.4 Flowback Process.....	7
2.5 Flowback Chemical Analysis.....	7
2.6 Response Surface Modelling.....	8

2.7 Genetic Algorithm (GA)	9
Chapter 3: Coupling Flow-Geochemical Model Development in Sandstone Reservoir	11
3.1 Introduction	11
3.2. Mathematical Model	15
3.2.1 Component Material Balance Equation.....	15
3.2.2 Gas and Aqueous Phase Properties	16
3.2.3 Aqueous Reactions	17
3.2.4 Mineral Dissolution and Precipitation	17
3.2.5 Ion Exchange	18
3.2.6 Flow and Geochemistry Coupling.....	20
3.2.7 Solution Method	22
3.3 Model Development of the Core Flooding Experiment.....	22
3.4 Validation Model History Match and Analysis.....	26
3.5 Summary	35
Chapter 4: Modelling of a Hydraulically Fractured Horizontal Well using Coupled Flow-Geochemical Model and Regression Modelling base on the Fracture Characteristics.....	36
4.1 Introduction	36
4.2 Methodology	43
4.2.1 Flow and Geochemistry Coupling.....	43
4.2.2 Validation of a Single Well Model.....	44

4.2.3 Modelling of a Hydraulically Fractured Horizontal Well	51
4.3. Results	56
4.3.1 Sensitivity Analysis of Fracture Parameters.....	56
4.3.2 Response Surface Model (RSM) Construction	62
4.3.3 RSM Model Validation and Interpretation.....	68
4.4 Summary	72
Chapter 5: Fracture Characterization Using RSM-GA Workflow	73
5.1 Introduction	73
5.2 Case #1 – Uniform and Non-Uniform Secondary Fracture Parameters.....	74
5.3 Case #2 – Heterogeneous Secondary Fracture DFN Model	81
5.4 Case #3 – Multi-Stage Horizontal Well Model.....	88
5.4.1 Multi-Stage Horizontal Well with Equal Primary Fracture Length and Even Spacing	89
5.4.2 Multi-Stage Horizontal Well with Equal Primary Fracture Length and Uneven Primary Fracture Spacing	95
5.5 Multi-Stage Horizontal Well with Unequal Primary Fracture Length and Uneven Primary Fracture Spacing.....	100
5.6 Summary	107
Chapter 6: Conclusions and Future Work.....	109
6.1 Key Conclusions	109
6.2 Contributions.....	110

6.3 Limitations and Recommendations for Future Work.....	110
Bibliography	113
Appendix A.....	143

List of Tables

Table 3-1 Chemical compositions of formation water, seawater, and low-salinity water (Fjedel et al., 2012)	23
Table 3-2 The properties of the sandstone models	25
Table 3-3 Geochemical modelling database (Computer Modelling Group 2022)	26
Table 4-1 Parameters of the shale gas model (Mehana and Fahes, 2016)	46
Table 4-2 Chemical compositions of formation water and high-salinity water (Mehana and Fahes, 2016)	47
Table 4-3 Geochemical modelling database (Computer Modelling Group 2021)	47
Table 4-4 Parameters of the shale gas model.....	54
Table 4-5 Fracture characteristics for the training dataset.....	58
Table 4-6 Response variables and R^2 of salinity profiles for the training dataset	64
Table 4-7 Response variables and R^2 of rate profiles for the training dataset.....	65
Table 4-8 Coefficients Beta for RSM-Salinity	67
Table 4-9 Coefficients Beta for RSM-Rate	68
Table 4-10 Fracture characteristics for testing dataset.	69
Table 4-11 RSM model predictions for the testing dataset.....	69
Table 5-1 Fracture parameters estimated using RSM-GA workflow for the non-uniform SF case.	76
Table 5-2 Fracture parameters estimated using RSM-GA workflow – DFN realizations are generated using the estimated parameters.....	83
Table 5-3 Fracture parameters predicted by RSM for multi-stage horizontal well with equal primary fracture length and even primary fracture spacing.....	92
Table 5-4 Fracture parameters predicted by RSM for multi-stage horizontal well with equal primary fracture length and uneven primary fracture spacing.....	97

Table 5-5 Fracture parameters predicted by RSM for multi-stage horizontal well with unequal primary fracture length and uneven primary fracture spacing..... 103

Table 5-6 Comparison of the total computing time with and without proxy models. 106

Table A-1 Fracture parameters estimated using RSM-GA workflow and its percentage error for the non-uniform secondary fracture model..... 143

Table A-2 Fracture parameters estimated using RSM-GA workflow and its percentage error for heterogeneous secondary fracture DFN model..... 143

Table A-3 Fracture parameters estimated using RSM-GA workflow and its percentage error for multi-stage horizontal well with equal primary fracture length and even primary fracture spacing. 143

Table A-4 Fracture parameters estimated using RSM-GA workflow and its percentage error for multi-stage horizontal well with equal primary fracture length and uneven primary fracture spacing 144

Table A-5 Fracture parameters estimated using RSM-GA workflow and its percentage error for multi-stage horizontal well with unequal primary fracture length and uneven primary fracture spacing 145

List of Figures

Figure 3-1. Schematic view: two-way coupling between the flow module and geochemistry module as implemented in GEM (CMG, 2022).....	21
Figure 3-2 1D model setup; the colour scale represents pH (Inj: Injection well; Pro: Production well).	24
Figure 3-3 (a) Relative permeability curves and (b) capillary pressure curves (Fjelde et al., 2012).	24
Figure 3-4. Historical matching of simulation predictions with experimental results: (a) Effluent Ca^{++} ion concentration, (b) Effluent Mg^{++} ion concentration, (c) Effluent pH value, and (d) Average oil saturation.	27
Figure 3-5. Low-salinity water injection: (a) Effluent Ca^{++} ion concentration, (b) Effluent Mg^{++} ion concentration, (c) Effluent pH value, and (d) Effluent SO_4^{--} ion concentration.	28
Figure 3-6. Seawater injection: (a) Effluent Ca^{++} ion concentration, (b) Effluent Mg^{++} ion concentration, (c) Effluent pH value, and (d) Effluent SO_4^{--} ion concentration.	29
Figure 3-7. Low-salinity water injection: (a) Change in the total number of moles of minerals in the reservoir, (b) Pore volume change, (c) Ion exchange equivalent fraction, and (d) Oil recovery factor.	30
Figure 3-8. Seawater injection: (a) Change in the total number of moles of mineral in the reservoir, (b) Pore volume change, (c) Ion exchange equivalent fraction in grid block (1 1 1), and (d) Oil recovery factor.	31
Figure 4-1. Logarithmically spaced, locally refined grid model structure (Inj: Injection well; Pro: Production well): Green-shale, Black-Fracture Conduit.	45
Figure 4-2. Historical matching of baseline model with results of Mehana and Fahes (2016): (a) Mineral moles change, (b) Cumulative gas recovery.	47
Figure 4-3. Ion concentration of flowback fluid comparison between new model result and baseline model result: (a) Na^+ ion concentration, (b) Ca^{++} ion concentration, (c) Mg^{++} ion concentration, (d) SO_4^{--} ion concentration.	49

Figure 4-4. Salinity profiles from field observation.	51
Figure 4-5. New horizontal well shale model: Green-shale, Black-Secondary Fracture Conduit, Red-Primary Fracture Conduit, Yellow-Horizontal Well Path.....	53
Figure 4-6. Relative permeability functions for low (LSW)) and high (HSW) salinity water systems: (a) gas-water and (b) water-oil.....	53
Figure 4-7. Ion concentration of flowback fluids between new horizontal well shale model and comparison model: (a) Na + ion, (b) Ca ² + ion, (c) Mg ² + ion and (d) SO ₄ ²⁻ ion.	55
Figure 4-8. Case 1-8 Schematic of horizontal well shale model: Green-shale, Black-Secondary Fracture Conduit, Red-Primary Fracture Conduit, Yellow-Horizontal Well Path.	57
Figure 4-9. Flowback fluids salinity at different fracture characteristics: (a) PF Length. (b) PF Permeability, (c) SF Coverage, (d) SF P32, (e) SF Aperture, and (f) SF Permeability.....	60
Figure 4-10. Gas rate at different fracture characteristics: (a) PF Length. (b) PF Permeability, (c) SF Coverage, (d) SF P32, (e) SF Aperture, and (f) SF Permeability.....	61
Figure 4-11. Salinity profile and gas rate curve fitting for base case: (a) Salinity curve fitting. (b) Gas rate curve fitting.....	63
Figure 4-12. Comparison between the predicted and true profiles using the RSM-Salinity model.	70
Figure 4-13. Comparison between the predicted and true profiles using the RSM-Rate model. .	71
Figure 5-1. True case for non-uniform secondary fracture model.....	75
Figure 5-2. Salinity and rate histories for non-uniform secondary fracture model: (a) Salinity curve fitting, (b) Gas rate curve fitting.	76
Figure 5-3. Uniform and non-uniform secondary fracture model constructed by RSM-Salinity: Green-shale, Black-Secondary Fracture Conduit, Red-Primary Fracture Conduit, Yellow-Horizontal Well Path.....	76
Figure 5-4. Uniform and non-uniform secondary fracture model constructed by RSM-Rate: Green-shale, Black-Secondary Fracture Conduit, Red-Primary Fracture Conduit, Yellow-Horizontal Well Path.	77

Figure 5-5. Salinity and Rate profile between true value and RSM response for cases 1, 1a, 1b, and 1c.....	79
Figure 5-6. Salinity and Rate profile between true value and RSM response for cases 2, 2a, 2b, and 2c.....	81
Figure 5-7. True case for heterogeneous secondary fracture DFN model.....	82
Figure 5-8. Salinity and rate histories for heterogeneous secondary fracture DFN model.....	83
Figure 5-9. The secondary fracture permeability distribution of the DFN model constructed by RSM-Salinity.	83
Figure 5-10. The secondary fracture permeability distribution of the DFN model constructed by RSM-Rate.	84
Figure 5-11. Salinity and Rate profile between the true value and RSM response for cases DFN 1-3.....	85
Figure 5-12. Salinity and Rate profile between the true value and RSM response for cases DFN 4-6.....	87
Figure 5-13. True case for equal primary fracture length and even primary spacing.....	89
Figure 5-14. Salinity and rate histories for multi-stage horizontal well with equal primary fracture length and even primary fracture spacing.	91
Figure 5-15. The secondary fracture permeability distribution of the Multi-stage horizontal well model with equal primary fracture length and even primary spacing constructed by RSM-Salinity, RSM-Rate (total), RSM (stage); the colour scale represents secondary fracture permeability distribution.	93
Figure 5-16. Multi-stage horizontal well model with equal primary fracture length and even primary spacing; the colour scale represents pressure distribution (psi) after 60 days.	93
Figure 5-17. The comparison between true production profile and predicted curve for multi-stage horizontal well with equal primary fracture length and even primary spacing : (a) Salinity profile, and (b) Gas rate curve.	94
Figure 5-18. True case for equal primary fracture length and uneven primary fracture spacing.	95

Figure 5-19. Salinity and rate histories for multi-stage horizontal well with equal primary fracture length and uneven primary fracture spacing	97
Figure 5-20. The secondary fracture permeability distribution of the Multi-stage horizontal well model with equal primary fracture length and uneven primary fracture spacing constructed by RSM-Salinity, RSM-Rate (total), RSM (stage); the colour scale represents secondary fracture permeability distribution.	98
Figure 5-21. Multi-stage horizontal well model with equal primary fracture length and uneven primary fracture spacing; the colour scale represents pressure distribution (psi) after 60 days. ..	99
Figure 5-22. The comparison between true production profile and predicted curve for multi-stage horizontal well with equal primary fracture length and uneven primary fracture spacing.	99
Figure 5-23. True case for unequal primary fracture length and uneven primary fracture spacing model.....	101
Figure 5-24. Salinity and rate histories for multi-stage horizontal well with	102
Figure 5-25. The secondary fracture permeability distribution of the Multi-stage horizontal well with unequal primary fracture length and uneven primary fracture spacing constructed by RSM-Salinity, RSM-Rate (total), RSM (stage); the colour scale represents secondary fracture permeability distribution.	104
Figure 5-26. Multi-stage horizontal well with unequal primary fracture length and uneven primary fracture spacing; the colour scale represents pressure distribution (psi) after 60 days.....	104
Figure 5-27. The comparison between true production profile and predicted curve for multi-stage horizontal well with unequal primary fracture length and uneven primary fracture spacing: (a) Salinity profile, and (b) Gas rate curve.	105

List of Symbols

RSM	=	Response Surface Modelling
GA	=	Genetic Algorithm
PTA	=	pressure transient analysis
RTA	=	rate transient analysis
MSE	=	Mean Squared Error
PF	=	Primary Fracture
SF	=	Secondary Fracture
$m(p)$	=	pseudo-pressure
q_g	=	gas rate
m	=	slope
A_{cw}	=	cross-sectional area to flow
x_e	=	effective well length
h	=	reservoir height
A_{cm}	=	total matrix/secondary fracture surface drainage area
y_e	=	primary fracture half length
L_f	=	secondary fracture spacing
\sqrt{t}	=	material balance time
c_t	=	total compressibility
μ	=	fluid viscosity
σ	=	shape factor
q_{Dl}	=	dimensionless flow rate
ω_f	=	storativity ratio
λ	=	dimensionless interporosity flow
n_g	=	number of gaseous components
n_{aq}	=	number of aqueous components
n_m	=	number of mineral components

- n_{ct} = number of total components
 ψ = constitutive equation
 n = old time level
 $n + 1$ = new time level
 u = number of explicit time step for grid block
 T_g = transmissibility of gaseous phase, mD·ft/(mPa·s)
 y = mole fraction
 p = pressure, psi
 P_c = capillary pressure, psi
 ρ = density, kg/ft³
 g = acceleration due to gravity, ft/s²
 d = Depth, ft
 D = diffusivity in the phase, ft²/day
 $V\sigma_{i,aaq}$ = intra-aqueous reaction rates, mol/ft³ · s
 $V\sigma_{i,mn}$ = mineral dissolution/precipitation rates, mol/ft³ · s
 q = injection rate, ft³/day
 N = number of moles of mineral
 X = clay mineral in the reservoir rock
 $j - X$ = component j adsorbed on the clay surface
 Δt = time step, days
 f_i = fugacity of component i
 H_i = Henry's constant for component i
 Q = activity product
 K_{eq} = chemical equilibrium constant, mol/ft²·s
 R_{aaq} = the number of aqueous reactions
 a_k = activity of component k
 $v_{k\alpha}$ = stoichiometry coefficient of component k in reaction α
 γ_k = activity coefficient of component k

- m_k = molality of component k (moles per kg of H_2O)
 r = rate of reaction
 \hat{A} = reactive surface area, ft^2/ft^3
 k = rate constant
 T = Temperature, F
 T_0 = reference temperature, F
 $E_{\alpha\beta}$ = activation energy for reaction β , J/mol
 R = universal gas constant
 \hat{A}^0 = reactive surface area at time 0, ft^2/ft^3
 ζ = equivalent fraction
CEC = cation exchange capacity
 ϕ = porosity
 ϕ^* = porosity without mineral precipitation/dissolution at the reference pressure p^*
 p^* = reference pressure, psi
 c_ϕ = rock compressibility, 1/psi
PV = number of pore volumes
FW = formation water
SW = seawater
LSW = low-salinity water

Chapter 1: Introduction

This chapter illustrates the background of unconventional reservoir exploration and some prevalent knowledge gaps and research motivations. It also presents the problem statement, research objectives, and thesis outline.

1.1 Background

Unconventional oil and gas reservoirs are emerging as critical sources of energy in North America as well as all over the world (Bocora, 2012; Hongjun et al., 2016; Law et al., 1993). These low-permeability reservoirs are commonly developed with multi-fractured horizontal wells. This technological breakthrough has significant implications for global energy security, economic development, and the optimization of hydrocarbon resources (Zhang, 2019; Zhao et al., 2015; King, 2014). A large volume of fracturing fluid is injected to create multiple fractures and to increase the reservoir contact per well. This fracturing fluid pumped into the formation is flown back before placing the well on production, preparing the fractured well for long-term hydrocarbon production (Kondash et al., 2017; Lester et al., 2015, Y; Zolfaghari et al., 2016).

However, many simulations of the hydraulically fractured reservoir do not consider or incorporate geochemistry. These practices frequently overlook the influence of geochemical interactions among injection fluids, crude oil, connate water, and minerals. This omission could have substantial implications for reservoir management, fracturing effectiveness, and, ultimately, production yield (Ghorbani et al., 2022; Muniruzzaman and Rolle, 2016; Brookfield et al., 2021; Alpers and Nordstrom, 1999).

In addition, accurate fracture characterization remains a challenge due to the limited data available and the simplification of the analytical model. Typically, rate data, especially in the early stage, is not sensitive to secondary fracture and is very useful for characterizing primary fractures. Recent literature, however, has indicated a promising alternative: using salinity or geochemical data from produced/flowback fluid for fracture characterization (Blauch et al., 2009; Gaudlip et al., 2008; Myers, 2008; Zolfaghari et al. 2014 and 2016). Following hydraulic fracturing operations, a large quantity of water flows back to the surface along with the gas, known as produced/flowback water. This produced/flowback water, which is relatively simple to collect at the wellhead for ion concentration analysis, provides a significant yet underutilized source of information.

In the past, the chemistry of produced/flowback water was usually only reported to the government/environmental agencies to prevent environmental pollution. However, within the petroleum industry, this data has not been explored to its full potential (Sharak, 2018; Zolfaghari et al. 2014 and 2016). Using the potential of this data could bridge current knowledge gaps, developing a more comprehensive fracture characterization workflow. This could inevitably lead to optimized fracturing techniques and more efficient hydrocarbon production.

1.2 Problem Statement

This section identifies and elaborates on the core problems within the scope of the research:

1. There is limited existing work that focused on the construction of a coupled flow-geochemistry numerical simulation model suitable for analyzing hydraulically fractured reservoirs using a commercial package and validation of such models with experimental data of tight oil/shale gas fractured wells in the literature;

3. There is no quantitative framework to correlate the salinity data of flowback water with fracture properties;
4. A workflow for fracture characterization that integrates the salinity of flowback water and gas rate is needed.

1.3 Research Objective

Simulation can be used to incorporate geochemical data to infer more information about complexity fracture geometry recycling. So, this work will use the simulation to solve the foregoing problems, and the corresponding objectives are listed as follow:

1. Develop a coupled flow and geochemical approach for hydraulically fractured reservoirs using commercial simulation packages, validate against other relevant simulation studies in the literature, and compare simulation results with field observations qualitatively.
2. Develop a systematic framework for correlating fracture properties with salinity of flowback fluid and gas rate and assess the utility of salinity data in estimating uncertain fracture properties.
3. Develop a workflow using the salinity of flowback fluid and gas rate to infer fracture properties for various fracture distributions.

1.4 Thesis Outline

This thesis consists of 6 chapters, and it is organized as follows:

Chapter 1 presents a general introduction of this thesis, including background information and research motivations, problem statement, research objectives and thesis outline.

Chapter 2 presents the literature review on concepts and developments in unconventional reservoirs, hydraulic fracturing, flowback processes, and advanced analytical techniques like response surface modelling and genetic algorithms.

Chapter 3 presents a simulation study where complex mechanisms and interactions are represented, including multiple ion exchange, mineral dissolution, wettability alteration, pH variation, and electrical double layers. The models are used to examine how the salinity of injected water may affect gas recovery.

Chapter 4 introduces a hydraulically fractured reservoir model incorporating multiple geochemical reaction mechanisms. Develop the RSM-Salinity and RSM-Rate prediction regression models. The models reveal the complex temporal relationships between the salinity of flowback fluid and/or gas rate with production time.

Chapter 5 presents a comprehensive workflow, synergizing the power of RSM and GA, to utilize the salinity profile of flowback fluid and gas rate for fracture characterization. A comprehensive range of scenarios was examined, stretching from Single-Stage Wells to Multi-Stage Horizontal Wells and from homogeneous to heterogeneous fracture models.

Chapter 6 presents the conclusions and contributions of this study. Recommendations for future work are also discussed.

Chapter 2: Literature Review

The Literature Review serves as the foundation upon which this study builds. It provides an overview of the body of knowledge that has informed this research, highlighting key theories, models, and findings in the areas most pertinent to this thesis. This chapter is organized into six main sections that discuss unconventional reservoirs, the fracturing process, flowback process, fracture network characterization, response surface modelling, and genetic algorithms.

2.1 Unconventional Reservoirs

Unconventional reservoirs are a class of hydrocarbon deposits distinguished from their conventional counterparts by their unique geological characteristics. These typically include low permeability and porosity, complex mineralogy, and diverse depositional environments. Common types of unconventional reservoirs include gas and oil shales, tight oil and gas formations, coalbed methane, oil sands, and gas-hydrate deposits. The exploitation of these resources has gained momentum in recent decades, thanks to advancements in extraction technologies. Notably, horizontal drilling and multi-stage hydraulic fracturing have emerged as critical innovations that enable the commercial viability of these otherwise difficult-to-reach resources. Horizontal drilling allows for more extensive contact with the formation, while multi-stage hydraulic fracturing creates multiple fractures at different intervals along a horizontal wellbore, thus significantly enhancing hydrocarbon recovery rates (Meyer et al., 2010; Soliman et al., 2010; Soliman et al., 2012).

2.2 Fracturing Process

The hydraulic fracturing technique is a form of reservoir stimulation that involves pumping a relatively large amount of fracturing fluid into the wellbore at a high pressure, sufficient to exceed the tensile strength of the reservoir rock. The objective is to create new fractures or expand existing natural fractures within the hydrocarbon-bearing formation. Once fractures are created, proppants such as sand, ceramic, or resin-coated beads are injected into these fractures to hold them open, facilitating the flow of hydrocarbons. This technique was first introduced in the petroleum industry in 1947, with commercial applications in 1950 (King, 2012). Modern improvements in fluid chemistry, proppant technology, and the application of multi-stage fracturing have greatly enhanced the efficiency and effectiveness of hydraulic fracturing.

2.3 Fracturing Fluid

Fracturing fluid is used to initiate and propagate fractures. Commonly used types include water-based, oil-based, and foam-based fluids (Wanniarachchi et al., 2017; Tang et al., 2022; Xiong et al., 1996). Water-based fluids are the most widely used due to their cost-effectiveness. Typically, the fluid consists of a mixture of water, proppants, and chemical additives, each selected to optimize the fracturing process. The choice of fracturing fluid composition can have far-reaching implications, affecting not only the immediate efficacy of the hydraulic fracturing operation but also the long-term productivity of the well. Despite its significance, prior numerical modelling studies have often overlooked the geochemical interactions between the fracturing fluid and the formation rock. These interactions can significantly influence both the short-term effectiveness

and long-term behaviour of the reservoir. Understanding these interactions is thus crucial for improving reservoir models and optimizing production.

2.4 Flowback Process

Following hydraulic fracturing, the flowback process entails the recovery of the fracturing fluid from the well. The chemistry of flowback fluid can provide insights into the efficiency of the fracturing process. While some studies have examined the chemical composition of flowback water, they have mostly been limited to environmental impact assessments rather than as a resource for improving reservoir understanding and management (Fu et al., 2021; Dong et al., 2022; He et al., 2022; Rosenblum et al., 2017). Some existing studies have explored the relationship between the chemistry of flowback fluids and the long-term performance of the reservoir. However, these have been mainly concentrated on environmental impact assessments rather than serving as a resource for improving reservoir understanding and management.

2.5 Flowback Chemical Analysis

Chemical analysis of flowback water offers a supplementary or alternative methodology for fracture characterization. Various researchers have conducted notable studies in this area. Woodroof et al. (2003), Sullivan et al. (2004), Willberg et al. (1998) and Asadi et al. (2008) all proposed models focusing on the chemical characteristics of flowback water to better understand and manage the fracturing process. Gdanski et al. (2007) took it a step further by adding a chemical component to their 2D numerical simulator for the history matching of flowback fluid composition.

Ghanbari et al. (2013) analyzed specifically salt concentrations in flowback water from hydraulically fractured wells in the Horn River Basin. They found that the complexity of the fracture network appeared to influence the salt concentration and load-recovery profile. Zolfaghari et al. (2014) carried out a set of experiments to trace the source of salts in the flowback water. Their findings offered valuable insights into the connection between the barium concentration in the flowback water and the complexity of the fracture network.

2.6 Response Surface Modelling

Response surface methodology (RSM), introduced by Box and Wilson (1951), encompasses a series of mathematical/statistical techniques for empirical model building and exploitation of the model. Through design and analysis, RSM seeks to relate a response to the input variables or factors that influence it, and the objective is to optimize this response. In engineering, RSM has been employed to optimize manufacturing processes, design experiments, and model complex systems (Myers et al., 2016; Deng and Cai, 2010; Sen and Swaminathan, 2004; Singh et al., 2010; Baş and Boyacı, 2007). In chemistry, RSM has facilitated the optimization of reaction conditions, formulation development, and prediction of chemical properties (Bezerra et al., 2008; Hanrahan and Lu, 2006; Ahn et al., 2010; Amini et al., 2010). Additionally, RSM has found applications in economics, marketing, and social sciences, aiding in understanding consumer behaviour, market response, and policy analysis (Shang et al., 2004; Januardi et al., 2021; Guo et al., 2021; Anderson and Whitcomb, 2016; Venkatesh and Goyal, 2010;). However, traditional RSM is rooted in static experimental designs, where relationships are explored at specific points in parameter space. While this approach has proven valuable in various applications, it neglects the temporal dimension that

characterizes many systems. Consider, for instance, processes in which variables evolve over time, such as chemical reactions, biological processes, and even economic phenomena. In such cases, relying solely on static experimental data fails to capture the full scope of the system's behaviour. To overcome this limitation, Coefficient-Driven Response Surface Modelling is a novel extension of RSM tailored to address dynamic behaviours. This approach is designed to unravel the intricate relationships that unfold over time by focusing on the coefficients of carefully selected nonlinear equations. By integrating temporal dynamics and coefficient analysis, RSM strives to enhance the predictive power of RSM, offering a more comprehensive understanding of complex systems.

2.7 Genetic Algorithm (GA)

The genetic algorithm was put forward by Professor J. Holland at the University of Michigan in 1975, which is an optimization technique inspired by the process of natural selection and genetics (Holland, 1975). It is widely used to solve complex optimization problems by mimicking the evolutionary principles observed in biological systems (Goldberg and Holland, 1988; Holland, 1992; Mitchell, 1998; Sivanandam et al., 2008; Srinivasan and Leung, 2022). The goal is to find the optimal values of these variables that minimize the objective function. The GA follows an iterative process, which consists of the following steps:

Initialization: Initialize an initial population of candidate solutions randomly or based on some prior knowledge. Each candidate solution represents a potential set of values for the independent variables.

Evaluation: Evaluate the fitness of each candidate solution by calculating the objective value using the defined objective function. The objective value quantifies the quality or performance of the solution in terms of fracture characterization.

Selection: Select the fittest individuals from the population to serve as parents for the next generation. The selection process is typically based on a probabilistic mechanism, where individuals with higher fitness have a higher chance of being selected.

Genetic Operators: Apply genetic operators, including crossover and mutation, to the selected parents to create new offspring. Crossover involves combining genetic information from two or more parents, while mutation introduces random changes to maintain diversity in the population.

Replacement: Replace a portion of the existing population with the newly created offspring. The replacement process ensures the evolution of the population towards better solutions over successive generations.

Termination: Repeat the evaluation, selection, genetic operators, and replacement steps for a specified number of generations or until a termination criterion is met. The termination criterion can be a predetermined number of iterations or when the improvement in the objective value becomes negligible.

Chapter 3: Coupling Flow-Geochemical Model Development in Sandstone Reservoir

3.1 Introduction

In the past few decades, water flooding and hydraulic fracturing have been applied extensively to improve oil recovery in conventional and unconventional reservoirs. The literature generally reports that the salinity of the injected fluids plays an important role in the process efficiency (Yousef et al., 2010; Zhang and Leung, 2022).

The potential for injection of engineered water (also known as smart water or low-salinity water or LSW) to enhance recovery was first discovered in sandstone reservoirs by Baptist (1954), Bernard (1967), and Martin (1959). In the 1990s, Jadhunandan and Morrow (1991) and Yildiz and Morrow (1996) reported the effect of brine composition on the recovery factor, which identified the possibility of improving waterflood by optimizing injection brine formulations. Numerous laboratory experiments (Tang and Morrow, 1997; Morrow et al., 1998; Tang and Morrow, 1999; Sharma and Filico, 2000; Morrow and Buckley, 2011; Chaturvedi et al., 2021) demonstrated that changing the salinity of the injected water can alter the reservoir recovery. Brady et al. (2012 and 2016) showed that the increase in salinity could increase the number of cations on the clay basal plane, leading to positively charged oil groups adsorbed onto the clay surface.

Numerical models have been used extensively to simulate flow and geomechanical responses of hydraulically fractured reservoirs. However, most previous modelling works did not consider geochemistry. For example, Zhong and Leung (2020a and 2020b) investigated the effect of fracture distribution on hydraulic-fractured shale-gas production by upscaling the stochastic 3D

discrete fracture network (DFN) model into an equivalent continuum dual-porosity dual-permeability (DPDK) model. Xu and Leung (2022) studied the impact of mesh alignment with DFN in a DPDK model. Liu et al. (2020 and 2021) presented a coupled two-phase flow/geomechanics model to investigate the feasibility and efficiency of inter-fracture water injection to enhance oil recovery. Wang and Leung (2015 and 2016) constructed a series of mechanistic simulation models consisting of both hydraulic fractures and stochastically-distributed secondary fractures to simulate imbibition, fluid re-distribution, and flow-back during shut-in and cleanup. Some authors incorporated geochemical experimental data and findings in their modelling work. For instance, Shabani and Zivar (2020) coupled flow with a geochemistry model package to simulate geochemical reactions during low-salinity water injection. Esene et al. (2018) used the CMG-GEM module to establish a geochemical model to study the wettability alteration during low salinity water flooding and proposed the term optimal salinity. However, none of these works has examined the impacts of injected fluid salinity and the corresponding rock-fluid interactions. At the same time, the mechanism by which geochemistry affects recovery is also unclear because the mechanisms that govern the interactions between crude oil, formation water, engineered water and rock are complex.

To consider geochemistry in the numerical simulation, several proposed mechanisms, including fines migration, multiple ion exchange, mineral dissolution, wettability alteration, pH variation, and electrical double layers, should be modelled. Tang and Morrow (1999) proposed that the presence of potentially mobile fines was a necessary condition for an increase in oil recovery during low-salinity waterflooding. During the typical waterflooding process, crude oil droplets would adhere to the fines on the pore walls as part of the trapped oil. When the salinity of the injected water decreases, the attractive force between the fines and the pore wall decreases,

enabling the fine particles to be separated from the pore wall. The enhanced oil recovery is attributed to partially stripping the mixed wet fines from the pore walls. On the other hand, other researchers would argue that the migrated fines would plug some pore throats and reduce the relative permeability of water, causing more water to flow to the unswept area and improving the displacement efficiency. (Muecke 1979; Fogden et al. 2011; Bedrikovetsky et al. 2012; Bhuvankar et al. 2022). Some researchers did not observe any fines migration during low-salinity water flooding (Webb et al., 2004; McGuire et al., 2005; Jerauld et al., 2008). Lager et al. (2006) indicated fines migration is not ubiquitous during low-salinity water flooding.

Some studies have shown that during low-salinity water flooding, the pH increases with the oil recovery factor (McGuire et al., 2005). At first, it was attributed to the dissolution of carbonate rock and the consumption of hydrogen ions. Appelo and Postma (2004) demonstrated that the cation exchange process is faster than mineral dissolution. The hydrogen ions present in the liquid phase would exchange with the previously adsorbed cations on the mineral surfaces. This reduction of hydrogen ions in the liquid phase would lead to an increase in pH value. However, other studies have shown no direct relationship between the increase in oil recovery caused by low-salinity injected water and pH value (Ehrlich and Wygal, 1977; Lager et al., 2006).

Lager et al. (2006 and 2008) have proposed that the multiple ion exchange is the key mechanism for increasing oil recovery during low-salinity water flooding. A chemical balance exists between the ion concentration in the connate water (or initial formation water), the ion concentration adsorbed on the clay surface, and the polar compounds in the crude oil. Positively charged ions in the connate water, such as Ca^{2+} and Mg^{2+} , are adsorbed on negatively charged clay surfaces. The polar oil compounds, mainly negatively charged, are adsorbed to these multivalent positive charge sites on the clay surface, forming an oil film on the clay surface and an Electrical Double Layer

(EDL) (Ligthelm et al., 2009). Therefore, macroscopically, the clay surface can be considered oil-wet. This balance is disturbed upon the injection of engineered fracturing fluids. For example, Ca^{2+} and other multivalent ions would be replaced by monovalent Na^+ (AlShalabi and Sepehrnoori, 2016; Aminian and ZareNezhad, 2019), and the crude oil adsorbed on the multivalent ions could also be desorbed. Therefore, this exchange of ions could cause the formation to change from oil-wet to mixed or water-wet (Amirian et al., 2017).

Since the concentration of each ion in the injected engineered water is very different from that of the formation water, it will disturb the existing equilibrium and cause source minerals (e.g., CaCO_3 , MgCO_3 , $\text{CaMg}(\text{CO}_3)_2$ and CaSO_4 , etc.) to dissolve or precipitate, thereby establishing a new equilibrium. In this process, polar components adsorbed on the rock surface are released with the dissolved minerals, thereby increasing water-wetness (Hiorth et al., 2010; Evje and Hiorth, 2010 and 2011), and it can also lead to changes in pore structure (Yousef et al., 2010 and 2011).

Moreover, Tang and Morrow (1999) observed a similar oil recovery and imbibition rate from a high-salinity engineered water injection and a low-salinity engineered water injection in cores aged in crude oil with no initial formation brine. Sharma and Filoco (2000) and Tang and Morrow (1997) obtained increased recovery as the salinity of the initial formation water decreased. These authors emphasize that the salinity of the initial formation water plays a key role in oil recovery. However, the initial salinity of the formation water results from an equilibrium state formed by long-term geological activities. It is generally impossible to alter the composition of the formation water directly; however, compositions of the injected water can be engineered with the optimal salinity. Hence, systematic studies must be carried out to determine the optimum salinity and concentration of the engineered water.

A geochemical model is established in this chapter based on an experimental core flood data set (Fjelde et al., 2012). The simulated effluent ion concentration, pH, and saturation are compared and validated with experimental measurements. The intent is to validate the formulation of the geochemical model and other physical processes. The reliability of ion-exchange equivalent fraction, pore volume evolution, and mineral molarity is demonstrated.

3.2. Mathematical Model

3.2.1 Component Material Balance Equation

The simulation is performed using CMG-GEM compositional simulator (CMG, 2022). The material balance equation is coupled with Darcy's law governing the flow and the geochemical model, which includes intra-aqueous reactions, mineral reactions, ion exchange reactions, and phase equilibrium reactions. Consider a system consisting of n_{ct} total components: n_g gaseous components, n_{aq} aqueous components, and n_m mineral components. The conservation equations for the different species are shown here (Nghiem and Rozon, 1988 and 1989; Nghiem et al., 2011; Collins et al., 1992):

$$\psi_i \equiv \Delta T_g^u y_{i,g}^u (\Delta p^{n+1} + \Delta P_{c,aq-g}^u - \rho_g^u g \Delta d) + \Delta T_{aq}^u y_{i,aq}^u (\Delta p^{n+1} - \rho_{aq}^u g \Delta d) + \sum_{q=g,aq} \Delta D_{i,q}^u \Delta y_{i,q}^u + V \sigma_{i,aq}^{n+1} + q_i^{n+1} - \frac{V}{\Delta t} (N_i^{n+1} - N_i^n) = 0, \quad i = 1, \dots, n_g, \quad 1$$

$$\psi_j \equiv \Delta T_{aq}^u y_{j,aq}^u (\Delta p^{n+1} - \rho_{aq}^u g \Delta d) + \Delta D_{i,aq}^u \Delta y_{i,aq}^u + V \sigma_{j,aq}^{n+1} + V \sigma_{j,mn}^{n+1} + q_j^{n+1} - \frac{V}{\Delta t} [(N_{j,aq}^{n+1} + N_{j-x}^{n+1}) - (N_{j,aq}^n + N_{j-x}^n)] = 0, \quad j = n_g + 1, \dots, n_g + n_{aq}, \quad 2$$

$$\psi_k \equiv V \sigma_{k,mn}^{n+1} - \frac{V}{\Delta t} (N_k^{n+1} - N_k^n) = 0, \quad k = n_g + n_{aq} + 1, \dots, n_{ct}. \quad 3$$

ψ stands for constitutive equation; the superscript n and $n + 1$ denote the old and new time levels, respectively; the superscript $u = n$ or $n + 1$ refers to either explicit and implicit coupling; the subscript g , aq and mn stand for gaseous and aqueous and mineral, respectively; T_g is the transmissibility of the gaseous phase, y is the mole fraction, p is the pressure, P_c is the capillary pressure, ρ is the density (kg/m^3), g is the acceleration due to gravity (m/s^2), d is the depth (m), D is the diffusivity in the phase, $V\sigma_{i,aq}$ is the intra-aqueous reaction rates, $V\sigma_{i,mn}$ is the mineral dissolution/precipitation rates, q is the injection or production rate, N is the number of moles of mineral, X denotes the clay mineral in the reservoir rock, and the subscript $j - X$ stands for the component j adsorbed on the clay surface, and Δt is the time step.

3.2.2 Gas and Aqueous Phase Properties

The phase behaviour is modelled using the Peng-Robinson EOS (Peng and Robinson, 1976; Soave, 1972). The gas viscosity is calculated using the Jossi, Stiel and Thodos correlation (Jossi et al., 1962). The aqueous phase density and viscosity are computed following the correlations presented in Rowe and Chou (1970) and Kestin et al. (1981). However, it's important to note that the effects of capillary pressure (P_c) are not incorporated into the phase equilibrium calculations within the CMG software but are only considered in the flow equations. This limitation is a notable shortcoming of the approach taken.

3.2.3 Aqueous Reactions

Nghiem et al. (2004) proposed a fully-coupled geochemical Equation-of-State model for simulating CO₂ storage and low-salinity water flooding. The aqueous reactions are modelled with chemical equilibrium constants.

$$Q_{\alpha} - K_{eq,\alpha} = 0, \alpha = 1, \dots, R_{aq}, \quad 4$$

with

$$Q_{\alpha} = \prod_{k=1}^{n_{aq}} a_k^{v_{k\alpha}}, \quad 5$$

Q_{α} is the activity product of the aqueous reaction α (Bethke, 1996; Kharaka et al., 1989). $K_{eq,\alpha}$ is the chemical equilibrium constant for the aqueous reaction α . R_{aq} is the number of aqueous reactions. n_{aq} is the number of components. a_k is the activity of component k . $v_{k\alpha}$ is the stoichiometry coefficient of component k in reaction α (Nghiem et al., 2004).

$$a_k = \gamma_k m_k, k = 1, \dots, n_{aq}, \quad 6$$

where γ_k is the activity coefficient of component k and m_k is the molality (moles per kg of H₂O). For a non-ideal solution, the activity coefficient can be calculated from the B-dot model (Bethke, 1996).

3.2.4 Mineral Dissolution and Precipitation

The rate law for the mineral dissolution and precipitation reaction is (Bethke, 1996):

$$r_{\beta} = \widehat{A}_{\beta} k_{\beta} \left(1 - \frac{Q_{\beta}}{K_{eq,\beta}} \right), \beta = 1 \dots, R_{mn}, \quad 7$$

β refers to the mineral reaction; r is the reaction rate, which is dependent on the surface area (\widehat{A}) and the rate constant k). K_{eq} is the chemical equilibrium constant; Q is the activity product; R_{mn} is the total number of mineral reactions. If $Q_{\beta}/K_{eq,\beta} > 1$, mineral precipitation occurs and if $Q_{\beta}/K_{eq,\beta} < 1$, mineral dissolution occurs. Therefore, $r < 0$ for dissolution and $r > 0$ for precipitation. The rate is zero when $Q_{\beta}/K_{eq,\beta} = 1$. The reaction rate constant k_{β} at any temperature (T) can be obtained from the following equation (Bethke, 1996):

$$k_{\beta} = k_{\beta 0} \exp \left[-\frac{E_{a\beta}}{R} \left(\frac{1}{T} - \frac{1}{T_0} \right) \right], \quad 8$$

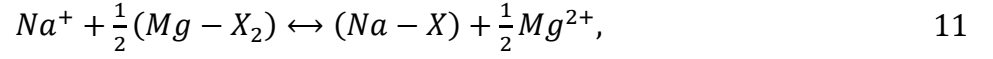
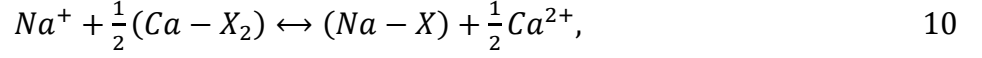
$E_{a\beta}$ is the activation energy for reaction β [J/mol], R is the universal gas constant, and $k_{\beta 0}$ is the reaction rate constant for reaction β at the reference temperature, T_0 . The reactive surface area of minerals per unit volume of porous media varies with mineral dissolution or precipitation. The following equation is used to calculate the reactive surface area (\widehat{A}_{β}) with change in the moles of minerals through dissolution or precipitation (Nghiem et al., 2004):

$$\widehat{A}_{\beta} = \widehat{A}_{\beta}^0 \frac{N_{\beta}}{N_{\beta}^0}, \quad 9$$

where \widehat{A}_{β}^0 is the reactive surface area at time 0, N_{β} is the number of moles of mineral β per unit grid block (bulk) volume at the current time, and N_{β}^0 is the number of moles of mineral β per unit grid block (bulk) volume at the initial time.

3.2.5 Ion Exchange

Two ionic exchange reactions are considered, where X denotes the clay mineral in the reservoir rock:



The ion-exchange reactions are modelled using the equilibrium constants. However, determining these equilibrium constants on the exchanger surfaces is difficult. According to the Gaines-Thomas convention (Appelo and Postma, 2005), the following selectivity coefficient formulation is used instead of the equilibrium constant (CMG, 2022).

$$K'_{Na/Ca} = \frac{\zeta(Na-X)[m(Ca^{2+})]^{0.5}}{[\zeta(Ca-X_2)]^{0.5}m(Na^+)} \times \frac{[\gamma(Ca^{2+})]^{0.5}}{\gamma(Na^+)}, \quad 12$$

$$K'_{Na/Mg} = \frac{\zeta(Na-X)[m(Mg^{2+})]^{0.5}}{[\zeta(Mg-X_2)]^{0.5}m(Na^+)} \times \frac{[\gamma(Mg^{2+})]^{0.5}}{\gamma(Na^+)}, \quad 13$$

where $\zeta(Na - X)$, $\zeta(Ca - X_2)$ and $\zeta(Mg - X_2)$ are the equivalent fraction of Na^+/Ca^{2+} and Na^+/Mg^{2+} on the exchanger surface, respectively.

The cation exchange capacity (CEC) is the amount of ions adsorbed on the rock surface. Thus the total moles of adsorbed ions of $Na - X$, $Ca - X_2$ and $Mg - X_2$ in a grid block are denoted as VN_{Na-X} , VN_{Ca-X_2} , and VN_{Mg-X_2} , where V is the grid block bulk volume. The following equation must be satisfied for a given value of CEC in the grid block (Esene et al., 2018).

$$VN_{Na-X} + 2VN_{Ca-X_2} + 2VN_{Mg-X_2} = V\phi(CEC), \quad 14$$

or

$$N_{Na-X} + 2N_{Ca-X_2} + 2N_{Mg-X_2} = \phi(CEC), \quad 15$$

where ϕ is the porosity, and N is the number of moles. Therefore, the equivalent fractions can be calculated:

$$\zeta(Na - X) = \frac{N_{Na-X}}{N_{Na-X} + 2N_{Ca-X_2} + 2N_{Mg-X_2}}, \quad 16$$

$$\zeta(Ca - X_2) = \frac{2N_{Ca-X_2}}{N_{Na-X} + 2N_{Ca-X_2} + 2N_{Mg-X_2}}, \quad 17$$

$$\zeta(Mg - X_2) = \frac{2N_{Mg-X_2}}{N_{Na-X} + 2N_{Ca-X_2} + 2N_{Mg-X_2}}, \quad 18$$

3.2.6 Flow and Geochemistry Coupling

As mineral dissolution and precipitation affect the void volume of the porous medium, a two-way coupling scheme (as shown in Figure 3-1) is implemented in GEM to couple the geochemical and flow calculations (CMG, 2022): the time-stepping in the flow module is performed first to obtain the pressure and temperature distribution. The pressure and temperature solutions are then passed to the geochemistry module to compute the total moles of minerals, which are used to update the porosity and permeability. The solution from the geochemistry module, including the updated porosity and permeability values, is transferred back to the flow module. The process is repeated within a time step until the convergence criteria are satisfied.

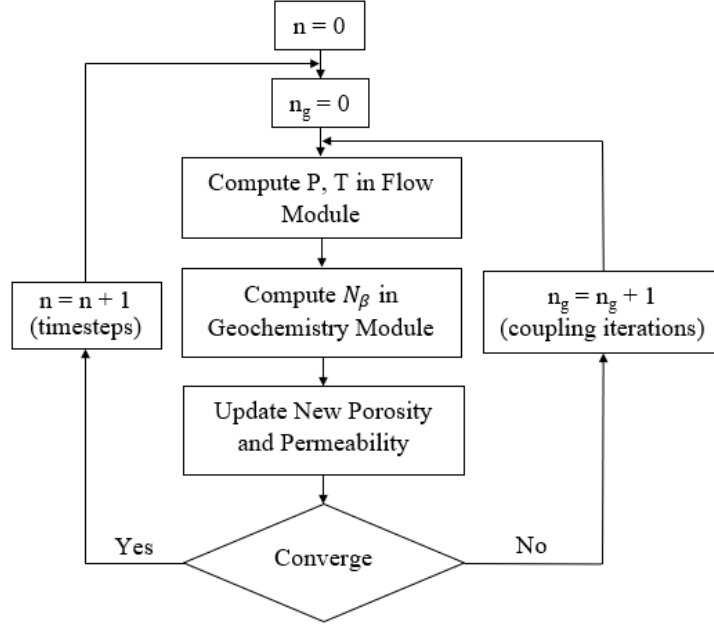


Figure 3-1. Schematic view: two-way coupling between the flow module and geochemistry module as implemented in GEM (CMG, 2022).

The porosity and permeability are updated within GEM. For example, the porosity is calculated as follows (Nghiem et al., 2004):

$$\widehat{\phi}^* = \phi^* - \sum_{\beta=1}^{n_m} \left(\frac{N_{\beta}}{\rho_{\beta}} - \frac{N_{\beta}^0}{\rho_{\beta}} \right), \quad 19$$

$$\phi = \widehat{\phi}^* [1 + c_{\phi}(p - p^*)], \quad 20$$

where ϕ is the updated porosity at pressure p after mineral precipitation/dissolution and compaction, ϕ^* is the porosity without mineral precipitation/dissolution at the reference pressure p^* , $\widehat{\phi}^*$ is the porosity at the reference pressure p^* after mineral precipitation/dissolution. N_{β} is the total moles of mineral β per bulk volume, N_{β}^0 is the total moles of mineral β per bulk volume prior

to mineral precipitation/dissolution at the reference pressure p^* , ρ_β is the mineral molar density, and c_ϕ is the rock compressibility.

The absolute permeability also changes with mineral dissolution and precipitation. The Kozeny-Carman equation is used (Kozeny, 1927; Carman, 1937):

$$\frac{k}{k^0} = \left(\frac{\phi}{\phi^0}\right)^3 \cdot \left(\frac{1-\phi^0}{1-\phi}\right)^2, \quad 21$$

where k^0 and ϕ^0 are the permeability and porosity at the reference pressure p^* , respectively.

3.2.7 Solution Method

The solution method is implemented in CMG (2022) and follows Nghiem et al. (2004)'s approach. A brief summary is provided here. The first elimination of chemical-equilibrium reactions reduces the number of flow equations. The volume constraint equations, the material balance equation, the flow equation, the injector and producer constraint equations, and the phase equilibrium equations were solved simultaneously using the Newton-Raphson method for each discretized grid block.

3.3 Model Development of the Core Flooding Experiment

A simulation model of the coreflood experiment reported by Fjelde et al. (2012) is constructed. A core plug extracted from the North Sea Sandstone Reservoir was used in their flooding experiment. The clay content in the rock was approximately 13% of the bulk sample by weight, and the cation exchange capacity was 2 meq/100g. Injections of synthetic formation water (FW), seawater (SW),

and low-salinity water (LSW) were tested at a constant core temperature of 80 °C , and approximately 10 pore volumes (PV) of brine were injected at each stage, as given in Table 3-1.

Table 3-1 Chemical compositions of formation water, seawater, and low-salinity water (Fjedel et al., 2012)

Ions	Formation water (mole/L)	Seawater (mole/L)	Low-salinity water (mole/L)
Ca ²⁺	0.14794	0.01299	0.00148
SO ₄ ²⁻	0.00089	0.02401	0.00001
Mg ²⁺	0.01746	0.04451	0.00018
Na ⁺	1.32622	0.45011	0.01326
Cl ⁻	1.67773	0.52513	0.01661
K ⁺	0.00562	0.01006	0.00006

A 1D model, as shown in Figure 3-2, is established using CMG-GEM compositional simulator (CMG, 2022) to model the coreflood experiments. Other relevant properties are shown in Table 3-2 and Table 3-3. The two relative permeability sets (one for high salinity and one for low salinity) provided by Fjelde et al. (2012) are adopted (as shown in Figure 3-3). The brine used in the simulation was slightly adjusted because potassium ions were not included in the model.

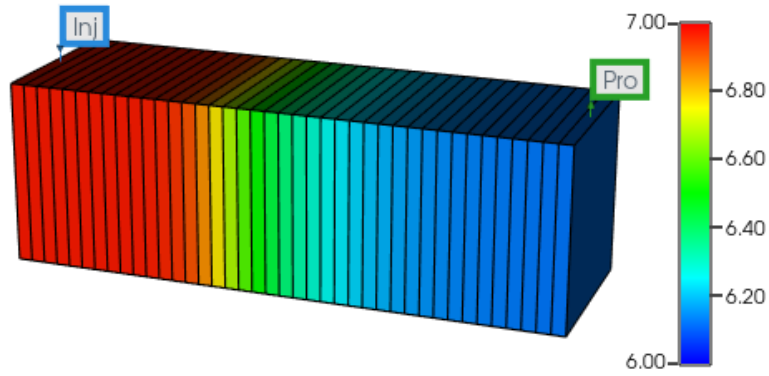


Figure 3-2 1D model setup; the colour scale represents pH (Inj: Injection well; Pro: Production well).

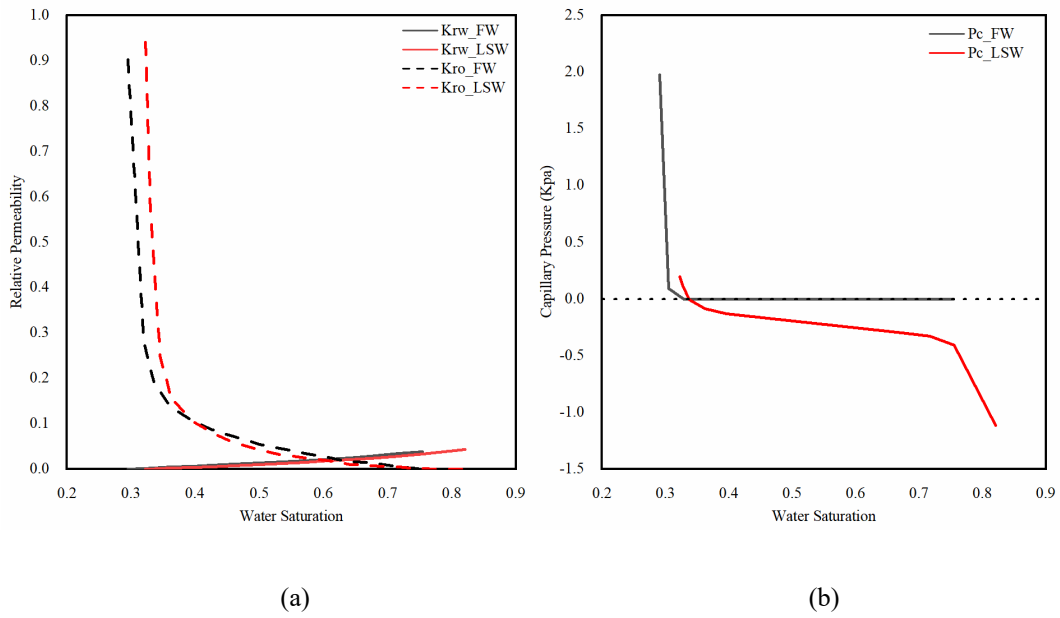


Figure 3-3 (a) Relative permeability curves and (b) capillary pressure curves (Fjelde et al., 2012).

Table 3-2 The properties of the sandstone models

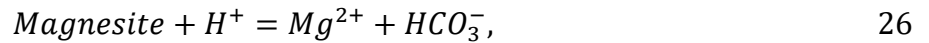
Property	Value
Model length	0.2625 ft
Model width and height	0.11066 ft
Mesh	40 × 1 × 1
Absolute permeability	164 mD
Porosity	0.28
Initial water saturation (Sw)	0.294
Initial oil saturation (So)	0.706
Injection velocity	0.002543 ft ³ /day
Pore volume (PV)	0.0009 ft ³
Temperature	80 °C

As discussed in the previous section, three types of reactions are modelled, and they are all reversible: (1) Aqueous phase reactions; (2) minerals are dissolved or precipitated; (3) Ion exchange:

Aqueous phase reactions:



Mineral reactions:





Ion exchange reactions:

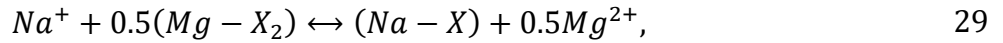
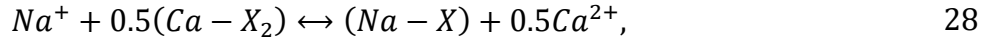


Table 3-3 Geochemical modelling database (Computer Modelling Group 2022)

Mineral	Area (ft ² /ft ³)	Activation energy (J/mol)	Log K_{eq} (mol/ft ² ·s) at 77 F
Calcite	825.99	23500	-0.5398
Magnesite	917.23	23500	-0.8677
Anhydrite	903.24	14300	-0.2964

3.4 Validation Model History Match and Analysis

The model predictions are compared with measured data from the core flooding experiments. According to Figure 3-4, the simulated results agree with the experimental data. To illustrate the relative impact of each mechanism on the recovery factor and produced fluid compositions, two sets of models are created based on the validated model: one where 10 PV of seawater is injected and another where 10 PV of low-salinity water is injected. Each set consists of 3 cases: (1) Base case with all mechanisms coupled; (2) without mineral dissolution and precipitation; (3) without ion exchange.

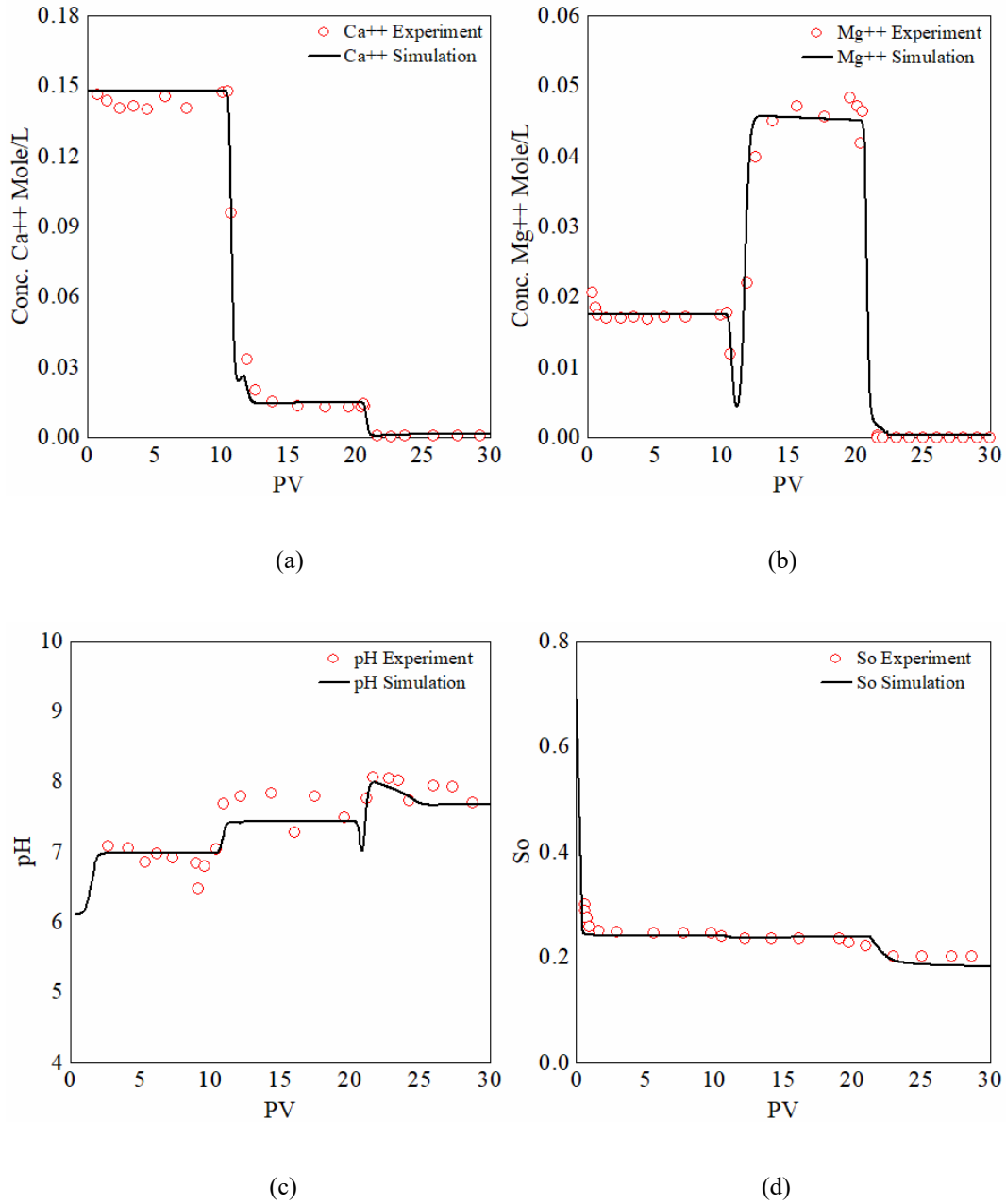


Figure 3-4. Historical matching of simulation predictions with experimental results: (a) Effluent Ca⁺⁺ ion concentration, (b) Effluent Mg⁺⁺ ion concentration, (c) Effluent pH value, and (d) Average oil saturation.

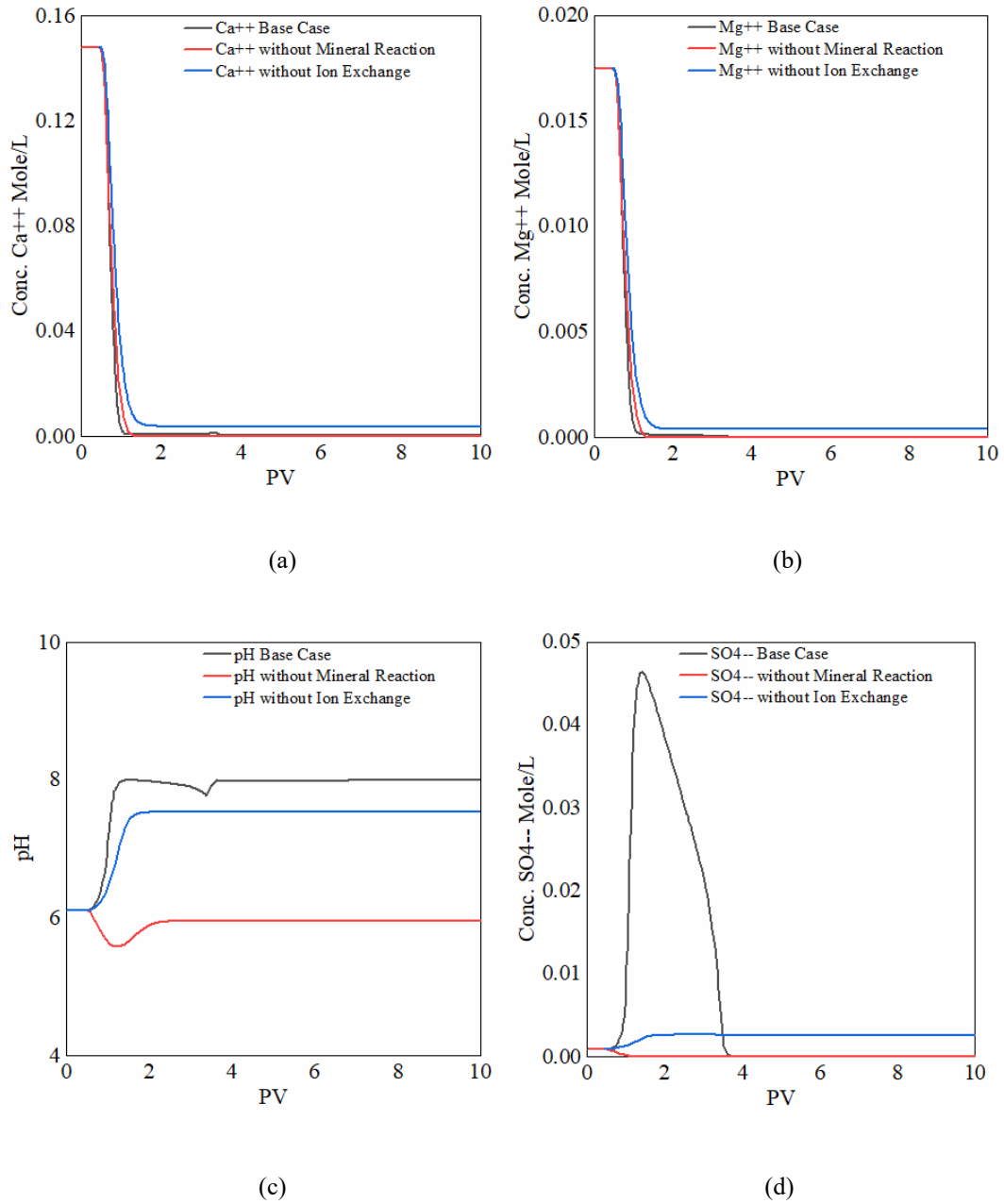


Figure 3-5. Low-salinity water injection: (a) Effluent Ca^{++} ion concentration, (b) Effluent Mg^{++} ion concentration, (c) Effluent pH value, and (d) Effluent SO_4^{--} ion concentration.

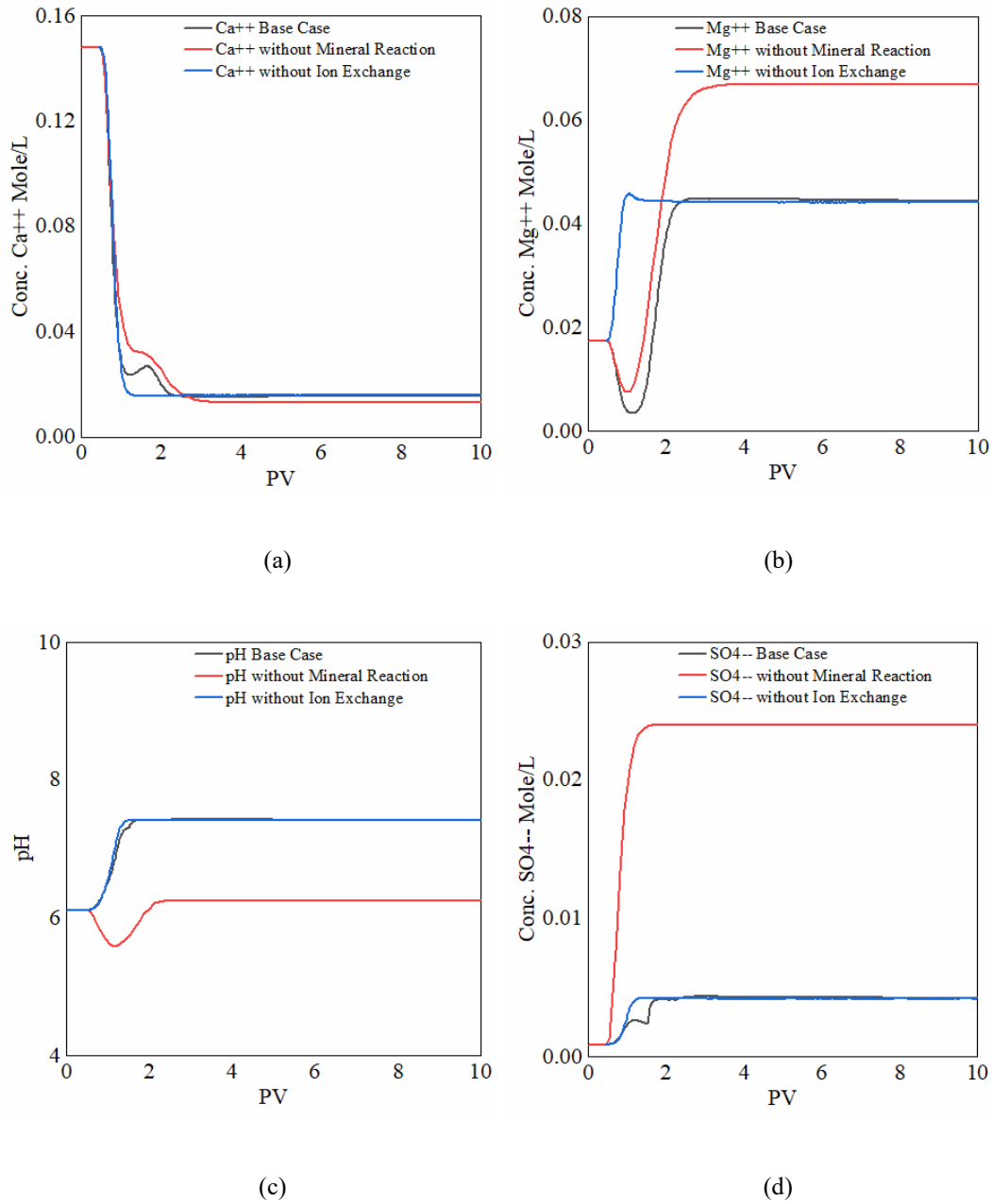


Figure 3-6. Seawater injection: (a) Effluent Ca^{++} ion concentration, (b) Effluent Mg^{++} ion concentration, (c) Effluent pH value, and (d) Effluent SO_4^{--} ion concentration.

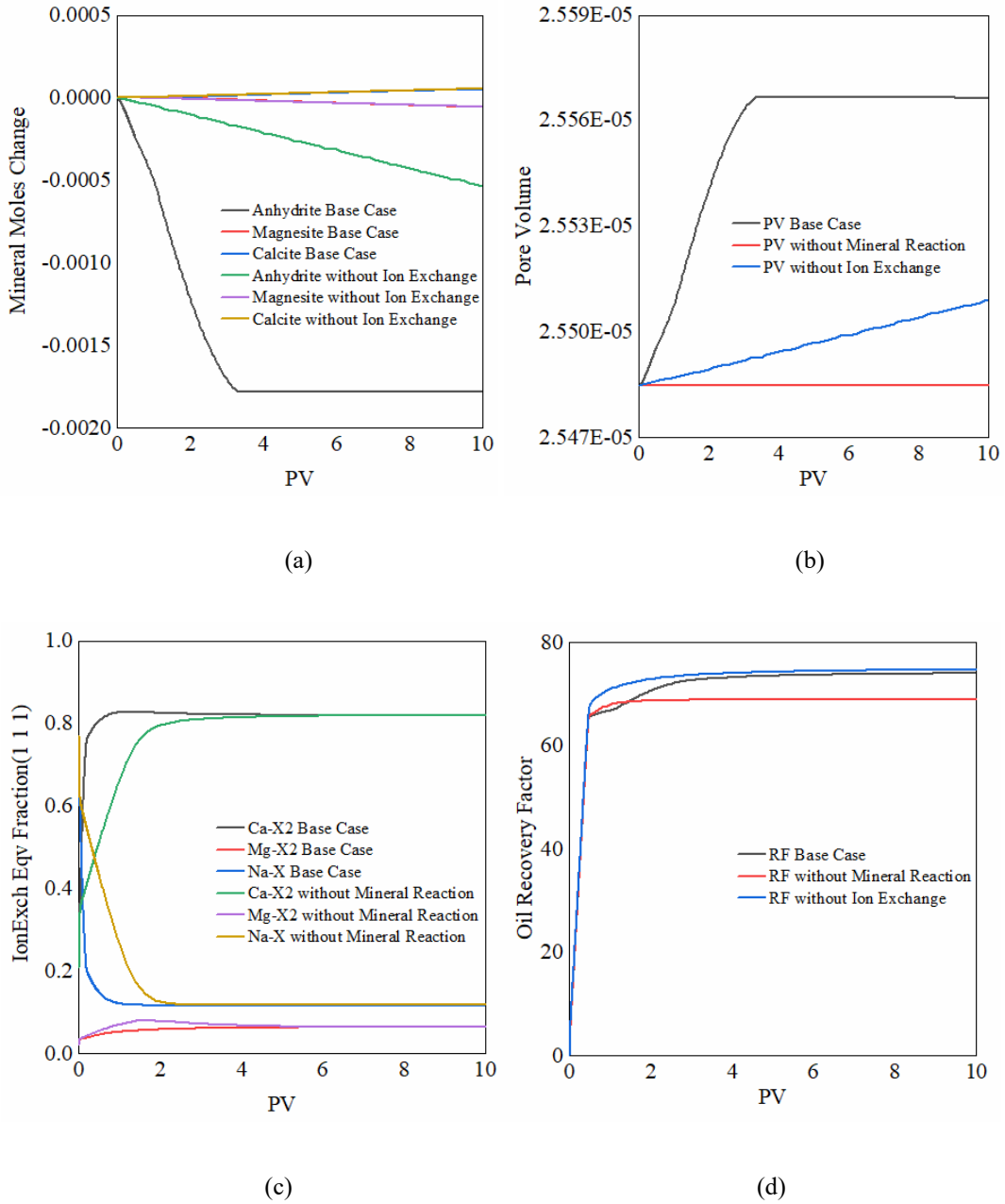


Figure 3-7. Low-salinity water injection: (a) Change in the total number of moles of minerals in the reservoir, (b) Pore volume change, (c) Ion exchange equivalent fraction, and (d) Oil recovery factor.

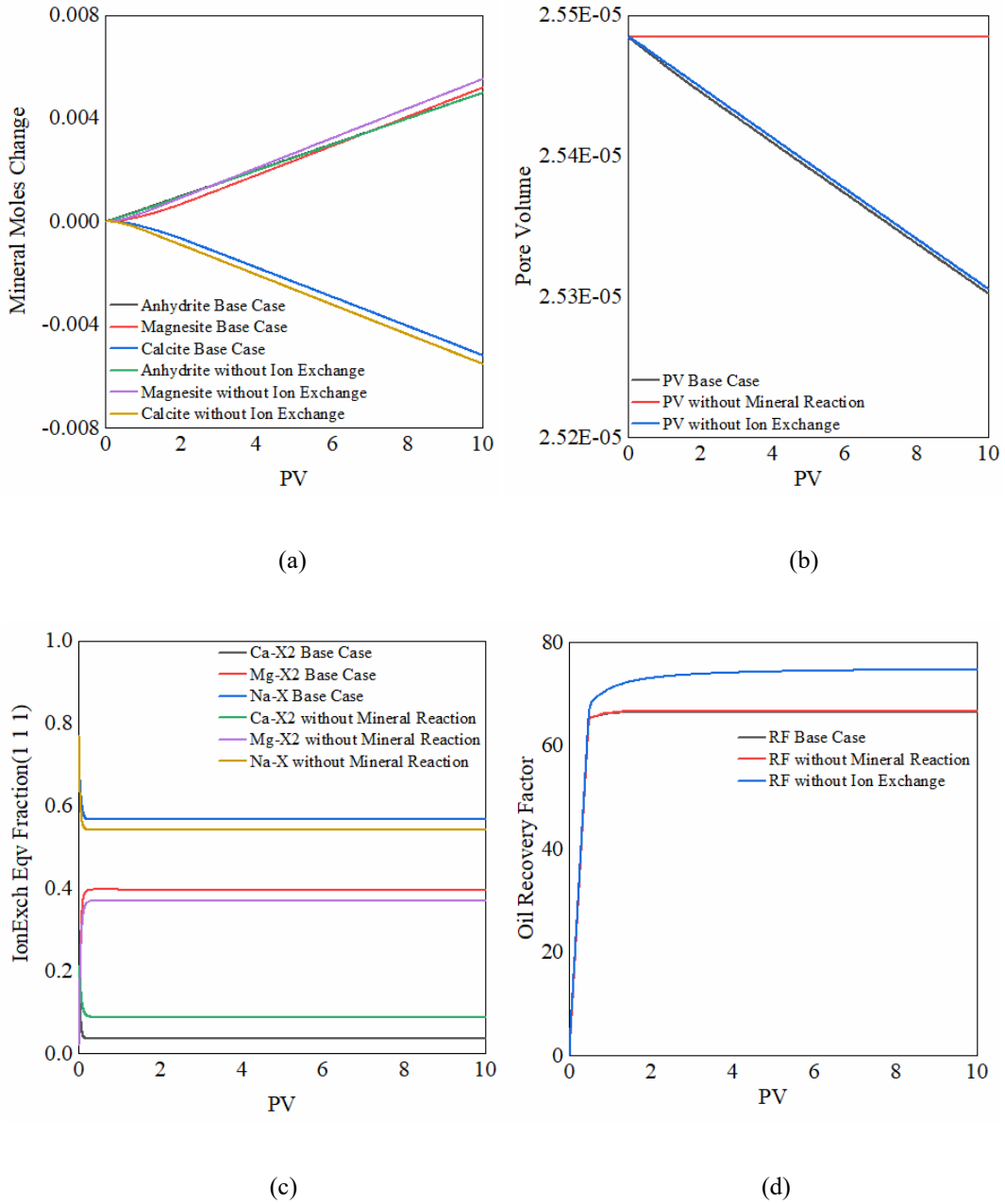


Figure 3-8. Seawater injection: (a) Change in the total number of moles of mineral in the reservoir, (b) Pore volume change, (c) Ion exchange equivalent fraction in grid block (1 1 1), and (d) Oil recovery factor.

The concentration of SO_4^{2-} ions in seawater is significantly higher than that of formation water (as shown in Table 3-1). Considering the base case in Figure 3-8a, more anhydrite is formed because

SO_4^{2-} ions reacted with Ca^{2+} ions to precipitate anhydrite. This observation is supported by the low concentration of SO_4^{2-} ions in the effluent (Figure 3-6d – SO_4^{2-} base case), compared to its concentration in the injected seawater (0.02401 mol/L in Table 3-1). Anhydrite precipitation consumes part of Ca^{2+} ions, and the Ca^{2+} ion concentration in seawater is lower than that in the formation water, so the $\text{Ca} - \text{X}_2$ adsorbed on the clay surface is rapidly converted into Ca^{2+} ions, resulting in a decrease in the equivalent fraction of $\text{Ca} - \text{X}_2$ (as shown in Figure 3-8c – $\text{Ca} - \text{X}_2$ base case). Since the Mg^{2+} ion concentration in seawater is greater than that in the formation water, the free Mg^{2+} are adsorbed on the clay and converted into $\text{Mg} - \text{X}_2$, causing an increase in the equivalent fraction of $\text{Mg} - \text{X}_2$ (as shown in Figure 3-8c – $\text{Mg} - \text{X}_2$ base case), while the desorption of Na^+ would lead to a decrease in the equivalent fraction of $\text{Na} - \text{X}$ (as shown in Figure 3-8c – $\text{Na} - \text{X}$ base case). It is worth noting that the ion concentrations in the effluent experience a sudden drop and increase at the beginning due to ion exchange. This phenomenon will be examined further later. Since both magnetite and anhydrite are precipitated, only calcite is dissolved. The dissolution rate of calcite is comparable to that of magnetite precipitation; the pore volume would decrease continuously throughout the process, as shown in Figure 3-8b, the base case.

When injecting low-salinity water, as shown in Figure 3-7a base case, the number of moles of anhydrite within the reservoir (i.e., simulation model) decreases rapidly, compared to a slight drop in the number of moles of magnesite, indicating that a large amount of anhydrite and a very small amount of magnesite are dissolved – a trend contrary to the observations for seawater injection where both would precipitate (Figure 3-7a the base case). In fact, the dissolution rate of anhydrite is significant, causing the SO_4^{2-} ion concentration in the effluent to increase dramatically to a peak, as shown in Figure 3-5d SO_4^{2-} base case. A large amount of Ca^{2+} produced by dissolution is

exchanged with $\text{Na} - \text{X}$ for $\text{Ca} - \text{X}_2$, as shown in Figure 3-7c, the base case, such that the equivalent fraction of $\text{Ca} - \text{X}_2$ increases, and the equivalent fraction of $\text{Na} - \text{X}$ decreases. During low-salinity water injection, the pore volume increases in the early stage because the dissolution rate is greater than that of precipitation. At the later stage, the dissolution rate of anhydrite slows down (Figure 3-7a – the base case), and the overall precipitation and dissolution rates are comparable, resulting in an essentially constant pore volume (Figure 3-7b – base case).

When ion exchange mechanisms are omitted, the results behave very differently from the base model. The effluent ion concentrations decrease smoothly with time (none of the sudden decreases and increases are present), as shown in Figure 3-6a Ca^{2+} for the base case and the one without ion exchange, suggesting that these fluctuations are attributable to ion exchange. In addition, as ion exchange could lead to wettability alteration, the recovery factors corresponding to seawater and low-salinity water injection would increase if ion exchange is ignored (Figure 3-7d and Figure 3-8d). Moreover, neglecting ion exchange would lead to an overestimation of the recovery factor, particularly in scenarios involving the injection of high-salinity water. During ion exchange, the monovalent and divalent ions adsorbed on the mineral are replaced by the free-state divalent ions and monovalent ions (e.g., $\text{Na} - \text{X}$ exchanges with Ca^{2+} or $\text{Ca} - \text{X}_2$ exchanges with Na^+), which causes an expansion of the double layer on the rock surface. This would mobilize previously unproduced oil adsorbed on divalent ions, enhancing oil recovery.

It is observed in Figure 3-7c and Figure 3-8c (the cases without mineral reactions) that the effluent ion concentrations follow a similar trend as the base case, and this similarity is attributed to the fact that ion exchanges are modelled. However, any observable differences reflect the important role of mineral dissolution. As shown in Figure 3-7a and b, when low-salinity water is injected, the dissolution rate of minerals is greater than the precipitation rate, causing the pore volume and

recovery to increase. This difference implies that without considering mineral reactions, recovery would be underestimated (Figure 3-7d – without mineral reaction). In contrast, Figure 3-8a and b show that the pore volume decreases when seawater is injected, as the mineral precipitation rate exceeds the dissolution rate. It implies that without considering mineral reactions, recovery would be overestimated (Figure 3-8d).

McGuire (2005) and Pal et al. (2019) suggested that an increased pH would amount to alkaline flooding, potentially reducing interfacial tension and improving oil recovery. However, in the practical scenarios, the pH is only 1 to 2 units higher than the injected level, with a peak value of approximately 8, which is much lower than the pH required for alkaline flooding (11 to 13) (Akhlaghi et al., 2020; MehdiBehrang et al., 2021; Awolayo et al., 2018). Figure 3-5c and 6c demonstrate that when mineral dissolution is omitted, the pH will fluctuate at the initial stage due to ion exchange before stabilizing at a level near 6, comparable to the pH of formation water. When ion exchange is omitted, the pH increases due to the consumption of hydrogen ions by mineral dissolution. It is worth noting that when seawater is injected, the pH profile for when ion exchange is omitted is the same as that of the base case, but the corresponding recovery factor is higher than that of the base case. The recovery factor for the injection of low-salinity water is also higher than that of the base case, while the pH is lower. Therefore, there is no clear relationship between the increased pH and improved recovery factor. Mineral dissolution and ion exchange process are the main contributors to increased oil recovery, a conclusion that is consistent with findings reported in the literature (Austad et al., 2010, Cissokho et al., 2010, Aksulu et al., 2012; Al-Saedi et al., 2019; Rezaei Doust et al., 2009).

3.5 Summary

This chapter presents a simulation study based on the complex interactions between the oil, original formation water, injected water, and rocks. The model setup is first verified with experimental data. Furthermore, based on the validated model, the impact of complex mechanisms and interactions on oil recovery and compositions of effluent fluids is discussed in detail. The key conclusions are summarized below:

1. This chapter proposes a coupled flow-geochemical model with multiple geochemical reaction mechanisms for simulating water injection with varying salinity in sandstone reservoirs.
2. Ion exchange and mineral dissolution/precipitation reactions are the main mechanisms affecting oil recovery. For low-salinity water flooding, mineral dissolution/precipitation reaction plays a major role in the recovery factor. For high-salinity water flooding, ion exchange is more important, while mineral dissolution/precipitation reaction does not significantly impact the recovery factor.

Chapter 4: Modelling of a Hydraulically Fractured Horizontal Well using Coupled Flow-Geochemical Model and Regression Modelling base on the Fracture Characteristics

4.1 Introduction

Hydraulic fracturing is an effective method for stimulating hydrocarbon production from unconventional tight/shale reservoirs (Hubbert, M.K. and Willis, 1957; Barati, R. and Liang, 2014; Liu et al., 2021). A considerable amount of fracturing fluid (also known as engineered water, smart water, or low-salinity water) with some chemical composition is injected during hydraulic fracturing; highly conductive complex fracture networks are formed, increasing reservoir contact per well (Cheng 2012; King 2012). Meanwhile, fracturing fluids with a chemical composition different from connate water would flow into the fracture network system, contributing to various complex geochemical interactions between the oil, original formation water, fracturing fluid, and rocks (Zhang and Leung, 2022). Following hydraulic fracturing operations, a large quantity of produced/flowback water flows back to the surface along with the gas.

In the 1990s, Jadhunandan and Morrow (1991) and Yildiz and Morrow (1996) reported the effect of brine composition on production performance and identified the benefits of optimizing injection brine formulations. Numerous laboratory experiments (Tang and Morrow, 1997; Morrow et al., 1998; Tang and Morrow, 1999; Sharma and Filico, 2000; Morrow and Buckley, 2011; Chaturvedi et al., 2021) demonstrated the effect of salinity of the injected water on recovery. Yousef et al. (2010) reported that the salinity of the injected fluids plays an important role in the process efficiency, a key factor in improving oil recovery. In addition, operators producing gas from

Haynesville, Marcellus, and Horn River shale formations have observed that the ion concentrations in flowback fluids are very different from the hydraulic fracturing fluid (Blauch et al., 2009; Gaudlip et al., 2008; Myers, 2008; Zolfaghari et al. 2014 and 2016). Blauch et al. (2009) conducted an analysis on the origin of salts found in Marcellus shale flowback fluids and proposed two explanations: (1) the dissolution of shale mineral components due to reaction with the fracturing fluid; (2) discharging of high-salinity formation water as a result of continuous compaction by the overlying rock layer during the hydrocarbon accumulation process. Bearinger (2013) noted that the composition of water recovered from induced hydraulic fractures differs from that of water recovered from reactivated secondary fractures. Ghanbari et al. (2013) analyzed the salinity of flow back fluids from hydraulically fractured horizontal wells completed in the Horn River Basin (HRB). They explained that the complexity of the fracture network can be inferred from certain characteristics of the salt-concentration/load-recovery profile. Zolfaghari et al. (2014 and 2016) also revealed a similar finding, supporting the use of geochemical or salinity flowback data for fracture characterization in hydraulically fractured wells.

Fracture characterization using production data has been a promising method for evaluating the fracturing efficiency and predicting long-term well productivity. A variety of pressure-transient analysis (PTA) and rate-transient analysis (RTA) have been developed (Fisher et al. 2005; Medeiros et al. 2008 and 2010; Bello 2009; Cheng et al. 2009; Song and Ehlig-Economides 2011; Samandarli et al. 2012; Ali et al. 2013). For instance, Fisher et al. (2005) characterized the induced-fracture network with fracture-mapping technologies and presented correlations between production response and various fracture parameters. Although RTA and PTA are widely used to characterize the fracture network, these methods consider several simplifications in the analytical solution formulations. For instance, Nwabia and Leung (2021a and 2021b) pointed out that using

traditional RTA to characterize the fracture networks can obtain some fracture parameters, including fracture half-length (X_f), length of the entire producing interval (L_w), number of transverse fractures (N), matrix permeability (k_m), formation thickness (h), matrix porosity (ϕ_m); however, complex heterogeneous fracture parameters cannot be readily obtained. Assisted history-matching utilizing optimization algorithms can adjust regional and local reservoir properties to align the model with observed production data, but these types of approaches can be tedious and time-consuming (Nwabia and Leung (2021a, 2021b) as they require repeated runs of the forward simulation models. In fact, extracting knowledge from production data and building reliable and fast models to characterize fracture properties have always been of great interest to fracturing design optimization. More importantly, many of these previous studies focus on history matching using rate data alone, the integration of geochemical data of produced fluids is limited, as they tend to focus on the qualitative observation of field data, and there is insufficient study, particularly numerical simulation analysis, to examine on the relationship between the characteristics of hydraulic fracturing and the ion concentration of flowback fluid.

With the wide application of big data and artificial intelligence (AI), data-driven modelling has achieved meaningful results for history matching or characterization of fracturing parameters. The genetic algorithm (GA) is a global optimization algorithm for all individuals, which is calculated by an iterative algorithm, and the parameter space is searched effectively by random technology. Based on the solution, the genetic algorithm can realize intelligent directional search and, based on the natural selection and genetic principles of all feasible solution spaces, gradually tend to the optimal solution and avoid the whole search of the whole solution space. It does not require the search space to be continuous, differentiable, and unimodal and is suitable for solving complex nonlinear spatial optimization problems (Amirjanov, 2015; Alvarez et al., 2009; Vesterstrom and

Thomsen, 2004; Rawlins, 2014). In this thesis, GA is adopted to history match the salinity and rate profiles of flowback fluid to estimate uncertain fracture parameters. To further speed up the process, Response Surface Modelling (RSM) (Box and Wilson, 1951) is used to create a proxy to flow simulations and establish the relationships between fracture parameters and salinity/rate responses.

In engineering, RSM has been employed to optimize manufacturing processes, design experiments, and model complex systems (Myers et al., 2016; Deng and Cai, 2010; Sen and Swaminathan, 2004; Singh et al., 2010; Baş and Boyacı, 2007). In chemistry, RSM has facilitated the optimization of reaction conditions, formulation development, and prediction of chemical properties (Bezerra et al., 2008; Hanrahan and Lu, 2006; Ahn et al., 2010; Amini et al., 2010). Additionally, RSM has found applications in economics, marketing, and social sciences, aiding in understanding consumer behaviour, market response, and policy analysis (Shang et al., 2004; Januardi et al., 2021; Guo et al., 2021; Anderson and Whitcomb, 2016; Venkatesh and Goyal, 2010). Here are some potential reasons for selecting RSM over other more sophisticated methods for this problem: (1) Simplicity and Interpretability (Vladislavleva et al., 2008; Dorie et al., 2016; Silva et al., 2007): RSM is relatively straightforward to implement and interpret, especially compared to more complex machine learning models. If the goal is to understand the relationship between variables and outcomes clearly, RSM offers an interpretable framework. This is particularly important in fields where explaining the model's behavior is as crucial as its predictive accuracy; (2) Experimental Design Integration (Khoo and Chen, 2001; Cheng et al., 2004; Boning and Mozumder, 1994): RSM is particularly useful in scenarios where experimental design plays a crucial role. It is adept at handling data from carefully designed experiments, optimizing the process by analyzing the effects of several variables simultaneously. This is less straightforward

in many machine learning models; (3) Low Data Requirement (Bezerra et al., 2008; Aslan, 2008): RSM can be more suitable for situations with limited data. Many advanced machine learning models require larger training datasets, while RSM can provide valuable insights even with smaller datasets, making it more cost-effective. Although more complicated machine learning models can better describe the complex relationships between inputs and outputs, for this particular problem, RSM is found to be sufficient since the numbers of input/output parameters and their associated ranges are small. The RSM modelling results are satisfactory for a specific set of parameter ranges.

To train the RSM models, a synthetic dataset is assembled from numerical simulations. The simulation responses (e.g., rate and salinity profiles) are treated as outputs, while various fracture parameters are considered as inputs. Sensitivity analyses of fracture parameters help identify the key factors influencing the system's response and guide the selection of input variables for the RSM. Nevertheless, it is worth mentioning that most previous modelling efforts coupling geochemical modules and complex fracture systems in hydraulically fractured reservoirs are rare. For example, Zhong and Leung (2020a and 2020b) investigated the effect of fracture distribution on hydraulic-fractured shale-gas production by upscaling the stochastic 3D discrete fracture network (DFN) model into an equivalent continuum dual-porosity dual-permeability (DPDK) model. Xu and Leung (2022) studied the impact of mesh alignment with DFN in a DPDK model. Liu et al. (2020 and 2021) presented a coupled two-phase flow/geomechanics model to investigate the feasibility and efficiency of inter-fracture water injection to enhance oil recovery. Wang and Leung (2015 and 2016) constructed a series of mechanistic simulation models consisting of both hydraulic fractures and stochastically-distributed secondary fractures to simulate imbibition, fluid re-distribution, and flow-back during shut-in and cleanup.

Therefore, the main research gap that this study aims to address is developing an efficient history-matching workflow to integrate geochemical (salinity) data and rate data from produced fluids collected during the flowback period. First, a numerical simulation model calibrated against experimental data is used to predict the salinity of produced fluids and the production behaviour of a hydraulically fractured well. A detailed sensitivity analysis of fracture parameters and other models is explored. The calibrated numerical simulation is used to create a training dataset to train a regression (response surface) model, which will be used as a proxy of numerical simulation. Next, the model is integrated into an optimization workflow to history match both rate and salinity data and infer uncertain primary and secondary fracture properties. Using response surface models and an automated optimization algorithm facilitates the inference of fracture parameters efficiently.

The mechanisms that govern the interactions between crude oil, formation water, engineered water and rock are complex. The most widely recognized mechanisms are multiple ion exchange and mineral dissolution/precipitation. Lager et al. (2006 and 2008) have proposed that the multiple ion exchange is the key mechanism for increasing oil recovery during low-salinity water flooding. There is a chemical balance between the ion concentration in the connate water (or initial formation water), the ion concentration adsorbed on the clay surface, and the polar compounds in the crude oil. Positively charged ions in the connate water, such as Ca^{2+} and Mg^{2+} , are adsorbed on negatively charged clay surfaces. The polar oil compounds, which are mainly negatively charged, are adsorbed to these multivalent positive charge sites on the clay surface, forming an oil film on the clay surface and an Electrical Double Layer (EDL) (Ligthelm et al., 2009). Therefore, macroscopically, the clay surface can be considered oil-wet. This balance is disturbed upon the injection of engineered fracturing fluids. For example, Ca^{2+} and other multivalent ions would be replaced by monovalent Na^+ (AlShalabi and Sepehrnoori, 2016), and the crude oil adsorbed on

the multivalent ions could also be desorbed. Therefore, this exchange of ions could cause the formation to change from oil-wet to mixed or water-wet (Amirian et al., 2017). Since the concentration of each ion in the injected engineered water is very different from that of the formation water, it will disturb the existing equilibrium and cause source minerals (e.g., CaCO_3 , MgCO_3 , $\text{CaMg}(\text{CO}_3)_2$ and CaSO_4 , etc.) to dissolve or precipitate, thereby establishing a new equilibrium. In this process, polar components adsorbed on the rock surface are released with the dissolved minerals, thereby increasing water-wetness (Hiorth et al., 2010; Evje and Hiorth, 2010 and 2011), and also it can lead to changes in pore structure (Yousef et al., 2010 and 2011).

In order to construct the numerical simulation model for hydraulically fractured reservoir, a model framework coupling flow-geochemical established describe in Chapter 3 will be used. This model is particularly relevant due to its comprehensive integration of geochemical mechanisms, including intra-aqueous reactions, mineral reactions, and ion exchange reactions, tested on conventional sandstone reservoirs. The appeal of this model lies in its ability to simulate and validate complex interactions between fluids and rocks, which are also pertinent to shale gas reservoirs. The model successfully simulated effluent ion concentration, pH, and saturation, aligning closely with experimental core flooding measurements. This alignment demonstrated the reliability of ion-exchange equivalent fraction, pore volume evolution, and mineral molarity. In addition, Mehana and Fahes (2016) built a synthetic numerical model based on the Haynesville shale vertical well. Their model incorporated the ion exchange and mineral dissolution mechanisms while omitting any aqueous reactions. They use the model to assess the impact of formation mineralogy and fracturing fluid composition on gas recovery. However, they did not present any analysis regarding the flowback fluid composition and the impacts of fracture characteristics.

This work aims to develop a systematic framework for correlating fracture properties with salinity of flowback fluid and gas rate during the flowback period. Firstly, a numerical simulation model validated against experimental data from Chapter 3 is used to predict the salinity of produced fluids and the production behaviour of a hydraulically fractured well, which is used to calibrate an existing hydraulically fractured shale well model (Mehana and Fahes, 2016). Next, the validated geochemical vertical well model is modified to simulate a single stage of hydraulic fracturing in a horizontal well - new horizontal well shale model. The calibrated new horizontal well shale model is used to create a training dataset to train a regression (response surface) model, correlating fracture properties with the salinity of flowback fluid and gas rate.

4.2 Methodology

4.2.1 Flow and Geochemistry Coupling

During water injection stimulation, when the driving agent with chemical composition different from the original formation water is injected into the formation, it will disrupt the initial geochemical balance and cause a series of geochemical reactions between the oil, original formation water, fracturing fluid, and rocks. In this process, the material balance equation is coupled with Darcy's law governing the flow and the geochemical model, which includes intra-aqueous reactions, mineral reactions, ion exchange reactions, and phase equilibrium reactions (Nghiem and Rozon, 1989; Nghiem et al., 2011; Collins et al., 1992;). In the previous section, we introduced that since mineral dissolution and precipitation will affect the void volume of porous media, a two-way coupling scheme is used to couple geochemical and flow calculations: the time-stepping in the flow module is performed first to obtain the pressure and temperature distribution.

The pressure and temperature solutions are then passed to the geochemistry module to compute the total moles of minerals, which are used to update the porosity and permeability. The solution from the geochemistry module, including the updated porosity and permeability values, is transferred back to the flow module. The process is repeated within a time step until the convergence criteria are satisfied. The solution method of this model follows the approach of Nghiem et al. (2004) to solve using the Newton-Raphson method for each discretized grid block.

4.2.2 Validation of a Single Well Model

The Mehana and Fahes's (2016) model of a Haynesville shale vertical well is used as a baseline for comparison. They presented a simulation model to assess the impact of formation mineralogy and fracturing fluid composition on gas recovery. However, they did not present any analysis regarding the flowback fluid composition and the impacts of fracture characteristics. A baseline model based on the setup in Mehana and Fahes (2016) is constructed. The parameters used in Mehana and Fahes (2016) are shown in Table 4-1, Table 4-2 and Table 4-3. To model the reservoir state after hydraulic fracturing, their model injected fracturing fluid at a rate of 400 bbl/day into the injection well for 1 day. The pressure near the well increases and fluid leaks off into the surrounding formation. Finally, the well is shut in for 30 days. In addition, their model incorporated the ion exchange and mineral dissolution mechanisms while omitting aqueous reactions. A logarithmically spaced, locally refined grid, dual permeability model (LS-LG-DK) was used in their study. . The baseline model results closely align with the limited results from Mehana and Fahes (2016), including mineral mole changes and gas recovery (as shown in Figure 4-1). At the

same time, the ion concentration of flowback fluid is also obtained (as shown by dotted line in Figure 4-2).

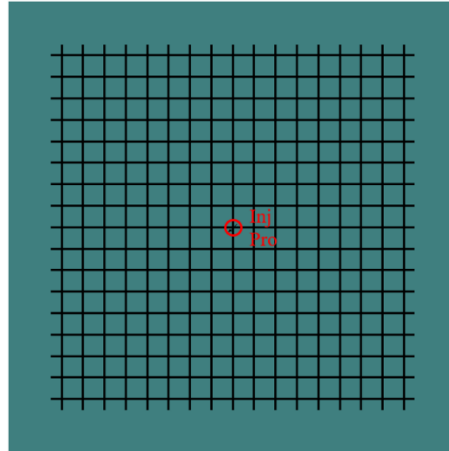
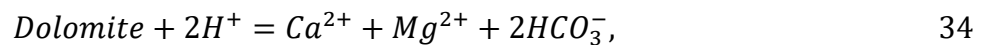
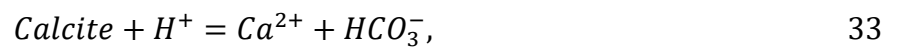


Figure 4-1. Logarithmically spaced, locally refined grid model structure (Inj: Injection well; Pro: Production well):
Green-shale, Black-Fracture Conduit.

Aqueous phase reactions:



Mineral dissolution and precipitation:



Ion exchange reactions:

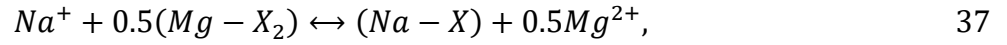
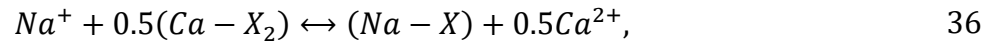


Table 4-1 Parameters of the shale gas model (Mehana and Fahes, 2016)

Property	Value
Model dimensions	420 × 420 × 100 ft
Reservoir pressure	5000 psi
Matrix porosity	0.07
Fracture porosity	0.01
Matrix permeability	0.00015 mD
Fracture conductivity	4.13 mD·ft
Natural fracture spacing	10 ft
Reservoir temperature	250 F
Shut-in time	1 month

Table 4-2 Chemical compositions of formation water and high-salinity water (Mehana and Fahes, 2016)

Ions	Formation water (mole/L)	High-salinity water (mole/L)
Ca ²⁺	4.8427E-1	1.6465E-2
SO ₄ ²⁻	3.6449E-3	2.4202E-2
Mg ²⁺	1.0060E+0	4.6356E-2
Na ⁺	2.7514E+0	4.5715E-1
HCO ₃ ⁻	5.8000E-3	1.9967E-4

Table 4-3 Geochemical modelling database (Computer Modelling Group 2021)

Mineral	Area (ft ² /ft ³)	Activation energy (J/mol)	Log <i>K_{eq}</i> (mol/ft ² ·s) at 77 F
Calcite	825.99	23500	-0.5398
Dolomite	873.24	52200	-0.6995
Anhydrite	903.24	14300	-0.2964

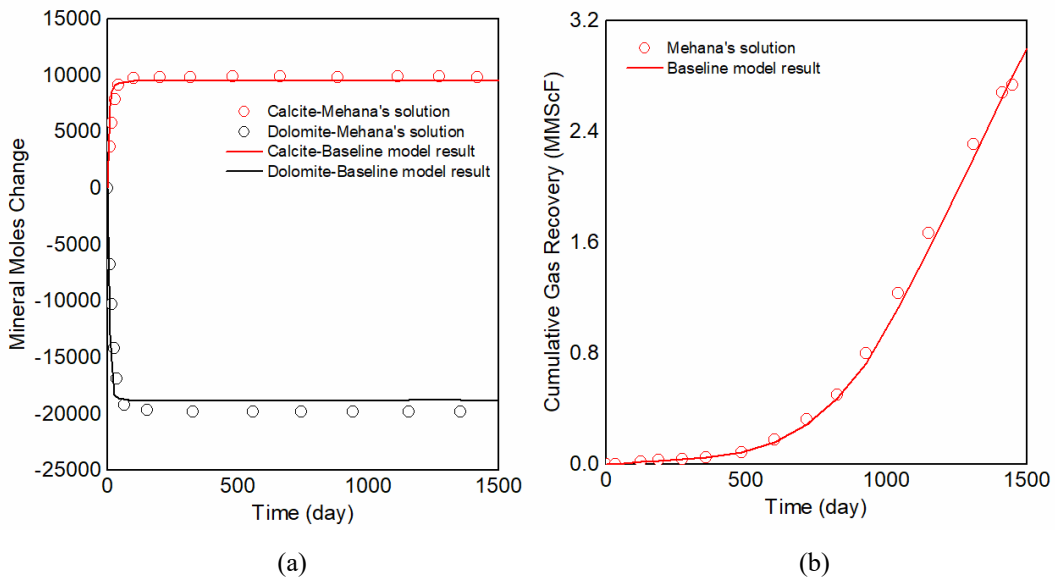
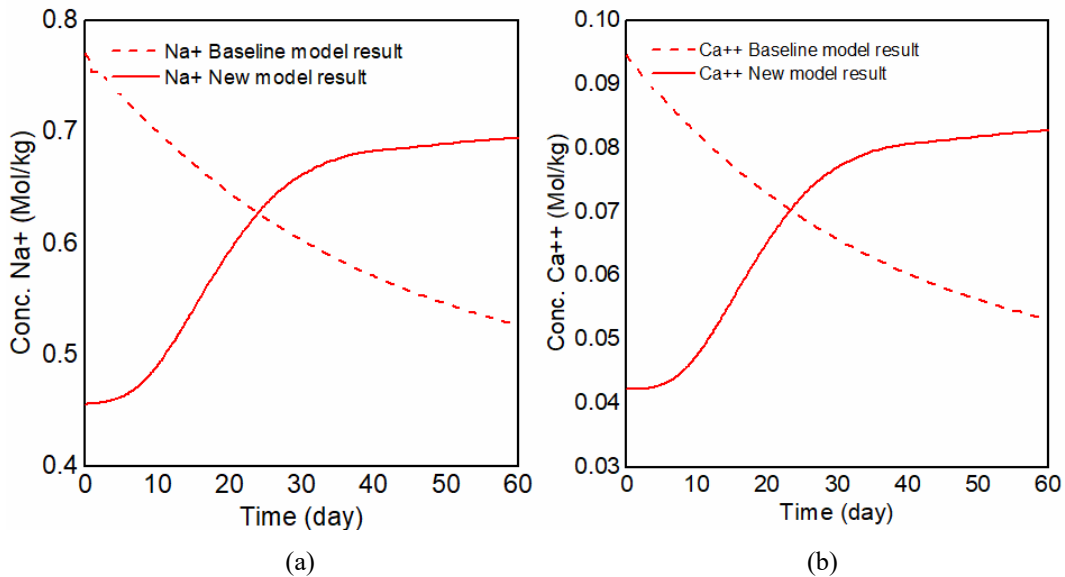


Figure 4-2. Historical matching of baseline model with results of Mehana and Fahes (2016): (a) Mineral moles change, (b) Cumulative gas recovery.

Next, aqueous reactions (Equations 30 to 32) omitted in the Mehana and Fahes's (2016) model are added, and the LS-LG-DK in the baseline model is replaced with a more accurate single porosity model with local grid refinement to create the "new model". The comparisons of ion concentration profiles of flowback fluid between the new and baseline models are shown in Figure 4-3, and a clear divergence is noted. The baseline model predictions tend to follow an opposite trend as those obtained with the new model; for example, the baseline model predicts a declining trend of SO_4^{--} ions, while the new model predicts an increasing trend. The discrepancies can be attributed to the primary factors that the aqueous phase reactions were not modelled in Mehana and Fahes's model.



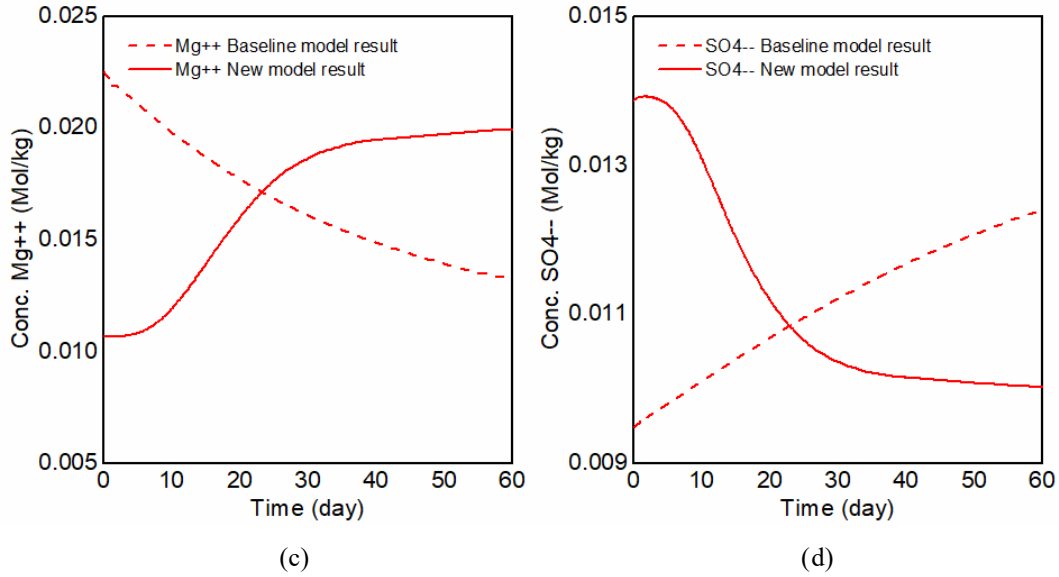
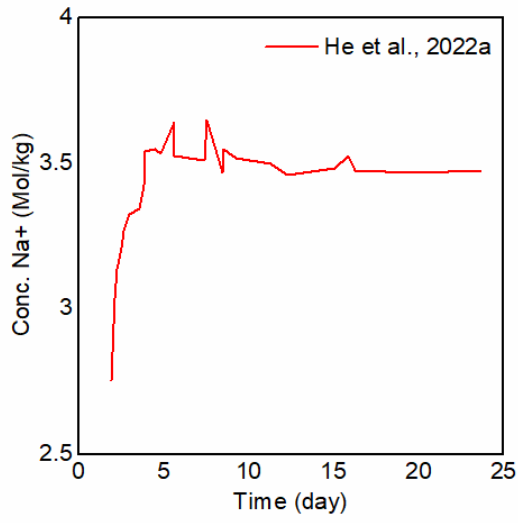
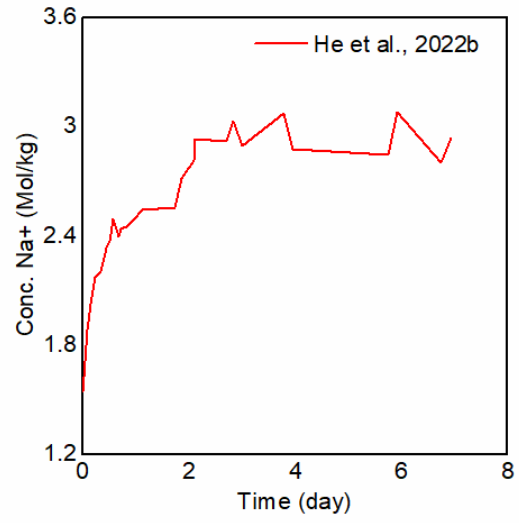


Figure 4-3. Ion concentration of flowback fluid comparison between new model result and baseline model result: (a) Na⁺ ion concentration, (b) Ca⁺⁺ ion concentration, (c) Mg⁺⁺ ion concentration, (d) SO₄⁻⁻ ion concentration.

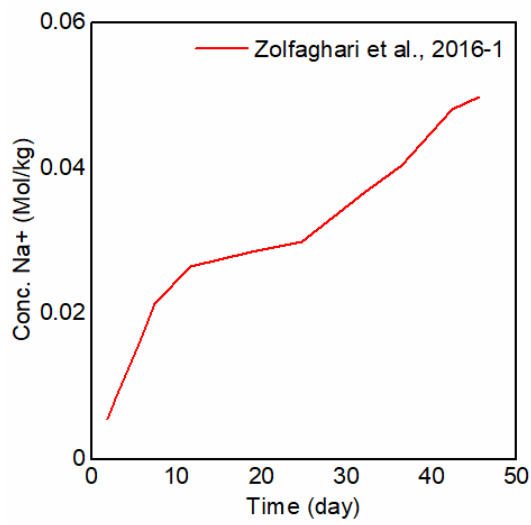
As documented in several field studies, the observed salinity trends in the updated model match real-world measurements. The research conducted by field observations (as shown in Figure 4-4) (He et al., 2022a and 2022b; Zolfaghari et al., 2014 and 2016; Blauch et al., 2009) serves as empirical validation, highlighting the potential impacts of all relevant geochemical mechanisms in simulation models. Such validation is crucial for the predictive models that reflect actual reservoir behaviour, demonstrating that geochemical interactions play an important role in hydraulic fracturing operations.



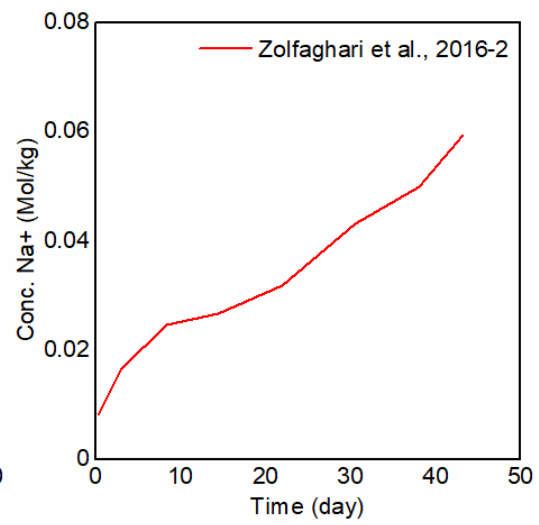
(a)



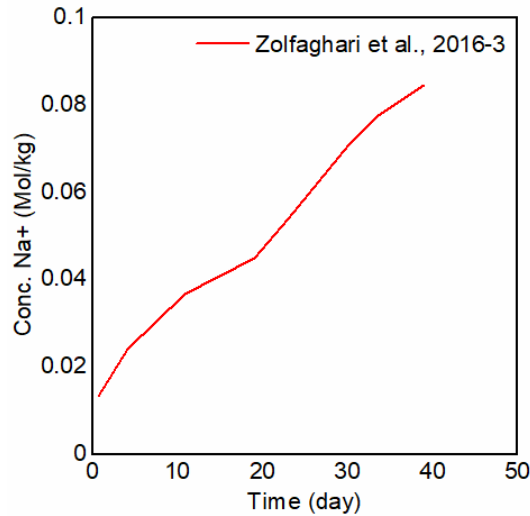
(b)



(c)



(d)



(e)

Figure 4-4. Salinity profiles from field observation.

4.2.3 Modelling of a Hydraulically Fractured Horizontal Well

The validated vertical well model is modified to simulate a single stage of hydraulic fracturing in a horizontal well. The "new horizontal well shale model" incorporates ion exchange reactions, mineral dissolution and precipitation reactions, as well as aqueous reactions. This model is constructed as a 2D numerical representation featuring three interactive components: matrix blocks, secondary fractures (SF), and hydraulic fractures (HF).

The model parameters are the same as the new model presented earlier (refer to Table 4-2 and Table 4-3, and Equations 30 to 37). The only difference is the fracture network configuration – a horizontal well with evenly spaced and symmetrical hydraulic fracture stages is assumed, and a single stage with two bi-wing hydraulic fractures (as shown in Figure 4-5) is simulated. The model includes a perforation at the intersection of the hydraulic fracture and the horizontal well, flanked

by evenly positioned secondary fractures. The basic parameters of the new horizontal well model are shown in

Table 4-4, and they are extracted from several references (Mehana and Fahes, 2018; Rubin, 2010; Wang and Leung, 2015; Zhong and Leung, 2020; Zhang and Leung, 2022).

The model uses two sets of published relative permeability curves (high salinity and low salinity) (as shown in Figure 4-6) to simulate the effect of wettability changes (Fakcharoenphol et al., 2014). To simulate the fluid injection during hydraulic fracturing, an injection rate of 3000 bbl/day for 3 hours is imposed, followed by a 3-hour shut-in, and this cycle is repeated three times. Subsequently, the well is shut in for 30 days. The model dynamically captures fluid movement, accounting for variable geochemical reactions and ensuring pressure and solute transport, and simulates realistic reservoir conditions after the hydraulic fracturing process. This study does not consider the fracture propagation process, as geomechanical simulation is not coupled. It simulates only the fluid movement during the injection, shut-in, and production phases. In other words, geomechanical effects and subsequent fracture opening, propagation, and closure are omitted. It aims to estimate fluid movement in pre-existing networks of primary and secondary fractures. Similar approaches were found in the literature where geomechanical simulation was not considered (Mehana and Fahes, 2018; Rubin, 2010; Wang and Leung, 2015; Zhong and Leung, 2020; Zhang and Leung, 2022).

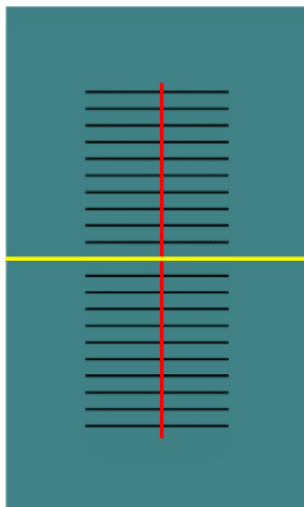


Figure 4-5. New horizontal well shale model: Green-shale, Black-Secondary Fracture Conduit, Red-Primary Fracture Conduit, Yellow-Horizontal Well Path.

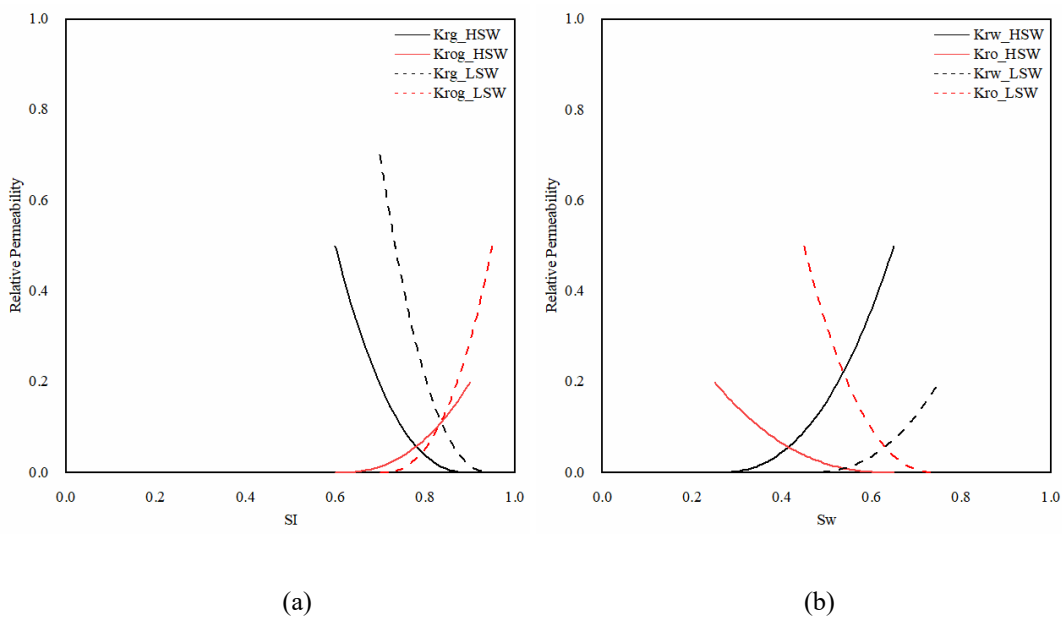


Figure 4-6. Relative permeability functions for low (LSW)) and high (HSW) salinity water systems: (a) gas-water and (b) water-oil

Table 4-4 Parameters of the shale gas model

Property	Value	Data Sources
Model dimensions	380 × 420 × 100 ft	Rubin, 2010
Reservoir pressure	5000 psi	Mehana and Fahes, 2018
Matrix porosity	0.07	Mehana and Fahes, 2018
Primary fracture porosity	1	Rubin, 2010
Secondary fracture porosity	0.6	Wang and Leung, 2015
Matrix permeability	0.00015 mD	Mehana and Fahes, 2018
Primary fracture permeability	10000 mD	Zhong and Leung, 2020
Primary fracture aperture	0.098425 ft	Zhong and Leung, 2020
Secondary fracture permeability	25 mD	Zhong and Leung, 2020
Secondary fracture aperture	0.00098425 ft	Zhong and Leung, 2020
Reservoir temperature	250 F	Mehana and Fahes, 2018
Shut-in time	35 days	Mehana and Fahes, 2018

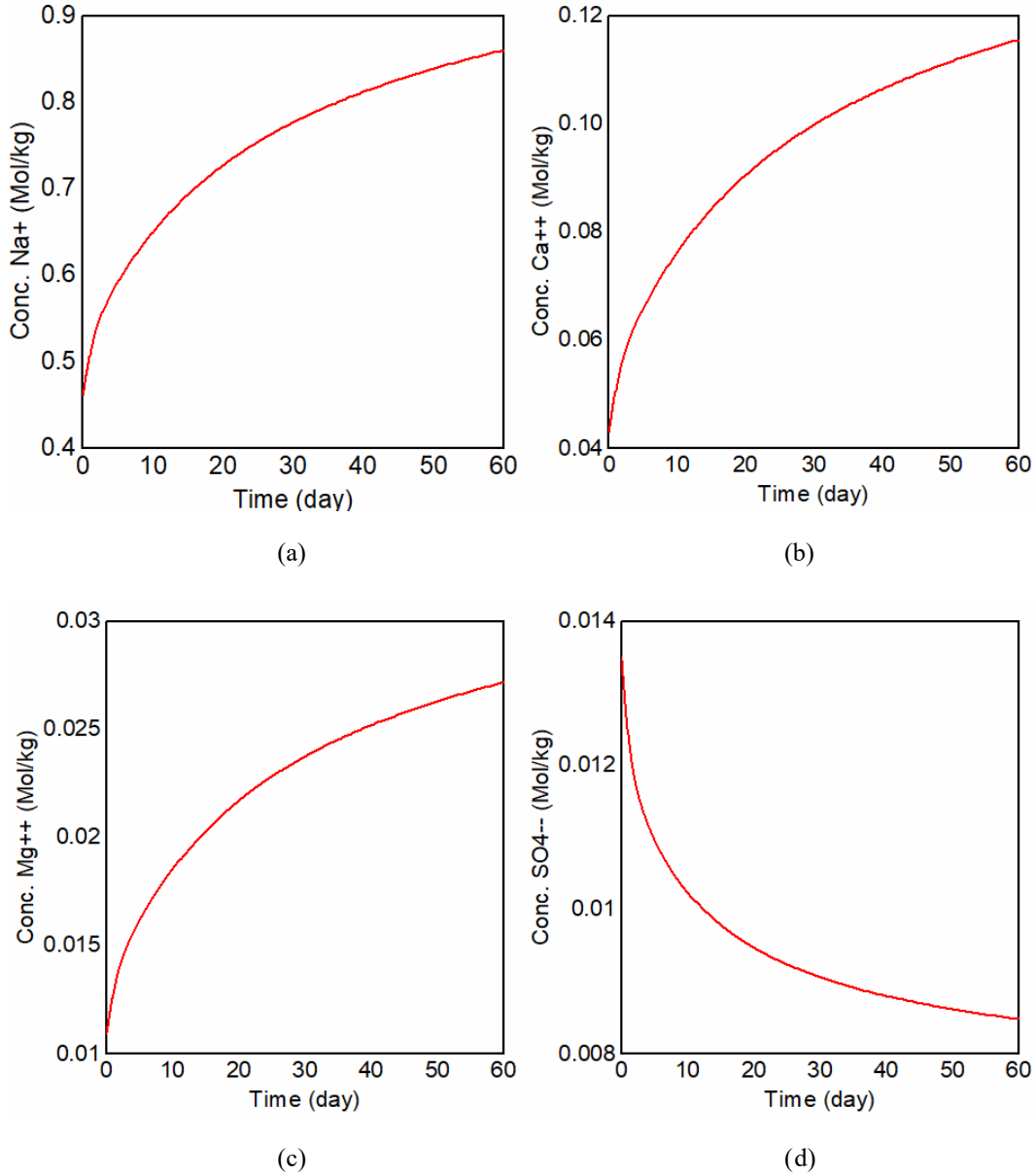


Figure 4-7. Ion concentration of flowback fluids between new horizontal well shale model and comparison model: (a) Na^+ ion, (b) Ca^{2+} ion, (c) Mg^{2+} ion and (d) SO_4^{2-} ion.

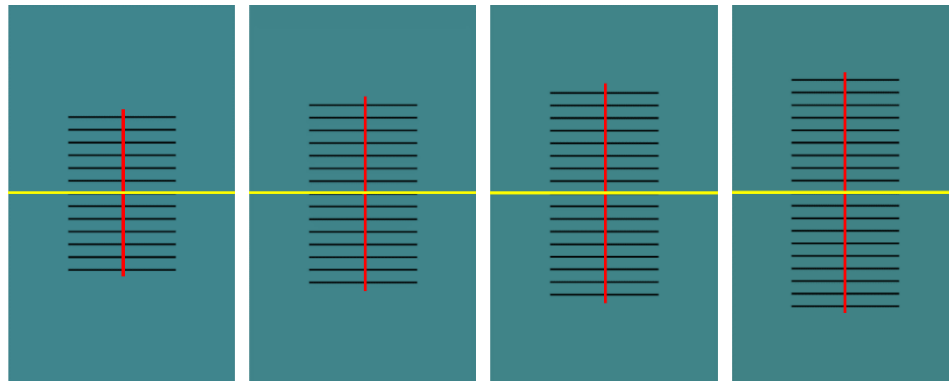
The ion concentration profiles of flowback fluids corresponding to the new horizontal well shale model are shown in Figure 4-7, where $t = 0$ is the time when the well re-opens after shut-in. They follow similar trends in Figure 4-3 in the previous section and correspond well with reported field observations (Figure 4-4) (He et al., 2022a and 2022b; Zolfaghari et al., 2014 and 2016; Blauch et

al., 2009). This further validates the accuracy of our developed model for subsequent analysis involving proxy/regression modelling.

4.3. Results

4.3.1 Sensitivity Analysis of Fracture Parameters

In this section, the simulation models will be used to examine the sensitivity of flowback fluid salinity to fracture network properties. Zolfaghari et al. (2014 and 2016) demonstrated using field data that the complexity of dendritic fracture systems can be related to the flowback fluid salinity (i.e., the concentration of Na⁺). For instance, for a less complex system, the salt recovery profile would increase gradually and then plateau at a certain level, while the salinity would continue rising when the fracture system is more complex. Yang and Wu (2017) pointed out that the fracture aperture may also affect the ion concentration of flowback water. More specifically, narrower fractures tend to produce flowback water with a higher concentration of ions. Given that multiple fracture system parameters would affect the salinity profile, the simulation model will be used to examine the impacts of individual parameters and capture the interplay between these parameters. The set of simulation models will be used to train two response surface models (one for flow rate and one for the salinity profiles in the subsequent sections). The selected primary fracture (PF) and secondary fracture (SF) parameters are (a) PF Length, (b) PF Permeability, (c) SF Coverage, (d) SF P22, (e) SF Aperture, and (f) SF Permeability. SF Coverage refers to the drainage area covered by the secondary fractures. The simulation domain is one hydraulic fracture stage, neglecting the interference between stages, as shown in Figure 4-8. The corresponding salinity and gas rate profiles are shown in Figure 4-9 and Figure 4-10, respectively.

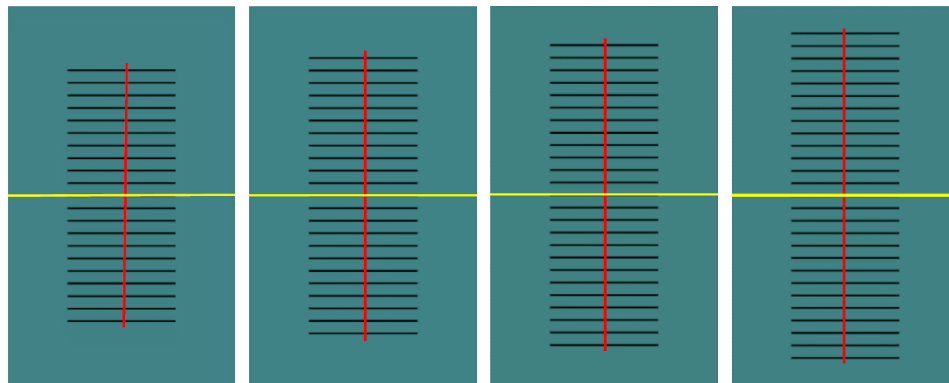


(a) case 1

(b) case 2

(c) case 3

(d) case 4



(e) case 5

(f) case 6

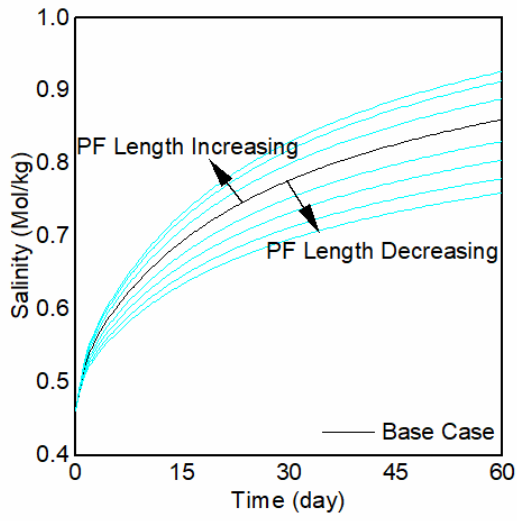
(g) case 7

(h) case 8

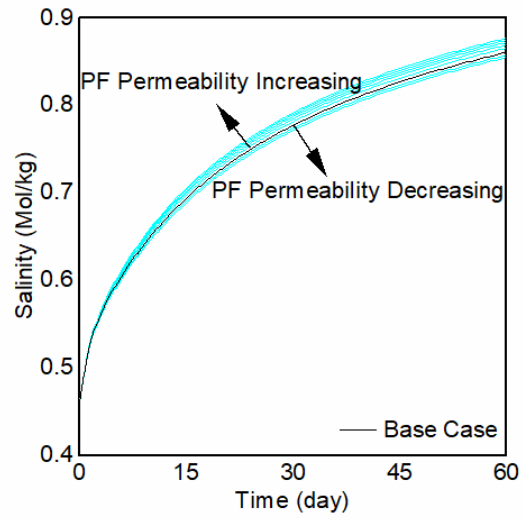
Figure 4-8. Case 1-8 Schematic of horizontal well shale model: Green-shale, Black-Secondary Fracture Conduit, Red-Primary Fracture Conduit, Yellow-Horizontal Well Path.

Table 4-5 Fracture characteristics for the training dataset

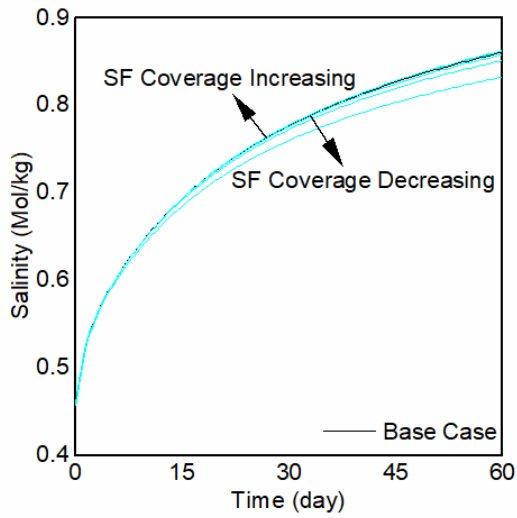
Case	PF Length (ft)	PF Permeability (mD)	SF Coverage (ft ²)	SF P32 ft ² /ft ³	SF Aperture (ft)	SF Permeability (mD)
1	260	10000	46800	0.1000	0.00098425	25
2	300	10000	54000	0.1000	0.00098425	25
3	340	10000	61200	0.1000	0.00098425	25
4	380	10000	68400	0.1000	0.00098425	25
5 (Base Case)	420	10000	75600	0.1000	0.00098425	25
6	460	10000	82800	0.1000	0.00098425	25
7	500	10000	90000	0.1000	0.00098425	25
8	540	10000	97200	0.1000	0.00098425	25
9	420	2500	75600	0.1000	0.00098425	25
10	420	5000	75600	0.1000	0.00098425	25
11	420	20000	75600	0.1000	0.00098425	25
12	420	30000	75600	0.1000	0.00098425	25
13	420	40000	75600	0.1000	0.00098425	25
14	420	50000	75600	0.1000	0.00098425	25
15	420	60000	75600	0.1000	0.00098425	25
16	420	10000	25200	0.1000	0.00098425	25
17	420	10000	42000	0.1000	0.00098425	25
18	420	10000	58800	0.1000	0.00098425	25
19	420	10000	92400	0.1000	0.00098425	25
20	420	10000	75600	0.0428	0.00098425	25
21	420	10000	75600	0.0620	0.00098425	25
22	420	10000	75600	0.0810	0.00098425	25
23	420	10000	75600	0.1190	0.00098425	25
24	420	10000	75600	0.1380	0.00098425	25
25	420	10000	75600	0.1572	0.00098425	25
26	420	10000	75600	0.1000	0.00019442	25
27	420	10000	75600	0.1000	0.00029163	25
28	420	10000	75600	0.1000	0.00043744	25
29	420	10000	75600	0.1000	0.00065617	25
30	420	10000	75600	0.1000	0.00147638	25
31	420	10000	75600	0.1000	0.00221456	25
32	420	10000	75600	0.1000	0.00332184	25
33	420	10000	75600	0.1000	0.00498277	25
34	420	10000	75600	0.1000	0.00098425	5
35	420	10000	75600	0.1000	0.00098425	10
36	420	10000	75600	0.1000	0.00098425	15
37	420	10000	75600	0.1000	0.00098425	20
38	420	10000	75600	0.1000	0.00098425	30
39	420	10000	75600	0.1000	0.00098425	35
40	420	10000	75600	0.1000	0.00098425	40
41	420	10000	75600	0.1000	0.00098425	45



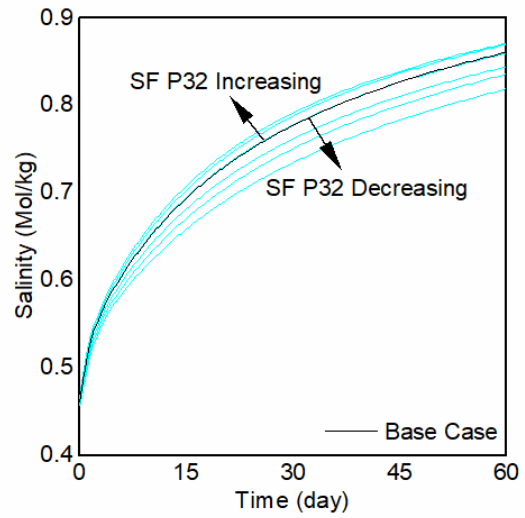
(a)



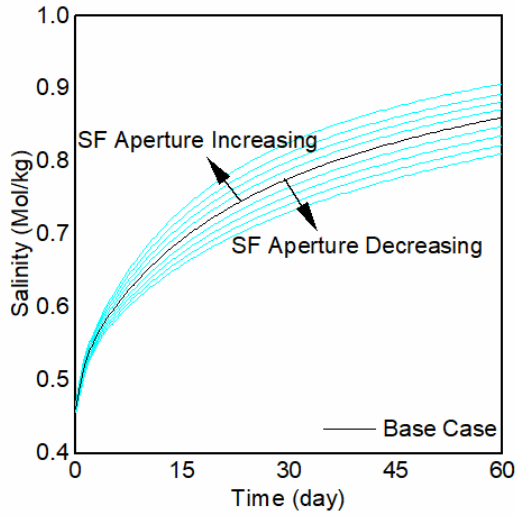
(b)



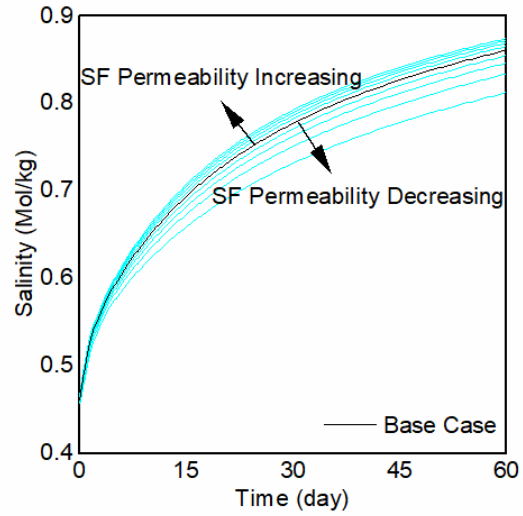
(c)



(d)

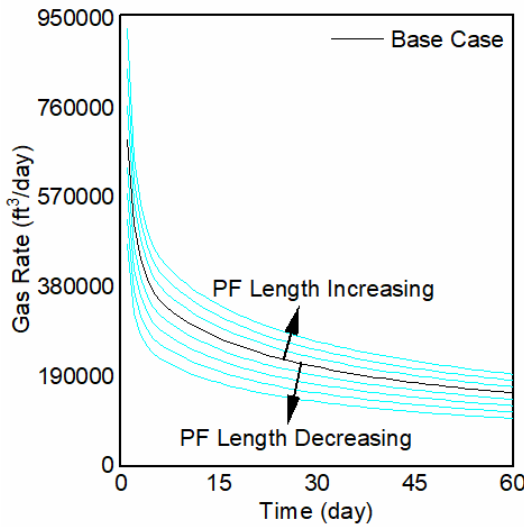


(e)

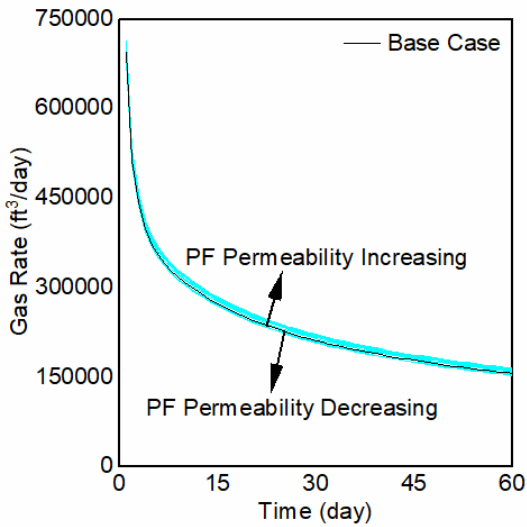


(f)

Figure 4-9. Flowback fluids salinity at different fracture characteristics: (a) PF Length, (b) PF Permeability, (c) SF Coverage, (d) SF P32, (e) SF Aperture, and (f) SF Permeability.



(a)



(b)

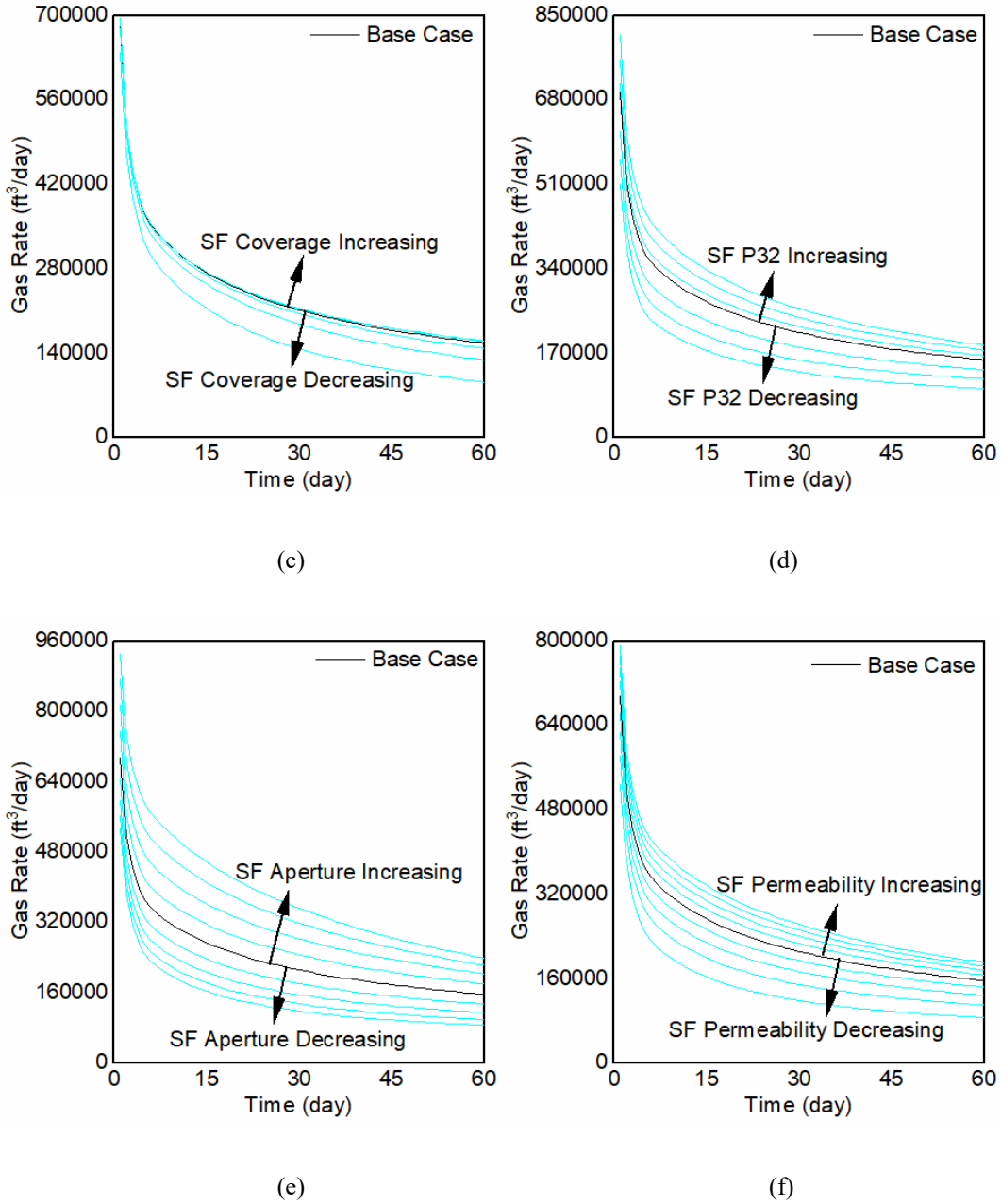


Figure 4-10. Gas rate at different fracture characteristics: (a) PF Length, (b) PF Permeability, (c) SF Coverage, (d) SF P32, (e) SF Aperture, and (f) SF Permeability.

The results illustrated in Figure 4-9 confirm the strong relationships between various fracture characteristics and the salinity levels in flowback fluid. When the conductivity of the fracture

network increases, the flowback fluid salinity and gas rate also increase. As expected, PF length has a significant impact, while PF permeability is less impactful, as seen in Figure 4-10. It is interesting to note that coverage of SF is less important than other properties of SF examined in these cases.

4.3.2 Response Surface Model (RSM) Construction

Given the lack of field data, the sensitivity analysis findings from section 4.3.1 are employed to construct a relationship between fracture characteristics and the salinity of flowback fluid and gas rate. The dataset size is small but enough for regression or response surface modelling (RSM). RSM is adept at capturing complex interactions through simplified empirical approximations of functional relationships. Through comparing multiple curve-fitting functions, including exponential, rational, logarithmic, power, and arps decline, two empirical relationships are selected to describe salinity and rate as a function of time. For the salinity of flowback fluid versus time (Figure 4-9), a logarithmic function (Equation 38) is selected. For the gas production rate, the Arps decline equation (Equation 39) was selected (Arps, 1945). An example of the curve-fitting process is shown in Figure 4-11. Response variables d , e , f , q_i , D_i and b , can be approximated by a low-degree polynomial described by Equations 38 and 39, as shown in Table 4-6 and Table 4-7.

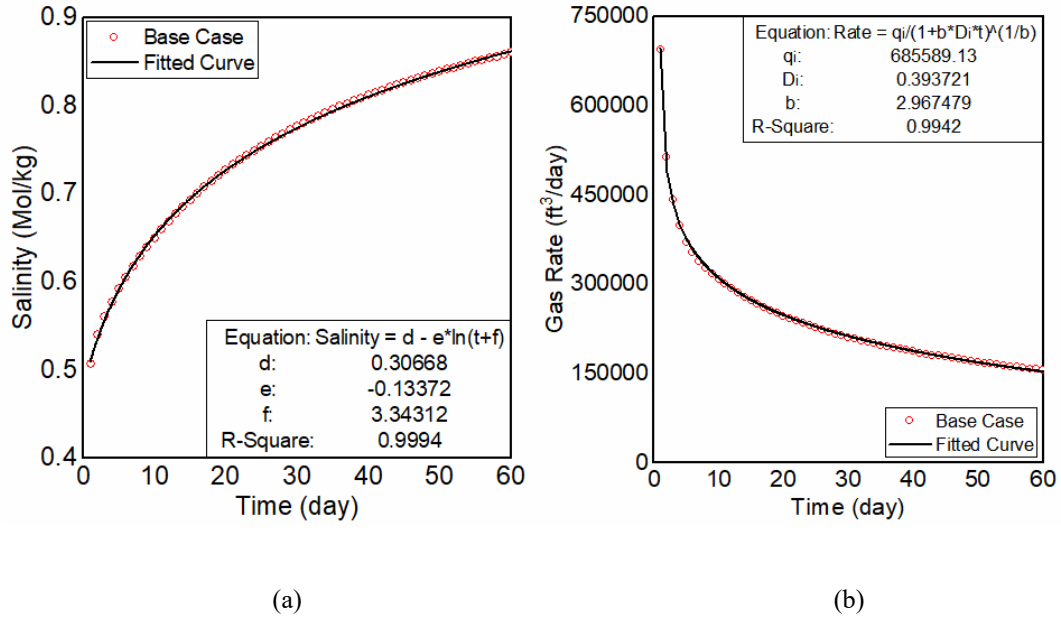


Figure 4-11. Salinity profile and gas rate curve fitting for base case: (a) Salinity curve fitting. (b) Gas rate curve fitting.

$$\widehat{\text{Salinity}}(t) = d - e \ln(t + f), \quad 38$$

$$\widehat{\text{Rate}}(t) = \frac{q_i}{(1 + b D_i t)^{1/b}}, \quad 39$$

Table 4-6 Response variables and R² of salinity profiles for the training dataset

Case	<i>d</i>	<i>e</i>	<i>f</i>	R ²
1	0.340010	-0.101050	3.670630	0.9994
2	0.333440	-0.107550	3.554820	0.9994
3	0.323940	-0.115970	3.501860	0.9994
4	0.314880	-0.124400	3.454130	0.9993
5	0.306680	-0.133720	3.343120	0.9994
6	0.294040	-0.143660	3.358340	0.9994
7	0.282090	-0.152380	3.397240	0.9994
8	0.273970	-0.157670	3.452290	0.9994
9	0.299880	-0.133800	3.548830	0.9994
10	0.304470	-0.133370	3.420500	0.9994
11	0.307580	-0.134720	3.283540	0.9994
12	0.307850	-0.135570	3.247180	0.9994
13	0.308000	-0.136300	3.219050	0.9994
14	0.308130	-0.136920	3.195200	0.9994
15	0.308260	-0.137470	3.173960	0.9994
16	0.358320	-0.114990	2.393270	0.9994
17	0.328810	-0.126460	2.923880	0.9994
18	0.313920	-0.131450	3.205370	0.9994
19	0.302590	-0.134910	3.421900	0.9994
20	0.288490	-0.126670	4.002310	0.9985
21	0.288170	-0.131230	3.849490	0.9988
22	0.308340	-0.129010	3.370580	0.9992
23	0.313840	-0.131910	3.232210	0.9994
24	0.315640	-0.134200	3.150190	0.9994
25	0.330610	-0.131170	2.910110	0.9994
26	0.318100	-0.117850	3.406940	0.9985
27	0.315530	-0.121600	3.358500	0.9988
28	0.311190	-0.125930	3.369140	0.9990
29	0.306950	-0.130320	3.388340	0.9992
30	0.310850	-0.135850	3.230700	0.9994
31	0.317480	-0.137210	3.072740	0.9994
32	0.324090	-0.138640	2.898430	0.9992
33	0.325750	-0.142150	2.759310	0.9989
34	0.314020	-0.119120	3.485900	0.9985
35	0.308430	-0.126030	3.432820	0.9989
36	0.305490	-0.130020	3.422940	0.9992
37	0.305130	-0.132400	3.392100	0.9993
38	0.309130	-0.134420	3.288890	0.9994
39	0.311880	-0.134790	3.235350	0.9994
40	0.314680	-0.134940	3.183740	0.9994
41	0.317430	-0.134950	3.134730	0.9994

Table 4-7 Response variables and R^2 of rate profiles for the training dataset

Case	q_i	D_i	b	R^2
1	464335.94	0.516424	3.128300	0.9991
2	516513.39	0.456826	3.065858	0.9993
3	570148.66	0.420410	3.019564	0.9991
4	626339.46	0.400008	2.986396	0.9997
5	685589.13	0.393721	2.967479	0.9992
6	755350.42	0.414838	2.976416	0.9993
7	834606.90	0.457872	3.003959	0.9992
8	922261.50	0.520971	3.043522	0.9999
9	671927.00	0.376064	2.923196	0.9992
10	680347.76	0.390400	2.948141	0.9991
11	691261.63	0.392736	2.986564	0.9993
12	695209.09	0.390474	2.997172	0.9994
13	699966.21	0.392061	3.007582	0.9994
14	701120.57	0.385851	3.008701	0.9995
15	703910.26	0.384669	3.012821	0.9996
16	619972.59	0.300431	1.977194	0.9995
17	665860.57	0.332961	2.490073	0.9990
18	682070.79	0.373097	2.814847	0.9998
19	687346.71	0.405062	3.027487	0.9998
20	507469.41	0.460998	2.642114	0.9993
21	556193.24	0.444747	2.824865	0.9998
22	611095.48	0.420508	2.929948	0.9993
23	701270.80	0.362239	2.978715	0.9990
24	743124.37	0.317604	2.896118	0.9994
25	787772.67	0.287803	2.809334	0.9898
26	530719.20	0.495633	2.351117	0.9998
27	558723.84	0.477952	2.489391	0.9995
28	593746.02	0.459548	2.653887	0.9998
29	641718.81	0.449829	2.836450	0.9994
30	737324.60	0.330389	3.027248	0.9996
31	786058.93	0.250771	2.951279	0.9991
32	826837.65	0.174060	2.716036	0.9994
33	861638.20	0.119215	2.371960	0.9999
34	526343.64	0.480149	2.345344	0.9998
35	578373.40	0.447803	2.591838	0.9991
36	620078.65	0.428995	2.767728	0.9990
37	655465.40	0.412110	2.888660	0.9997
38	711843.59	0.375051	3.016096	0.9996
39	734882.24	0.356410	3.042404	0.9991
40	755111.73	0.337952	3.051893	0.9996
41	773339.01	0.320818	3.049871	0.9992

The coefficients (d, e, f, q_i, D_i, b) are individually treated as a distinct response variable, and two sets of RSM models are constructed as shown below. In each model, the same independent variables (x_1, x_2, \dots, x_6) are used. This process was executed using Matlab® R2022a (MathWorks, 2022a).

$$\begin{aligned} coefficient_{salinity}(d, e, f) = \beta_0 + \beta_1 x_1 + \beta_2 x_1^2 + \beta_3 x_2 + \beta_4 x_2^2 + \beta_5 x_3 + \beta_6 x_3^2 + \beta_7 x_4 + \\ \beta_8 x_4^2 + \beta_9 x_5 + \beta_{10} x_5^2 + \beta_{11} x_6 + \beta_{12} x_6^2, \end{aligned} \quad 40$$

$$\begin{aligned} coefficient_{Rate}(q_i, D_i, b) = \beta_0 + \beta_1 x_1 + \beta_2 x_1^2 + \beta_3 x_2 + \beta_4 x_2^2 + \beta_5 x_3 + \beta_6 x_3^2 + \beta_7 x_4 + \\ \beta_8 x_4^2 + \beta_9 x_5 + \beta_{10} x_5^2 + \beta_{11} x_6 + \beta_{12} x_6^2, \end{aligned} \quad 41$$

x_1, x_2, \dots, x_6 refer to the six independent variables examined in the previous section: PF length, PF permeability, PF aperture, SF coverage, SF P32, SF aperture, and SF permeability, respectively.

$\beta_0, \beta_1, \dots, \beta_{12}$ are the adjustable RSM coefficients; their final values are detailed in Table 4-8 and Table 4-9.

Table 4-8 Coefficients Beta for RSM-Salinity

Beta	d	e	f
β_0	3.238323E-01	-1.563993E-02	7.161781E+00
β_1	4.386262E-04	-4.480361E-06	-1.713403E-02
β_2	-7.564449E-07	-2.289949E-07	1.855159E-05
β_3	2.876893E-07	-1.096603E-07	-1.233272E-05
β_4	-4.400383E-12	3.142018E-14	1.358058E-10
β_5	-2.228068E-06	-7.688263E-07	4.282431E-05
β_6	1.262078E-11	4.443315E-12	-2.431814E-10
β_7	3.695601E-01	-2.339818E-01	-1.765518E+01
β_8	-9.591130E-02	9.604481E-01	4.313155E+01
β_9	-2.830638E+00	-1.306492E+01	-1.488103E+02
β_{10}	1.413668E+03	1.895517E+03	-1.587512E+03
β_{11}	-7.716417E-04	-9.411953E-04	-2.899635E-03
β_{12}	1.871083E-05	1.204991E-05	-1.173613E-04
R2	0.9946	0.9909	0.9910

Table 4-9 Coefficients Beta for RSM-Rate

Beta	q_i	D_i	b
β_0	-2.566732E+05	1.810090E+00	2.721618E+00
β_1	-1.049860E+03	-5.982627E-03	-1.509276E-02
β_2	3.247988E+00	7.206343E-06	1.653701E-05
β_3	1.173979E+00	6.519562E-07	4.398591E-06
β_4	-8.852903E-06	-1.195750E-11	-3.371741E-11
β_5	2.559904E+00	3.314941E-06	4.042474E-05
β_6	-1.588229E-05	-1.471128E-11	-2.231825E-10
β_7	4.634453E+06	-4.959761E-01	1.207355E+01
β_8	-1.093529E+07	-5.322857E+00	-5.386805E+01
β_9	1.709453E+08	-1.548566E+02	5.335782E+02
β_{10}	-2.150519E+10	1.449914E+04	-1.174084E+05
β_{11}	8.880960E+03	-4.822421E-03	4.105786E-02
β_{12}	-5.734041E+01	1.984139E-05	-4.961534E-04
R2	0.9969	0.9966	0.9996

4.3.3 RSM Model Validation and Interpretation

The RSM-Rate and RSM-Salinity models developed in the previous section are validated here using a set of testing datasets. Four specific cases are outlined in Table 4-10, and the ranges of x_1, x_2, \dots, x_6 are the same as the training dataset. The RSM predictions are shown in Table 4-11, and they are then substituted into Equations 38 and 39 to generate a salinity and rate profile for each case. The comparisons of these profiles are shown in Figure 4-12 and Figure 4-13. The mismatch between these predicted profiles and the actual profiles of the testing dataset is represented by R2 values in the figures. The high R2 values (> 0.95) demonstrate that the RSM models can accurately

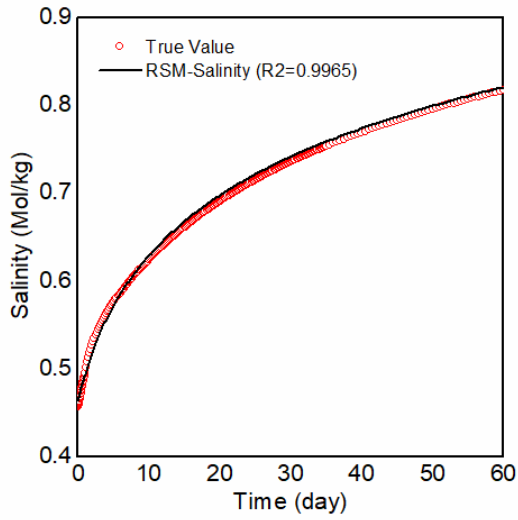
capture the underlying relationships between fracture parameters and the salinity of flowback fluid, as well as gas rate, for the ranges of fracture characteristics modelled here. A key limitation is that the model may not yield reasonable results if the ranges of x_1, x_2, \dots, x_6 are different than those used in the training dataset.

Table 4-10 Fracture characteristics for testing dataset.

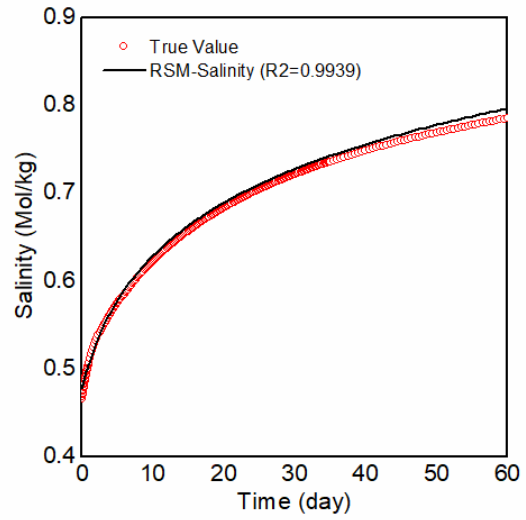
Case	PF Length (ft)	PF Permeability (mD)	SF Coverage (ft ²)	SF P32 ft ² /ft ³	SF Aperture (ft)	SF Permeability (mD)
1	420	16000	75600	0.0452	0.00042563	18
2	300	18000	54000	0.0767	0.00125862	16
3	380	8000	68400	0.0395	0.00113284	34
4	340	20000	61200	0.0529	0.00084517	28

Table 4-11 RSM model predictions for the testing dataset.

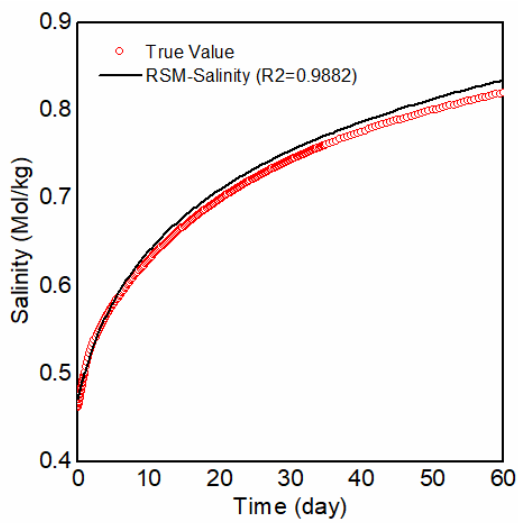
Case	d	e	f	q_i	D_i	b
1	0.289518	-0.119260	4.059341	391882.32	0.565532	2.361870
2	0.326481	-0.105829	3.749960	430508.99	0.494471	2.907142
3	0.298396	-0.121267	3.996217	490727.63	0.413910	2.797281
4	0.311389	-0.112510	3.885105	426349.75	0.483952	2.830000



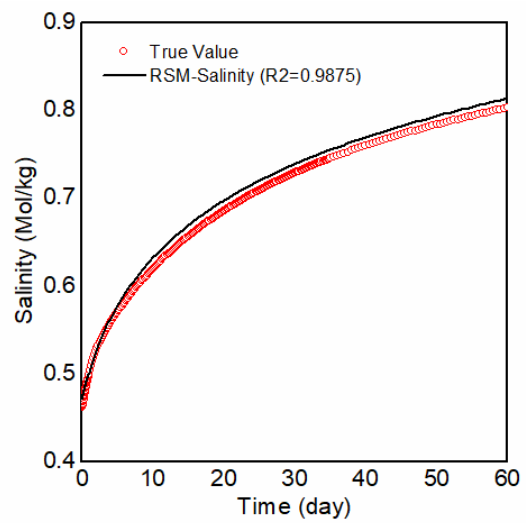
(a)



(b)

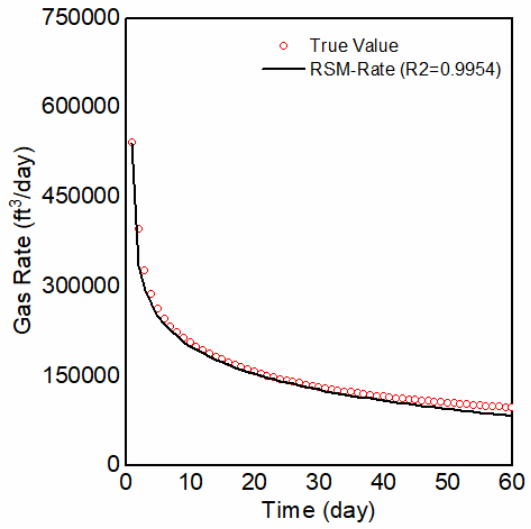


(c)

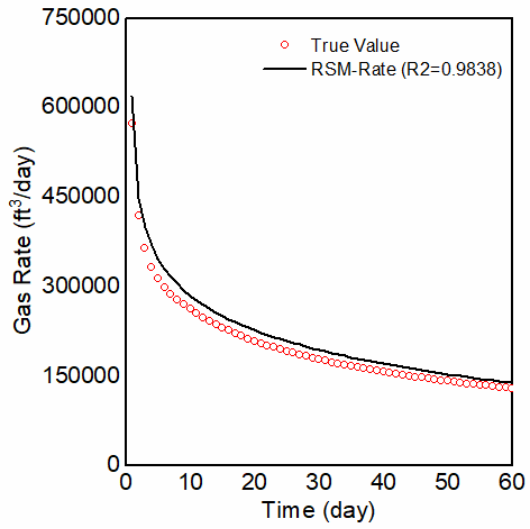


(d)

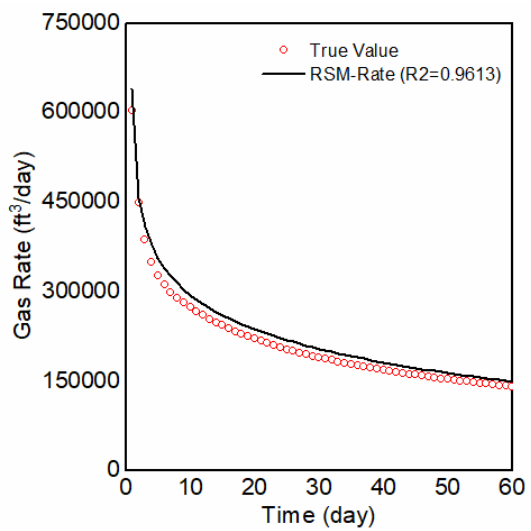
Figure 4-12. Comparison between the predicted and true profiles using the RSM-Salinity model.



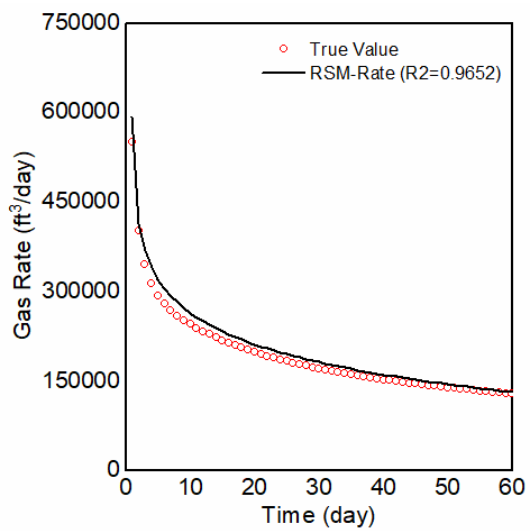
(a)



(b)



(c)



(d)

Figure 4-13. Comparison between the predicted and true profiles using the RSM-Rate model.

4.4 Summary

1. The chapter introduces a hydraulically fractured reservoir model that incorporates multiple geochemical reaction mechanisms. This enables a more nuanced and accurate representation of complex geochemical behaviours within fractures, filling a significant gap in the existing literature.
2. This chapter is based on the RSM and uses the sensitivity analysis results of the hydraulically fractured horizontal well model to establish the RSM-Salinity and RSM-Rate prediction models. The models reveal the complex temporal relationships between the salinity of flowback fluid and production time. Validation exercises demonstrate its robust predictive capabilities, with R2 values consistently above 0.95, confirming the model's reliability and applicability.

Chapter 5: Fracture Characterization Using RSM-GA Workflow

5.1 Introduction

The developed RSM models in Chapter 4 are used as a proxy for detailed flow simulations and integrated into a Genetic Algorithm (GA) optimization workflow for history matching of production and salinity profiles and for the inference of uncertain fracture parameters; in other words, the GA algorithm is used to adjust or perturb the fracture parameters, while the RSM proxies are used for the forward model calculations. The methodology is implemented in the Genetic Algorithm Optimization Toolbox of Matlab® R2022a (MathWorks, 2022a). The choice of GA for this research was driven by specific considerations of the problem rather than the general advantages of GAs. Other global optimization techniques, such as particle swarm optimization (PSO) or simulated annealing (SA), could potentially serve similar purposes, but GA was selected for its unique suitability (Sivanandam et al., 2008; Srinivas and Patnaik, 1994). GAs are particularly effective in searching complex, multimodal landscapes where other algorithms might get trapped in local optima. This is because GAs work with a population of solutions, enabling them to explore multiple regions of the search space simultaneously. Flexibility and Adaptability (Horn and Goldberg, 1995; De Jong, 1993; Kinnear, 1994): GAs are highly adaptable to different types of optimization problems without needing major modifications to their basic structure. They can handle a variety of objective functions and constraints, including non-differentiable, discontinuous, and highly non-linear functions. Parallelism (Bertoni and Dorigo, 1993; Alba and Troya, 2002; Gorges-Schleuter, 1990): The population-based approach of GAs is inherently parallel, making them suitable for parallel computing architectures. This can lead to significant reductions in computational time, especially for large and complex problems. Global Search

Capability (Smith et al., 1992; El-Mihoub et al., 2006): GAs are designed to perform a global search, which makes them suitable for problems where the global optimum is required, and the search space is large or poorly understood. Reduced Requirement for Derivative Information ((Bezerra et al., 2008; Aslan, 2008)): Unlike gradient-based methods, GAs do not require derivative information, which makes them applicable to problems where such information is difficult or impossible to calculate. Therefore, the problem of using salinity of flowback fluid to characterize fracture characteristics can be solved by establishing an intelligent optimization system based on genetic algorithm. The objective functions are the mean squared error (MSE) between the observed and predicted flowback fluid salinity or gas rate.

5.2 Case #1 – Uniform and Non-Uniform Secondary Fracture Parameters

The RSM models are trained using simulations with uniform SF parameters. Therefore, this section explores the feasibility of using these RSM proxies for predicting the salinity and rate profiles for non-uniform secondary fracture scenarios if "average SF parameters" are considered in the RSM proxies.

In this section, a true case with non-uniform SF parameters is constructed (as shown in Figure 5-1). The simulation profiles are used as histories or true values (as shown in Figure 5-2), and the RSM-GA workflow is used to estimate a single set of fracture parameters. In order to avoid the GA being stuck at a local minimum, the GA is run multiple times with different initial guesses. If it converges to approximately the same solution across multiple runs, this suggests that the result is a global optimum rather than a local minimum. The RSM-GA results are shown in Table 5-1. In one case, these GA estimates are considered to represent a uniform SF model case (case 1 and case 2); in

another case, these GA estimates correspond to averages of a non-uniform SF model case with certain standard deviations (SF permeability, aperture, and length). Therefore, for non-uniform secondary fracture scenarios, three SF parameters: permeability, aperture, and length are assumed to follow Gaussian distributions (Zhong and Leung, 2020a and 2020b; Sun and Schechter, 2015), and the standard deviation for each parameter is calculated as 10% of the average value predicted by GA; secondary fractures are randomly distributed on both sides of the horizontal well. Three realizations from RSM-Salinity and RSM-Rate are sampled and shown in Figure 5-3 (cases 1a, 1b, and 1c) and Figure 5-4 (cases 2a, 2b, and 2c). To assess the accuracy of predicted fracture properties, the Percentage Error (PE) for each variable was calculated by comparing the predicted values to the true values, with the detailed results provided in the Appendix A. This method was consistently applied across all examined cases.

$$\text{Percentage Error (PE)} = \left| \frac{\text{True Value} - \text{Predicted Value}}{\text{True Value}} \right| \times 100\%, \quad 42$$

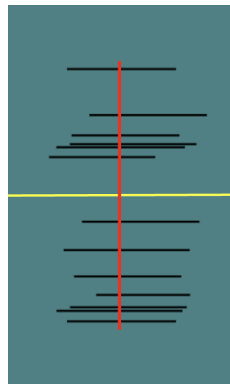


Figure 5-1. True case for non-uniform secondary fracture model.

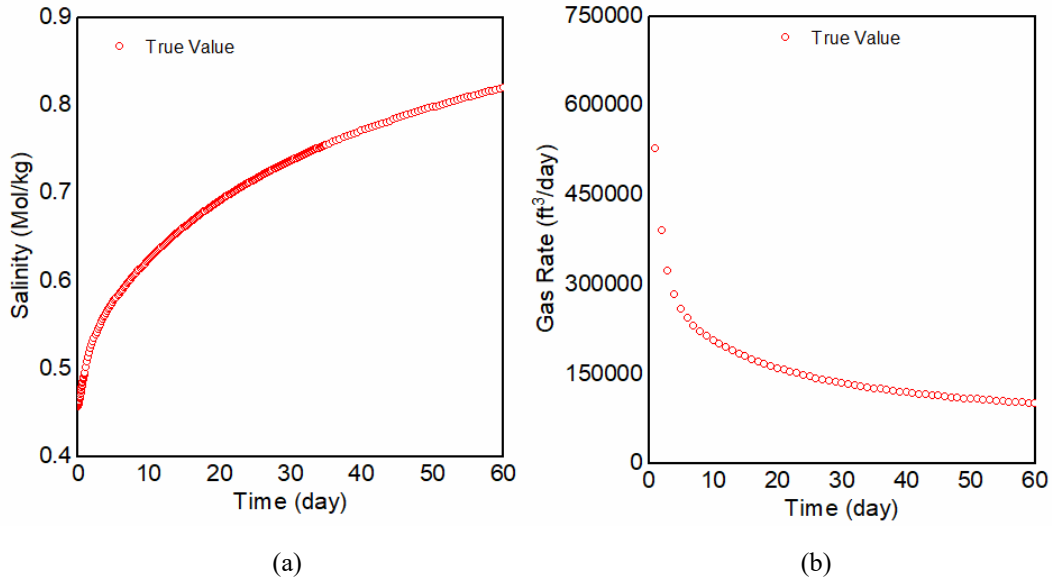


Figure 5-2. Salinity and rate histories for non-uniform secondary fracture model: (a) Salinity curve fitting, (b) Gas rate curve fitting.

Table 5-1 Fracture parameters estimated using RSM-GA workflow for the non-uniform SF case.

Parameter	PF Length (ft)	PF Permeability (mD)	SF Coverage (ft ²)	SF P32 (ft ² /ft ³)	SF Aperture (Average) (ft)	SF Permeability (Average) (mD)
RSM-Salinity	417	7233	74495	0.0639	0.00042947	33
RSM-Rate	425	6797	73886	0.0641	0.00044885	39

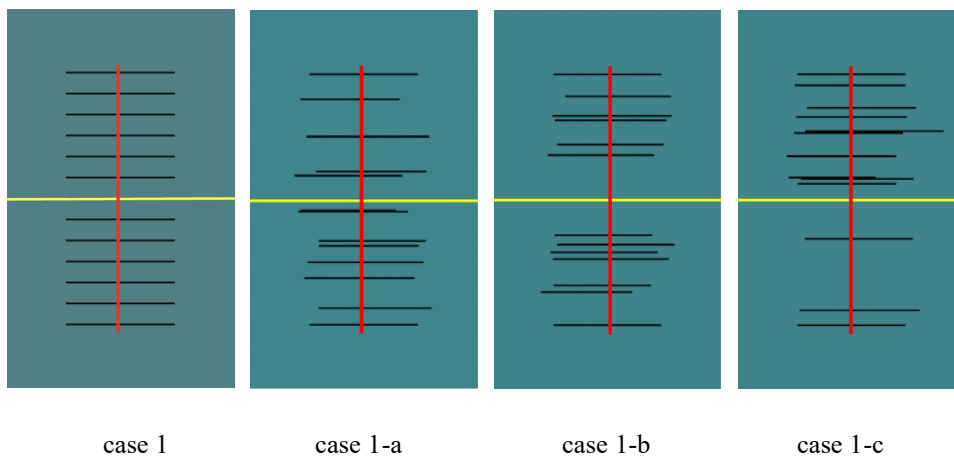


Figure 5-3. Uniform and non-uniform secondary fracture model constructed by RSM-Salinity: Green-shale, Black-Secondary Fracture Conduit, Red-Primary Fracture Conduit, Yellow-Horizontal Well Path.

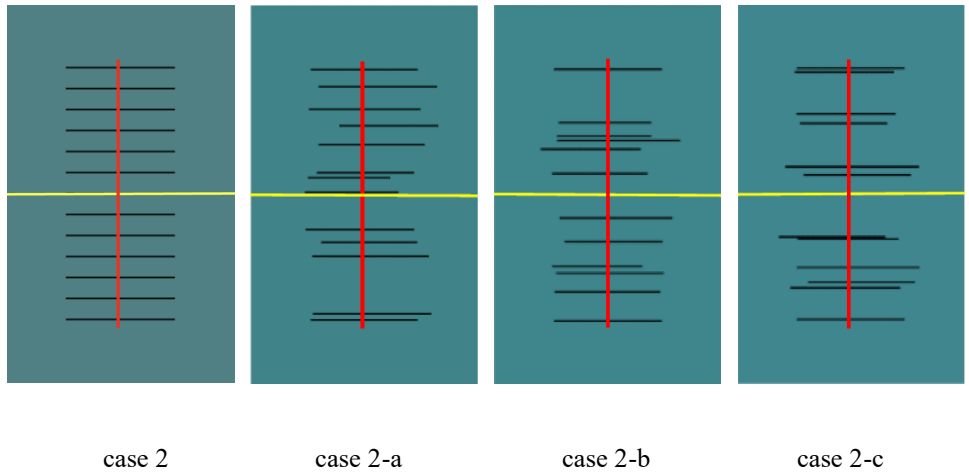
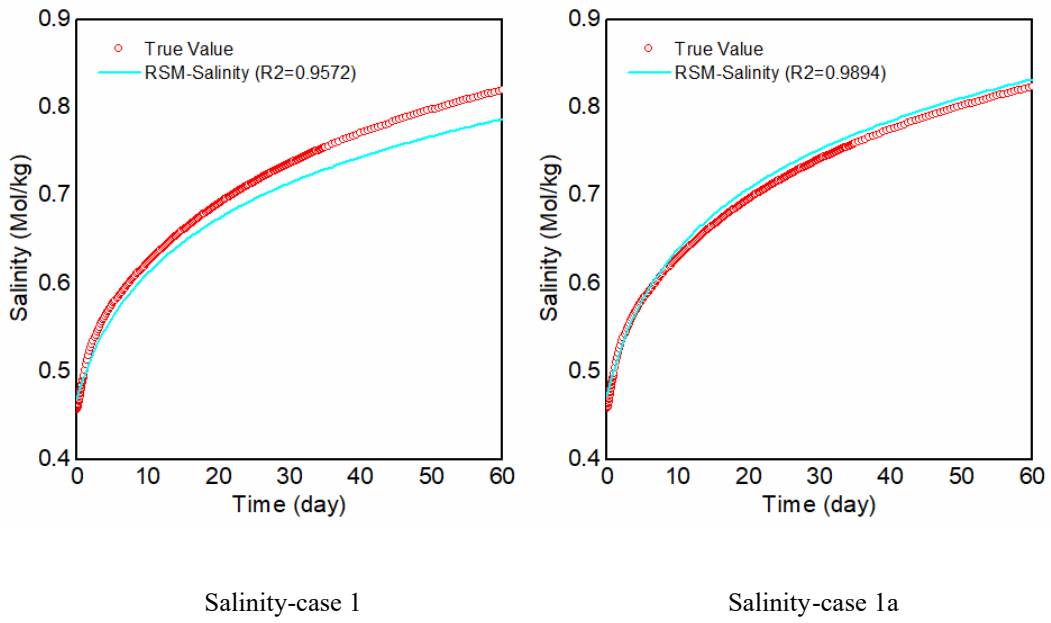
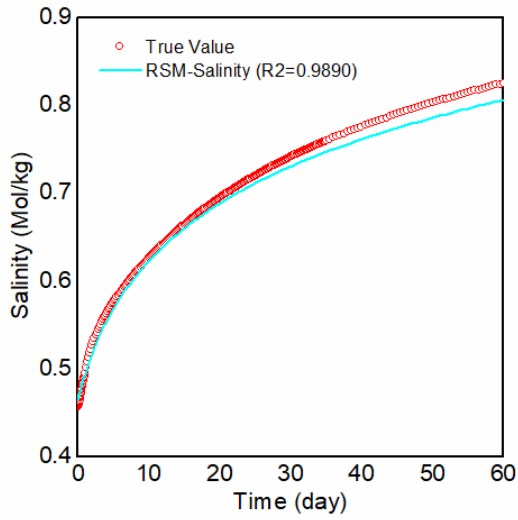
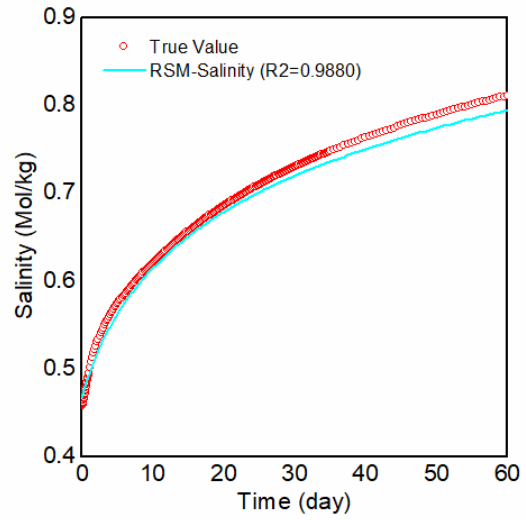


Figure 5-4. Uniform and non-uniform secondary fracture model constructed by RSM-Rate: Green-shale, Black-Secondary Fracture Conduit, Red-Primary Fracture Conduit, Yellow-Horizontal Well Path.

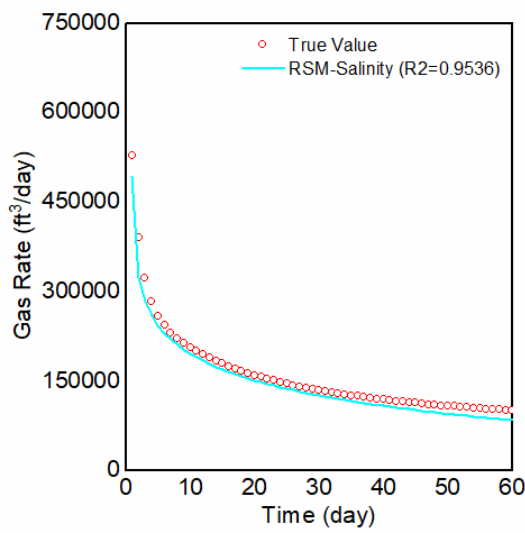




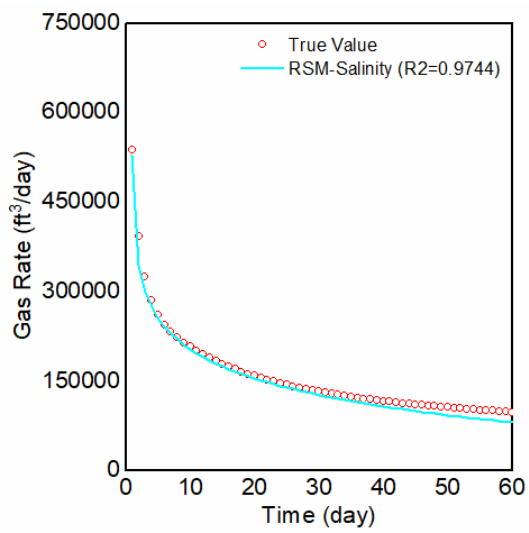
Salinity-case 1b



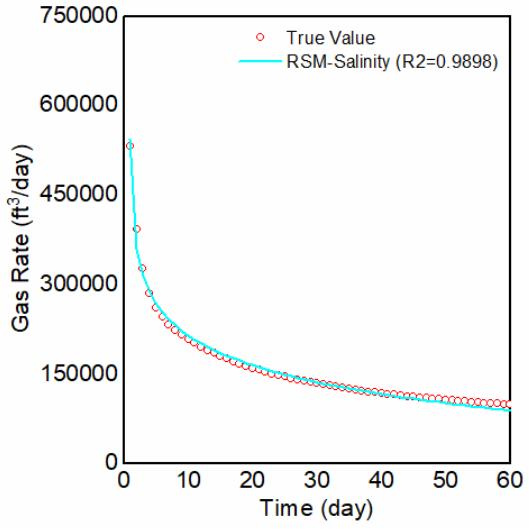
Salinity-case 1c



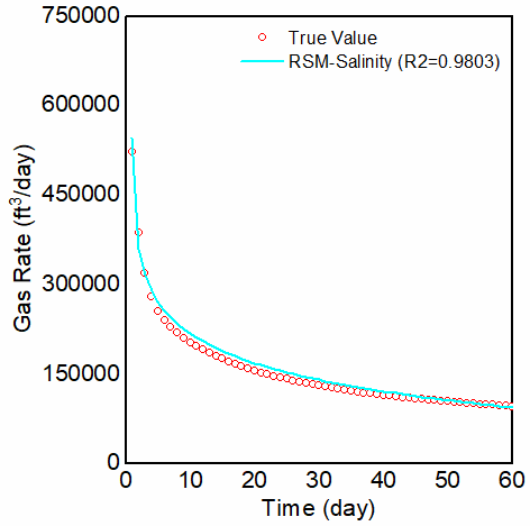
Rate-case 1



Rate-case 1a

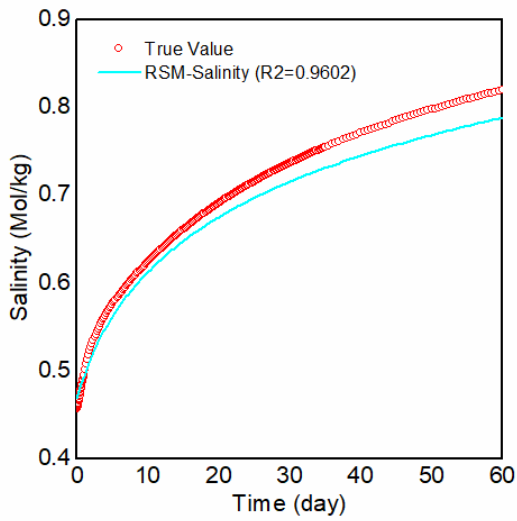


Rate-case 1b

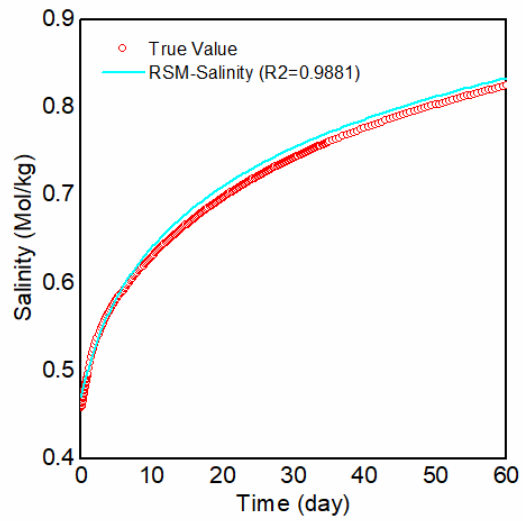


Rate-case 1c

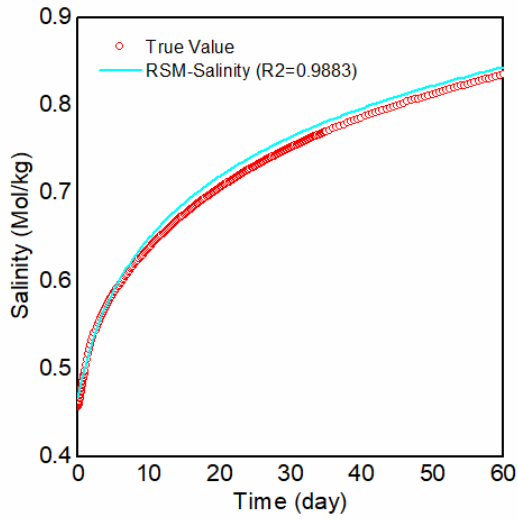
Figure 5-5. Salinity and Rate profile between true value and RSM response for cases 1, 1a, 1b, and 1c.



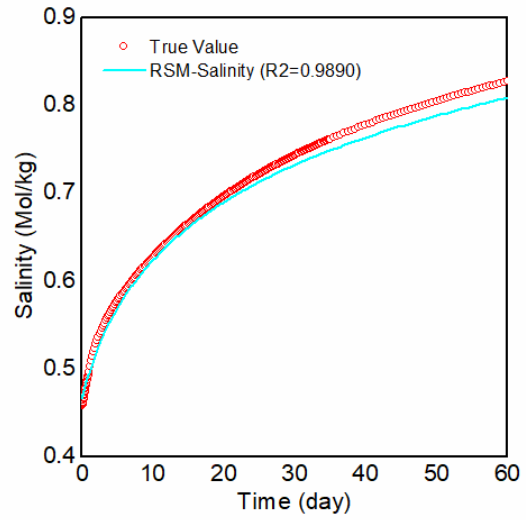
Salinity-case 2



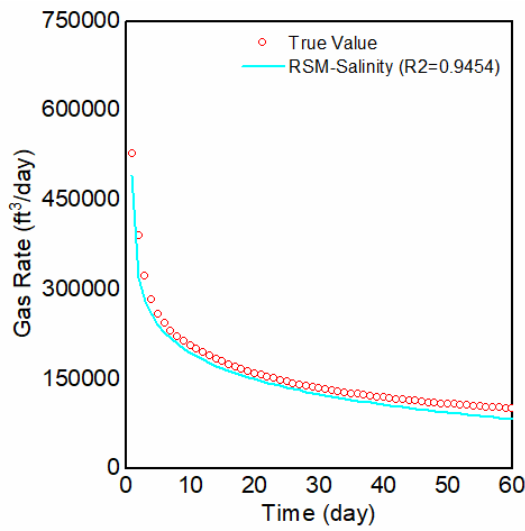
Salinity-case 2a



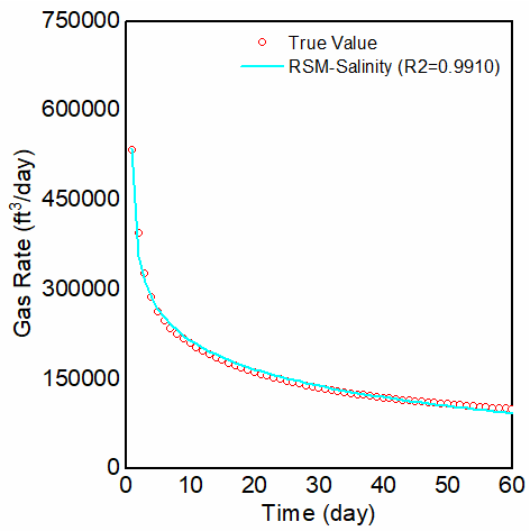
Salinity-case 2b



Salinity-case 2c



Rate-case 2



Rate-case 2a

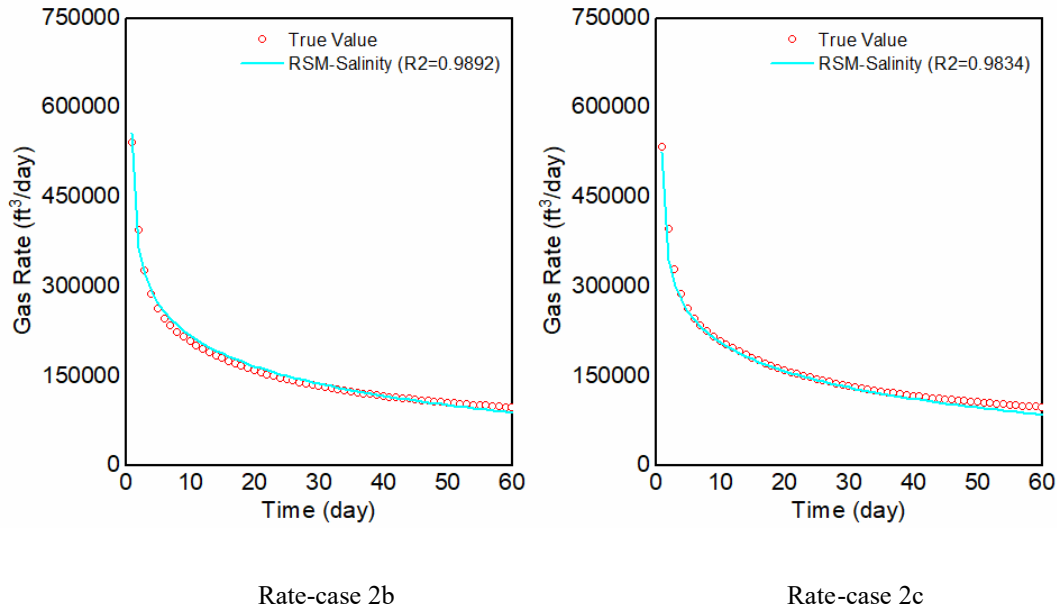


Figure 5-6. Salinity and Rate profile between true value and RSM response for cases 2, 2a, 2b, and 2c.

The models in Figure 5-3 and Figure 5-4 are subjected to detailed flow simulation again, and the simulated salinity and rate profiles are presented in Figure 5-5 and Figure 5-6. There is a good agreement between the simulated profiles using the fracture parameters estimated using the RSM-GA workflow and the introduction of variability through Gaussian noise (cases 1-a, 1-b, and 1-c; and cases 2a, 2b, and 2c) and the production history of the true cases. The agreement is good even for the uniform secondary fracture scenario (using constant secondary fracture parameters), demonstrating the utility of the RSM-GA models for estimating average fracture values.

5.3 Case #2 – Heterogeneous Secondary Fracture DFN Model

This section will apply the RSM models and GA workflow to a true case that is more complex and realistic. The Discrete Fracture Network (DFN) method is used to generate a complex network of

secondary fractures for the true case (as shown in Figure 5-7). The Fisher et al. (2005) conceptualization of a complex hydraulic fracture system was adopted to construct the DFN model using FRACMAN® (Golder Associates, 2018). PF parameters, SF coverage and P32 are constant and taken from Case #1 (section 5.2), while SF aperture and SF permeability follow the same Gaussian distributions described in Case #1. The simulation profiles are used as histories or true values (as shown in Figure 5-8), and the RSM-GA workflow described in section 5.1 is used to estimate a single set of fracture parameters (as shown in Table 5-2). Meanwhile, using the RSM-GA estimates and introducing variability through Gaussian noise described in section 5.2, three realizations of DFN are randomly generated, respectively (as shown in Figure 5-9 and Figure 5-10).

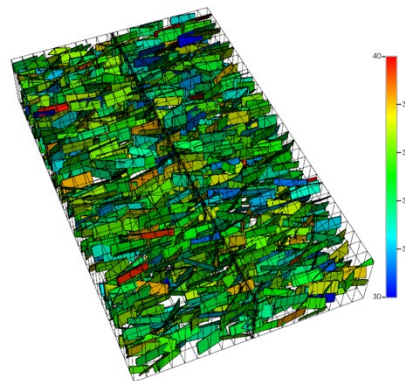


Figure 5-7. True case for heterogeneous secondary fracture DFN model.

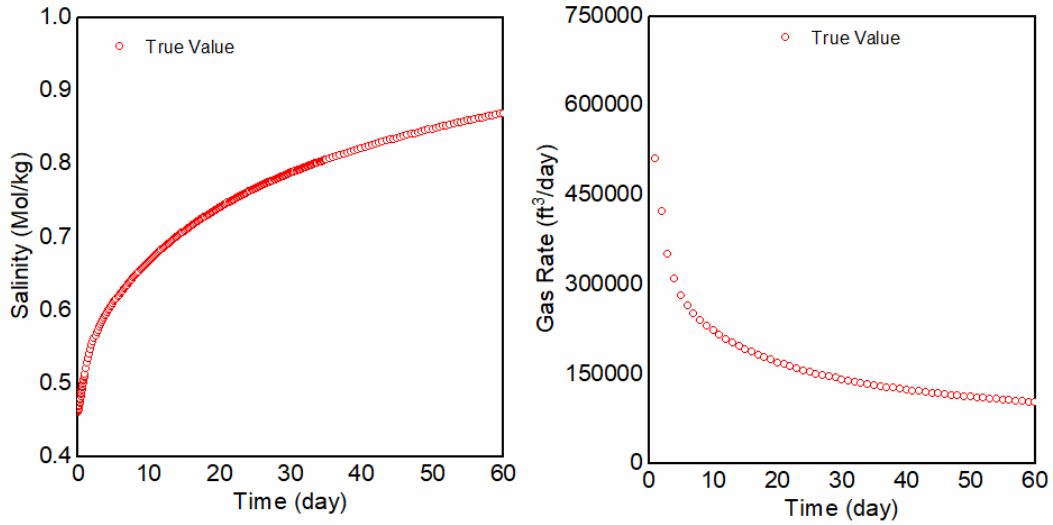


Figure 5-8. Salinity and rate histories for heterogeneous secondary fracture DFN model.

Table 5-2 Fracture parameters estimated using RSM-GA workflow – DFN realizations are generated using the estimated parameters.

Parameter	PF Length (ft)	PF Permeability (mD)	SF Coverage (ft ²)	SF P32 (ft ² /ft ³)	SF Aperture (Average) (ft)	SF Permeability (Average) (mD)
RSM-Salinity	414	7336	80034	0.0585	0.00041578	38
RSM-Rate	429	7346	80131	0.0588	0.00046167	30

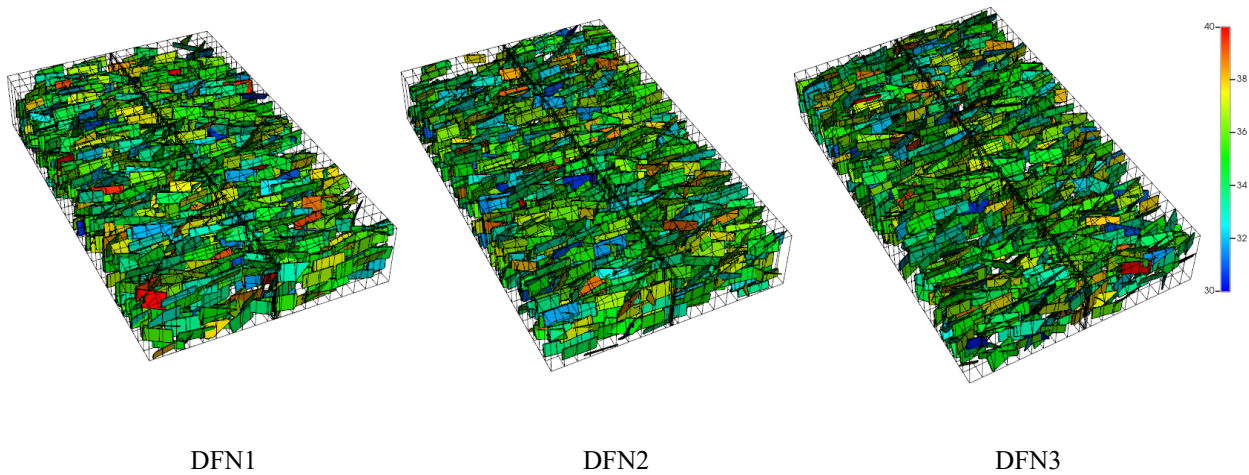


Figure 5-9. The secondary fracture permeability distribution of the DFN model constructed by RSM-Salinity.

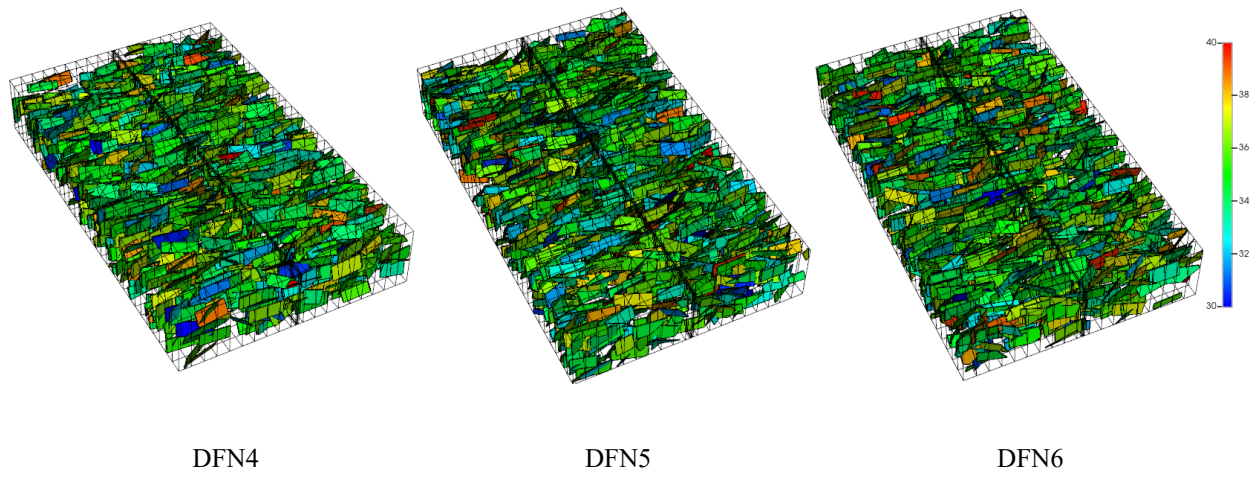
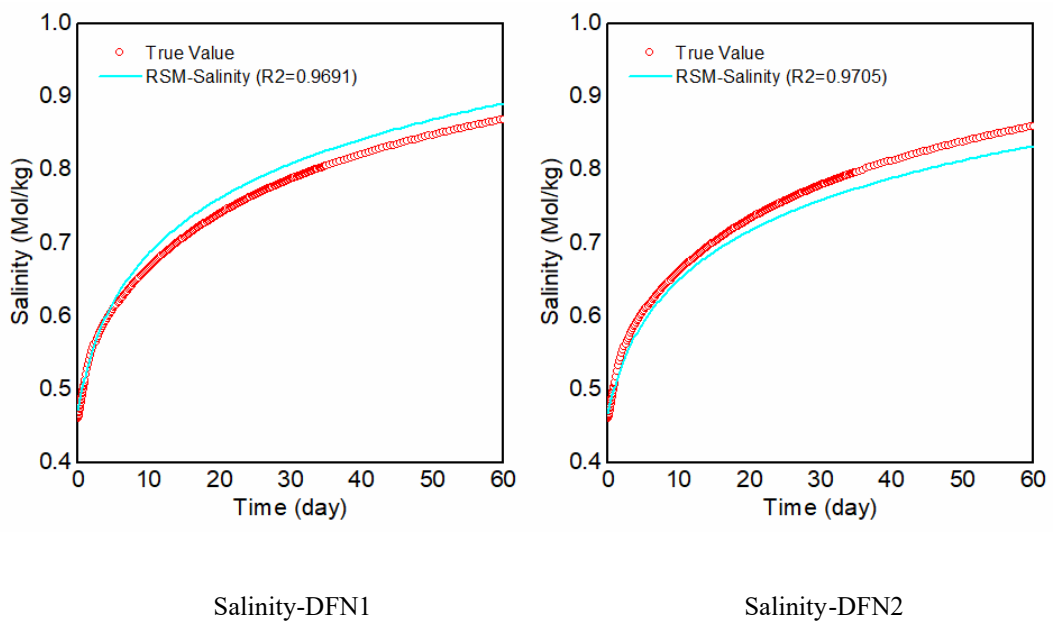
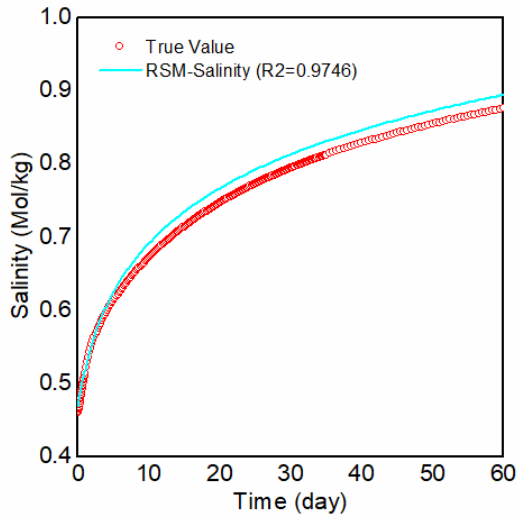
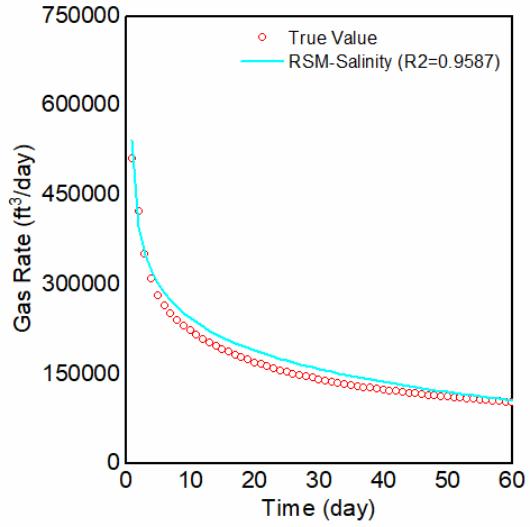


Figure 5-10. The secondary fracture permeability distribution of the DFN model constructed by RSM-Rate.

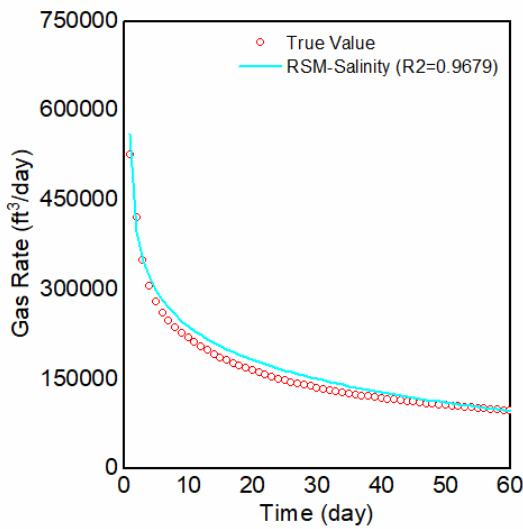




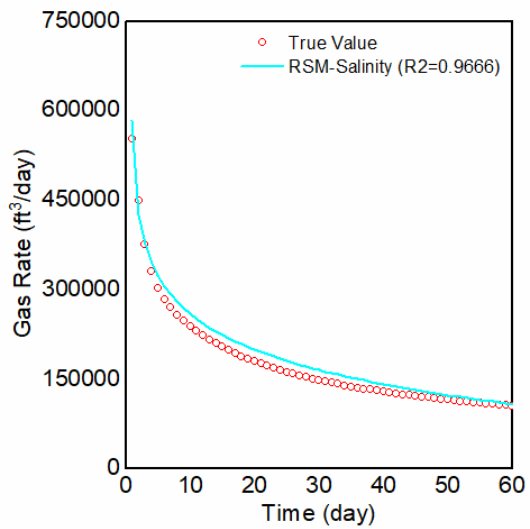
Salinity-DFN3



Rate-DFN1

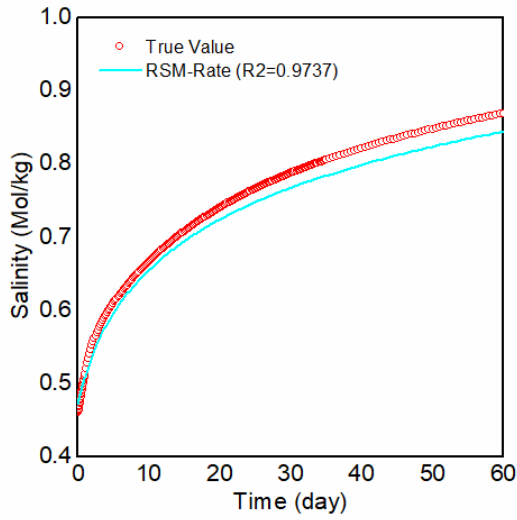


Rate-DFN2

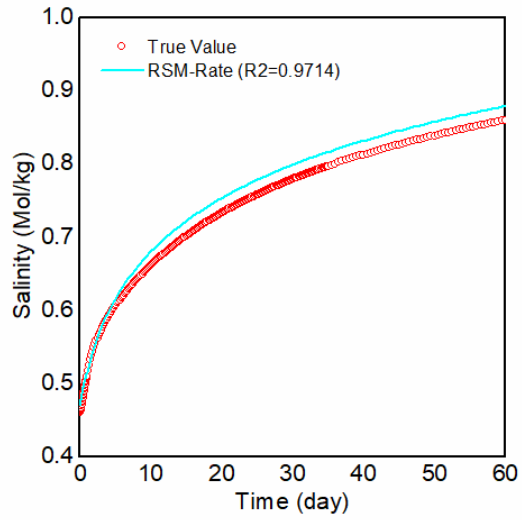


Rate-DFN3

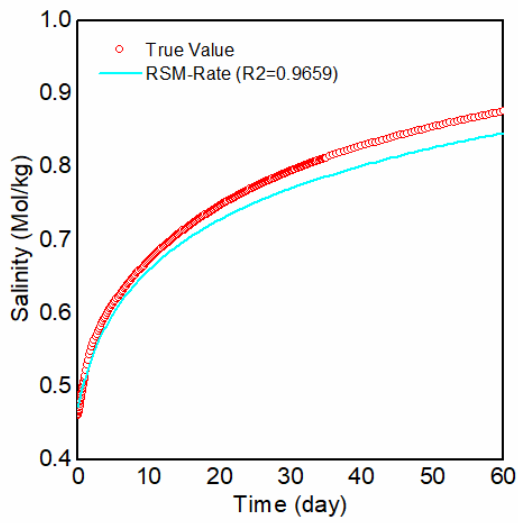
Figure 5-11. Salinity and Rate profile between the true value and RSM response for cases DFN 1-3.



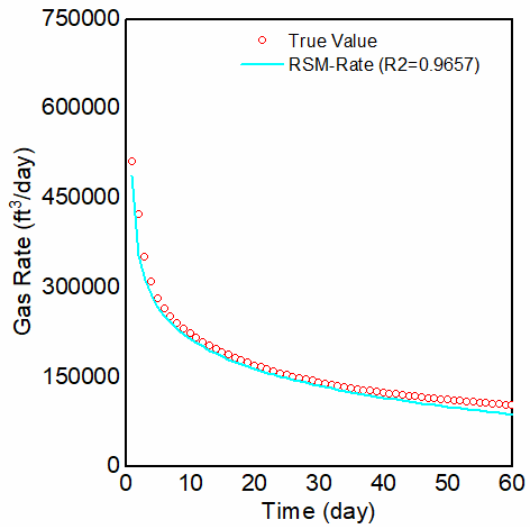
Salinity-DFN4



Salinity-DFN5



Salinity-DFN6



Rate-DFN4

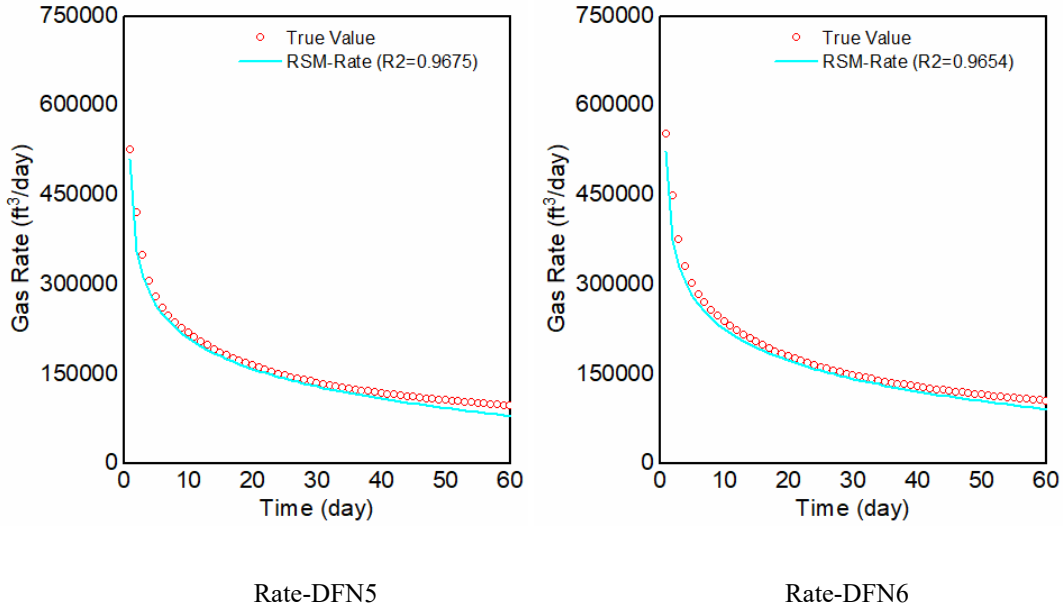


Figure 5-12. Salinity and Rate profile between the true value and RSM response for cases DFN 4-6.

Compared with matching the non-uniform secondary fracture model in section 5.2, the agreement between the simulated profiles from models in Figure 5-9 and Figure 5-10 and the histories will produce some sensitivities. This behaviour is reflected in R² values in Figure 5-11 and Figure 5-12. The main reason for this sensitivity may be the assumptions in the RSM model step: all secondary fractures are interconnected with the primary fractures. In this application to a realistic DFN model, fractures are randomly distributed, and some secondary fractures may not be directly connected to the primary fracture, leading to an underestimation of secondary fractures P32. Despite this limitation, it is essential to recognize the overarching predictive power of the RSM methodology under complex conditions. Figure 5-11 and Figure 5-12 confirm that RSM maintains an impressive level of overall accuracy, even when local heterogeneity and random distribution of fractures are introduced into the model.

5.4 Case #3 – Multi-Stage Horizontal Well Model

In this section, a horizontal well with five hydraulic fracturing stages is modelled. The goal is to explore how interference between the stages may affect the utility of the RSM-GA modelling approach trained using a single fracturing stage model with uniform SF properties.

In addition, in general, only the overall production curve can be obtained from multi-stage horizontal wells. For the assumptions of our RSM model, we can only obtain the average value of fractures in multi-stage horizontal wells. However, with the development of technology, such as the emergence of Distributed Temperature Sensing (DTS) and Distributed Acoustic Sensing (DAS) (Carpenter, 2016; Ghahfarokhi et al., 2018 and 2021; Kjetil et al., 2012; Sookprasong et al., 2014), we can obtain the gas rate curve of each stage.

A limitation comes out when considering the salinity of flowback water. Because the salinity of flowback water can only be measured from the wellhead, representing the entire horizontal well. Typically, measuring the salinity of flowback fluid requires collecting flowback water samples at the wellhead and sending them to the laboratory to measure their ion concentration. In the early stage of the flowback, the more intensive the collection times, the better. In the later stage, the collection time can be appropriately relaxed. For instance, Osselin et al., (2018) collected flowback water through 1L plastic bottles. Samples were collected every 20 m^3 until 100 m^3 of flowback and every 100 m^3 until 7 days of flowback, a total of 24 times. The samples were analyzed for concentrations of major ions, and presented a mathematical model that allows the calculation of the amount of fracturing fluid recovered.

In view of these considerations, the subsequent phase will use three types of production curves, the rate curve of each stage from DAS/DTS, the averaged total rate curve from the wellhead

(calculated by dividing the overall gas rate by the number of stages), and the salinity of flowback water from the wellhead to test the feasibility of the RSM model in multi-stage horizontal wells.

5.4.1 Multi-Stage Horizontal Well with Equal Primary Fracture Length and Even Spacing

Firstly, explore the efficacy of the RSM methodology in a horizontal well with five hydraulic fracturing stages with equal primary fracture length and even primary fracture spacing (as shown in Figure 5-13). Based on the previous assumptions, the histories or true values shown in Figure 5-14 can be obtained: the salinity of flowback fluid from the wellhead, the total rate curve from the wellhead, and the rate curve of each stage from DAS/DTS. The RSM-GA workflow is used to estimate fracture parameters, and the results are shown in Table 5-3. The DFN method described in section 5.3 generates complex networks of secondary fractures, and local grid refinement is used to build primary fractures. Three realizations from RSM-Salinity, RSM-Rate (total), and RSM-Rate (stage) are sampled and shown in Figure 5-15.

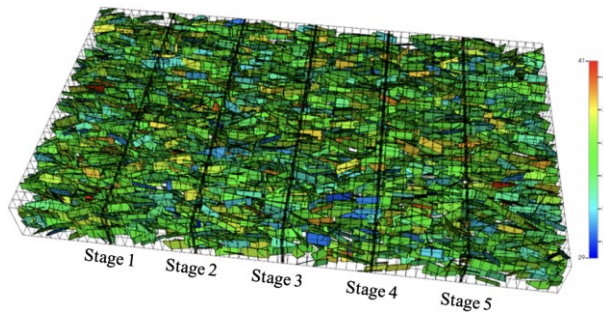
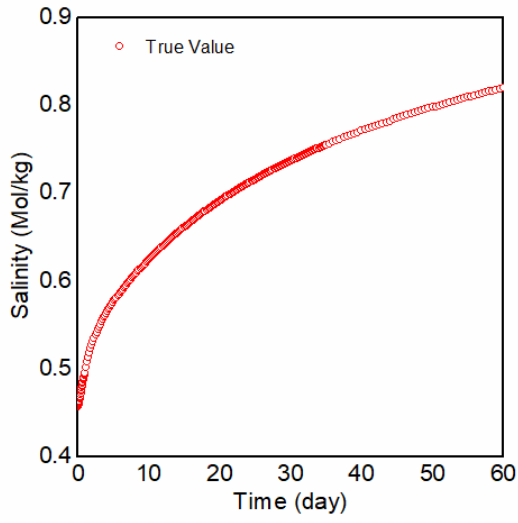
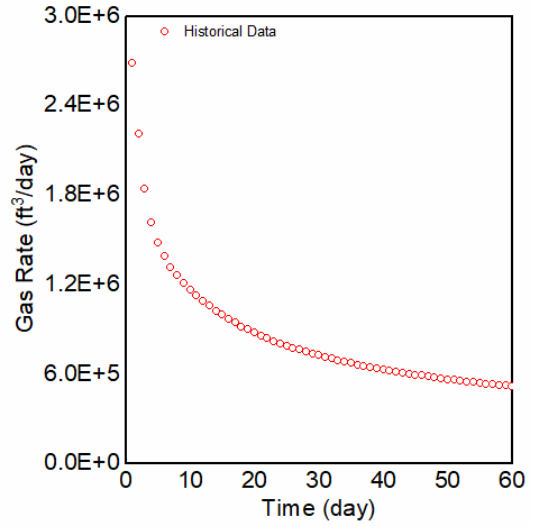


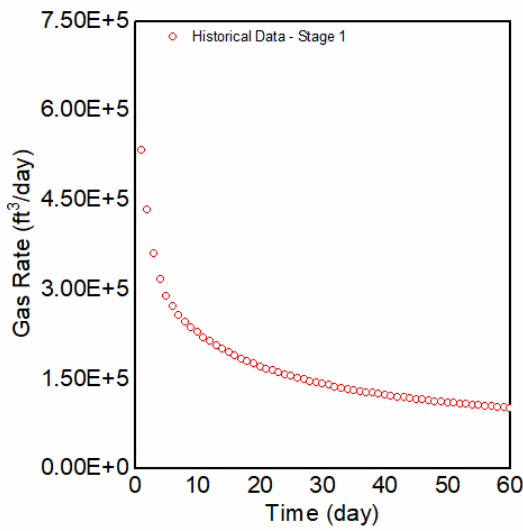
Figure 5-13. True case for equal primary fracture length and even primary spacing.



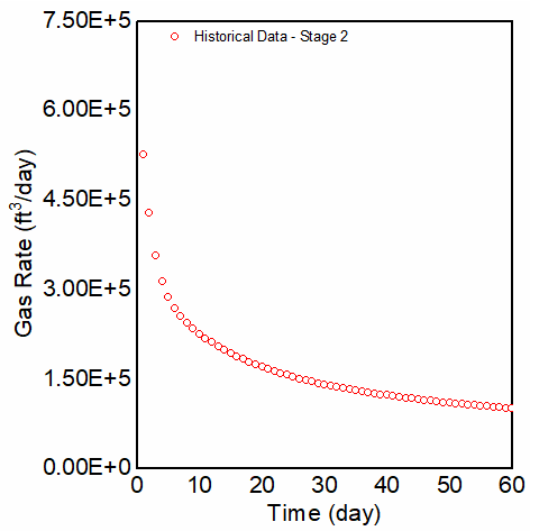
Salinity



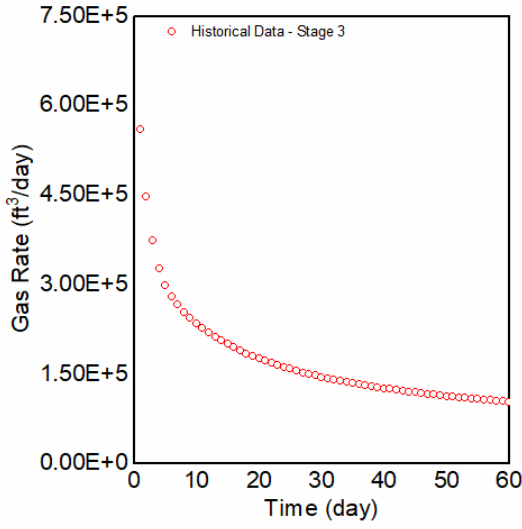
Rate (total)



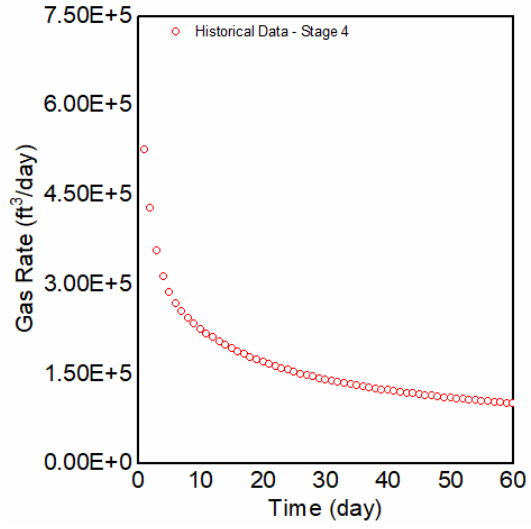
Rate (stage 1)



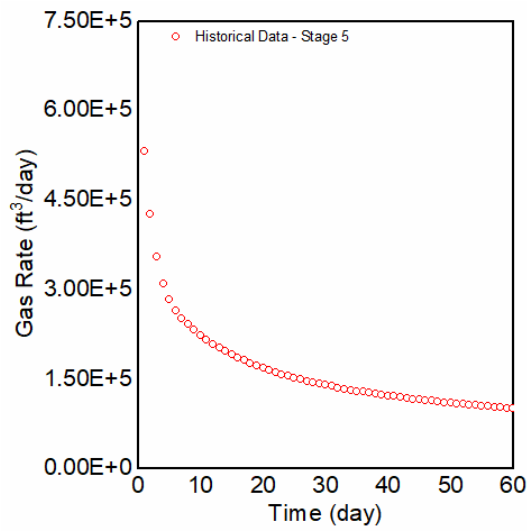
Rate (stage 2)



Rate (stage 3)



Rate (stage 4)

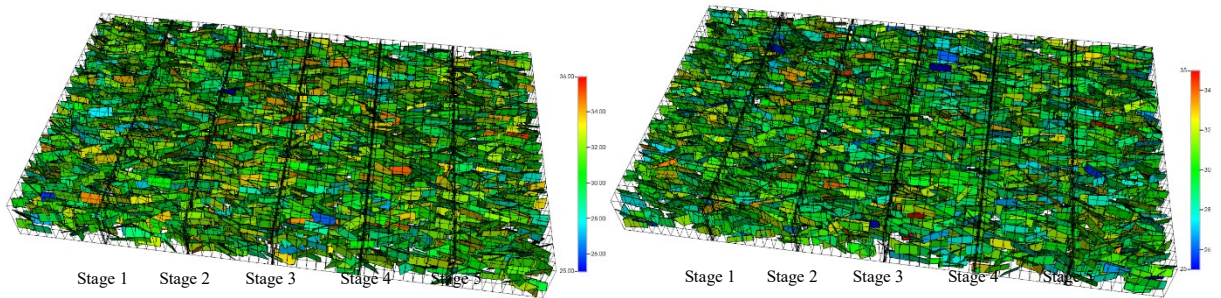


Rate (stage 5)

Figure 5-14. Salinity and rate histories for multi-stage horizontal well with equal primary fracture length and even primary fracture spacing.

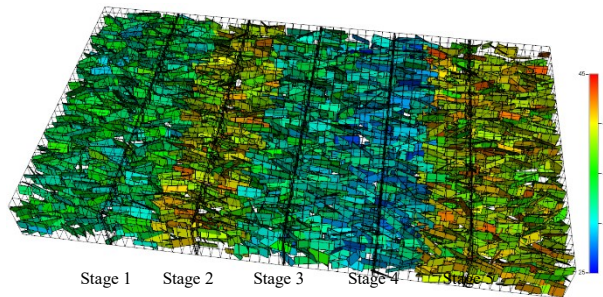
Table 5-3 Fracture parameters predicted by RSM for multi-stage horizontal well with equal primary fracture length and even primary fracture spacing.

Parameter	PF Length (ft)	PF Permeability (mD)	SF Coverage (ft ²)	SF P32 (ft ² /ft ³)	SF Aperture (Average) (ft)	SF Permeability (Average) (mD)
RSM-Salinity	426	7268	69963	0.0574	0.00047001	31
RSM-Rate (total)	428	7324	79953	0.0578	0.00040942	30
RSM-Rate (stage 1)	426	7316	70381	0.0575	0.00045611	33
RSM-Rate (stage 2)	407	7284	70354	0.0572	0.00041126	39
RSM-Rate (stage 3)	432	6685	78598	0.0586	0.00046237	32
RSM-Rate (stage 4)	414	7258	70141	0.0575	0.00047015	30
RSM-Rate (stage 5)	408	6689	70579	0.0578	0.00040468	39



RSM-Salinity

RSM-Rate (total)



RSM-Rate (stage)

Figure 5-15. The secondary fracture permeability distribution of the Multi-stage horizontal well model with equal primary fracture length and even primary spacing constructed by RSM-Salinity, RSM-Rate (total), RSM (stage); the colour scale represents secondary fracture permeability distribution.

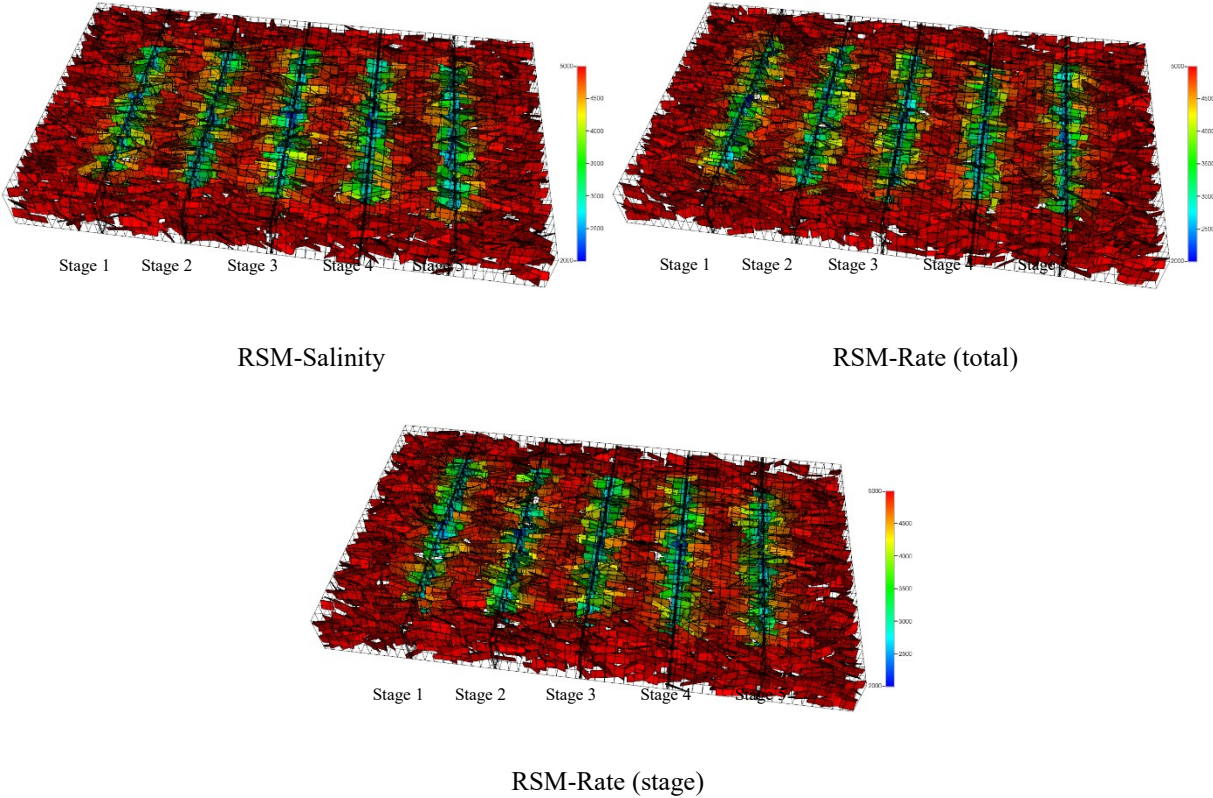


Figure 5-16. Multi-stage horizontal well model with equal primary fracture length and even primary spacing; the colour scale represents pressure distribution (psi) after 60 days.

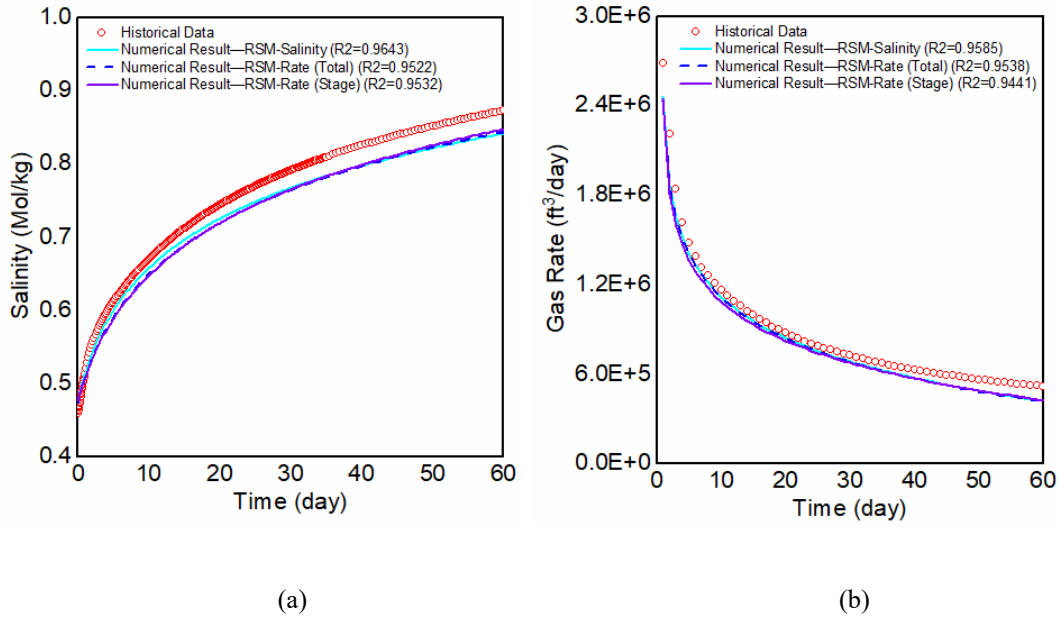


Figure 5-17. The comparison between true production profile and predicted curve for multi-stage horizontal well with equal primary fracture length and even primary spacing : (a) Salinity profile, and (b) Gas rate curve.

The models in Figure 5-15 are subjected to detailed flow simulation again, and the pressure distribution and the simulated salinity and rate profiles are presented in Figure 5-16 and Figure 5-17. The pressure distribution in Figure 5-16 indicates the five stages of the multi-stage horizontal well are effectively isolated, exhibiting minimal stage-to-stage interference. Given the uniformity in the primary fracture spacing, the RSM-Rate (stage) for each stage is a reliable indicator of individual fracture parameters. The results affirm that RSM-Salinity, RSM-Rate (total), and RSM-Rate (stage) offer high predictive accuracy under conditions of equal primary fracture length and even primary fracture spacing when there is no interference between stages.

5.4.2 Multi-Stage Horizontal Well with Equal Primary Fracture Length and Uneven Primary Fracture Spacing

This section will explore the feasibility of the RSM-GA modelling approach for multi-stage horizontal well with equal primary fracture length and uneven primary fracture spacing (as shown in Figure 5-18), exploring how interference between the stages may affect the history matching. The simulation profiles are used as histories or true values (as shown in Figure 5-19), and the RSM-GA results are shown in Table 5-4. Three realizations described in 5.4.1 are sampled and shown in Figure 5-20.

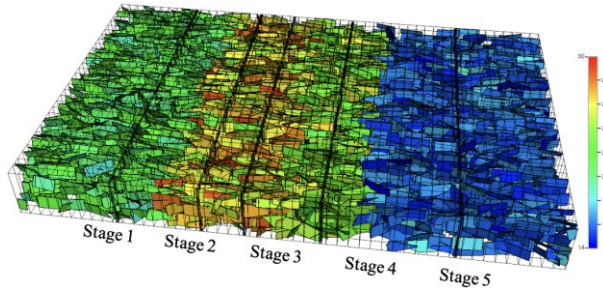
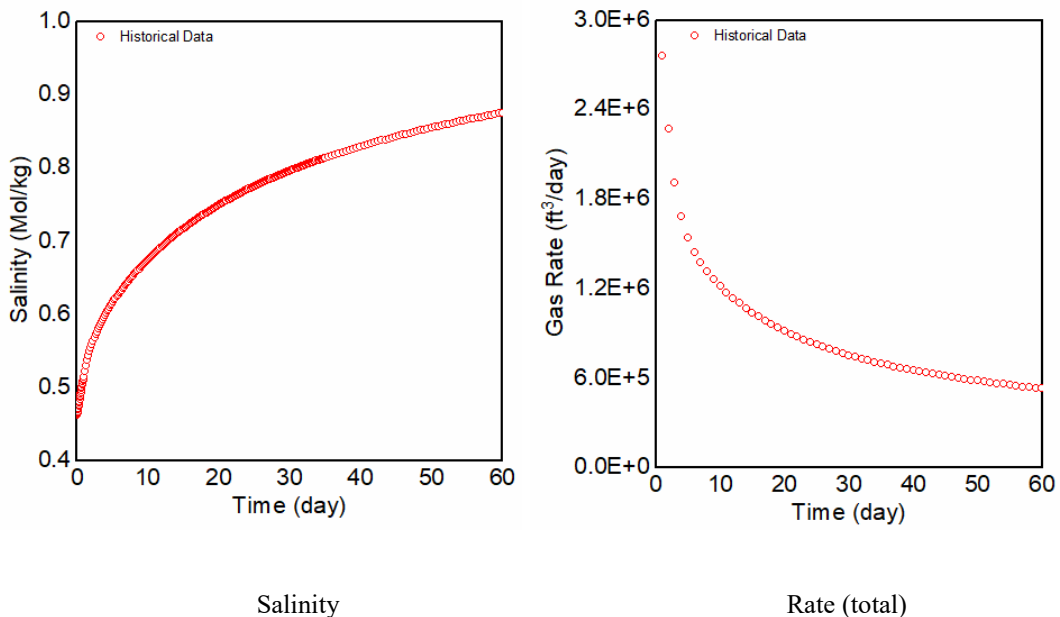
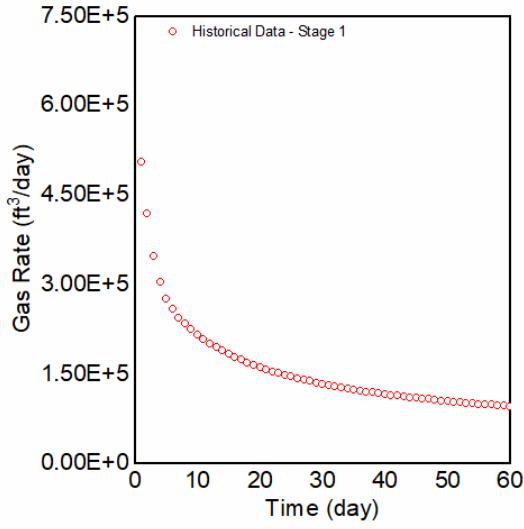
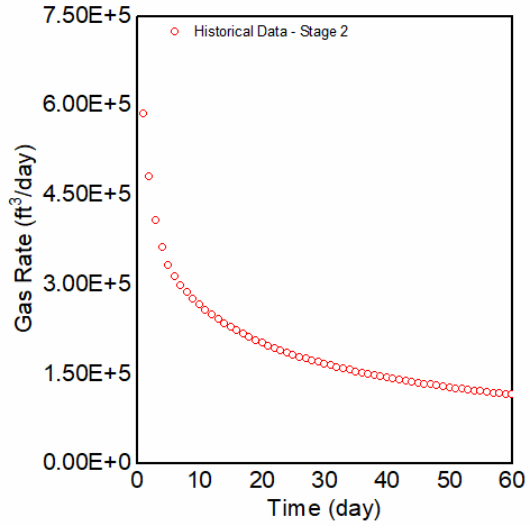


Figure 5-18. True case for equal primary fracture length and uneven primary fracture spacing.

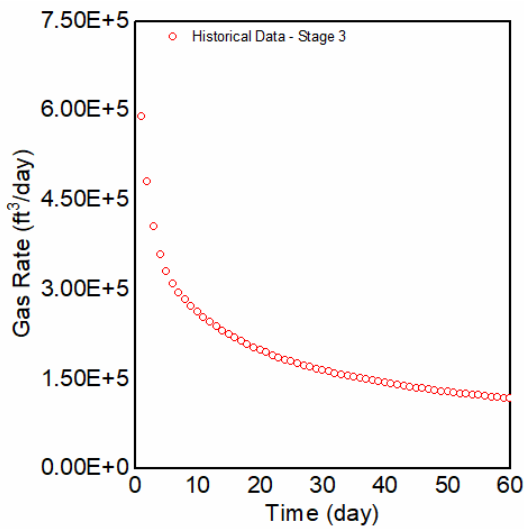




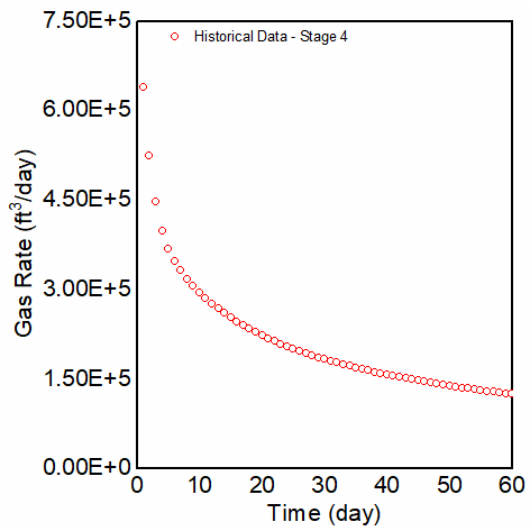
Rate (stage 1)



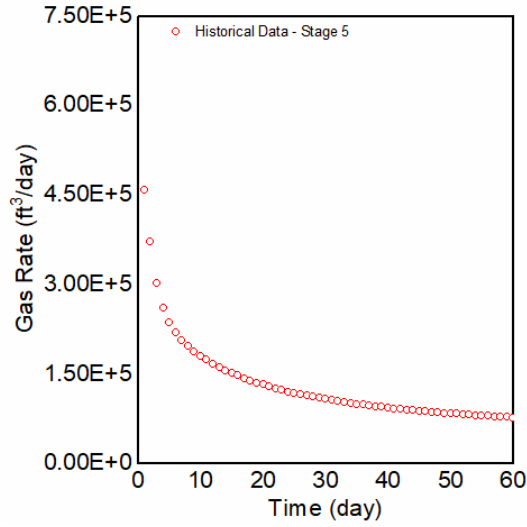
Rate (stage 2)



Rate (stage 3)



Rate (stage 4)



Rate (stage 5)

Figure 5-19. Salinity and rate histories for multi-stage horizontal well with equal primary fracture length and uneven primary fracture spacing.

Table 5-4 Fracture parameters predicted by RSM for multi-stage horizontal well with equal primary fracture length and uneven primary fracture spacing.

Parameter	PF Length (ft)	PF Permeability (mD)	SF Coverage (ft ²)	SF P32 (ft ² /ft ³)	SF Aperture (Average) (ft)	SF Permeability (Average) (mD)
RSM-Salinity	426	11547	57841	0.0685	0.00057768	25
RSM-Rate (total)	413	12519	55135	0.0627	0.00052523	18
RSM-Rate (stage 1)	424	11461	82218	0.0611	0.00046192	17
RSM-Rate (stage 2)	432	11590	41590	0.0764	0.00074882	20
RSM-Rate (stage 3)	415	11444	52906	0.0724	0.00071238	19
RSM-Rate (stage 4)	417	12544	58268	0.0664	0.00056019	28
RSM-Rate (stage 5)	413	12312	78462	0.0535	0.00033929	18

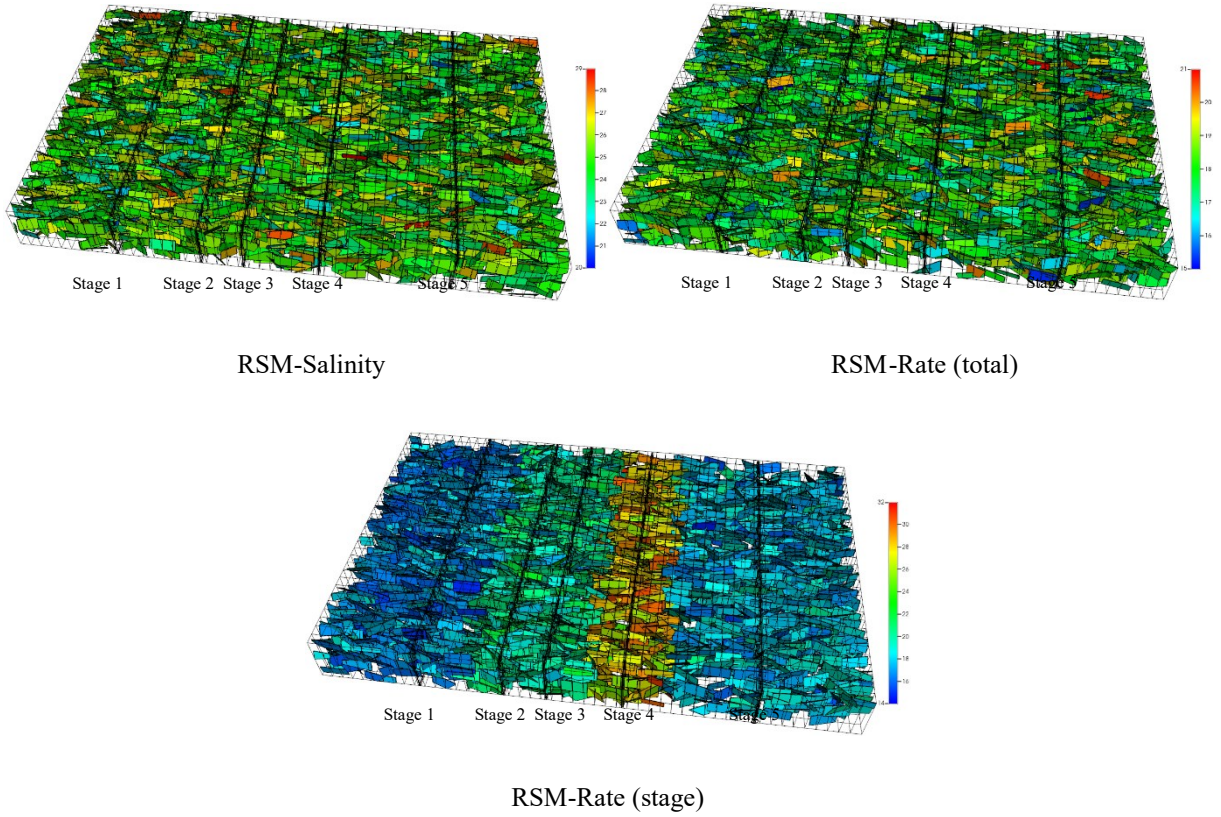
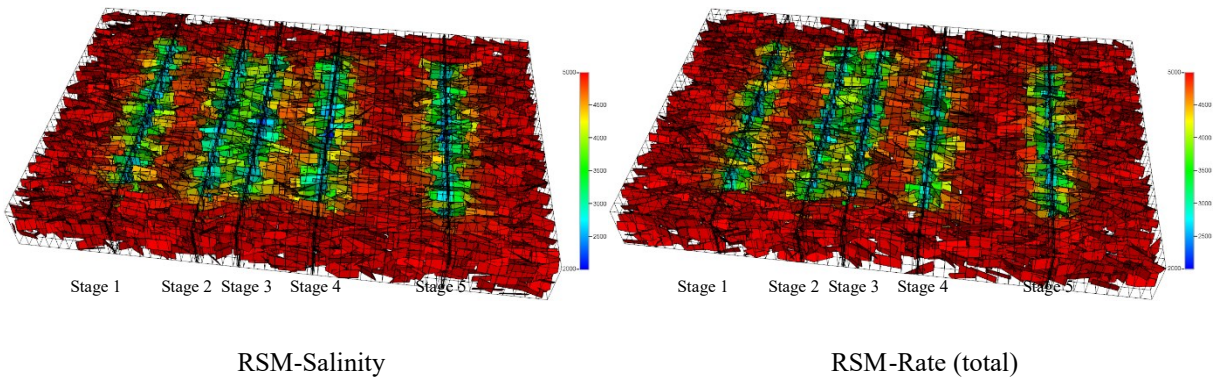


Figure 5-20. The secondary fracture permeability distribution of the Multi-stage horizontal well model with equal primary fracture length and uneven primary fracture spacing constructed by RSM-Salinity, RSM-Rate (total), RSM (stage); the colour scale represents secondary fracture permeability distribution.



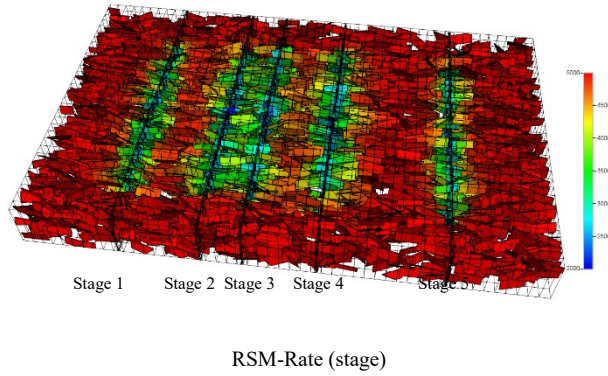


Figure 5-21. Multi-stage horizontal well model with equal primary fracture length and uneven primary fracture spacing; the colour scale represents pressure distribution (psi) after 60 days.

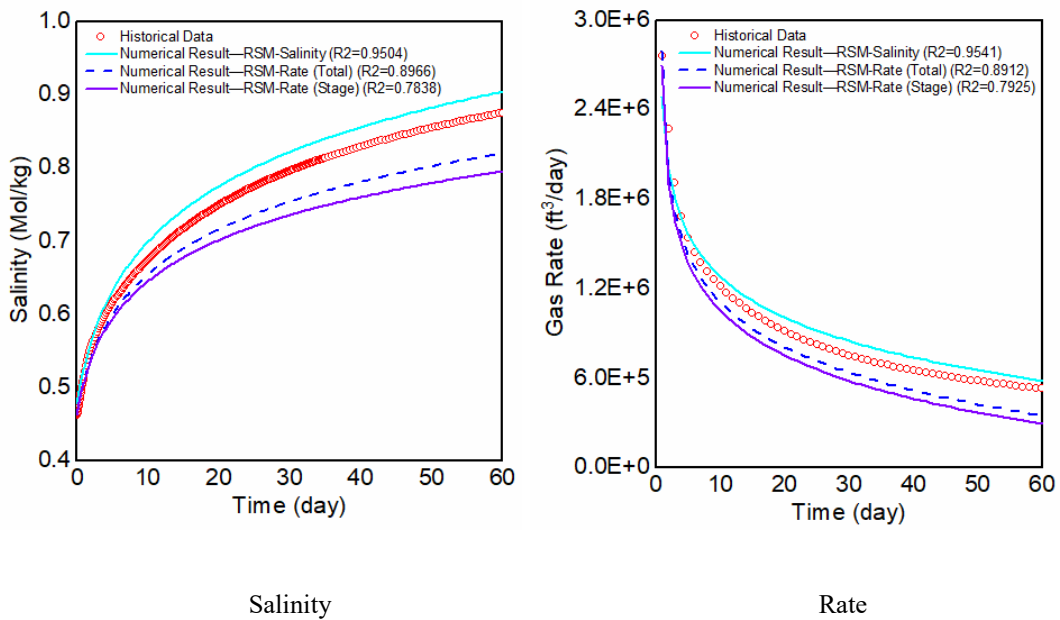


Figure 5-22. The comparison between true production profile and predicted curve for multi-stage horizontal well with equal primary fracture length and uneven primary fracture spacing.

After detailed flow simulation, Figure 5-21 depicts the pressure distribution after 60 days into production, clearly showing interdependence between Stages 1-4, especially stages 2-4.

Conversely, Stage 5 remains largely isolated, exerting minimal influence on Stage 4. Compared with Figure 5-17 in section 5.4.1, there is a certain sensitivity in the history matching results (Figure 5-22, especially in the reconstructed model by RSM-Rate (stage), which may be attributable to inter-stage interference. Through comparison, it was found that the model reconstructed with fracture parameters predicted by RSM-Salinity is closer to the historical production curve. This shows that in the case of the multi-stage horizontal well with equal primary fracture length and uneven primary fracture spacing, the prediction accuracy of RSM-Salinity is higher than RSM-Rate (total) and RSM-Rate (stage).

5.5 Multi-Stage Horizontal Well with Unequal Primary Fracture Length and Uneven Primary Fracture Spacing

This section will apply the RSM models and GA workflow to a multi-stage horizontal well with unequal primary fracture length and uneven primary fracture spacing (as shown in Figure 5-23), also called the completion heterogeneity model (Clarkson 2021), which captures the complexity often encountered in field applications. A case with unequal primary fracture length, uneven primary fracture spacing, and complex secondary fractures generated by DFN is constructed. The simulation profiles are used as histories or true values (as shown in Figure 5-24). The RSM-GA results are shown in Table 5-5. Three realizations are sampled and shown in Figure 5-25.

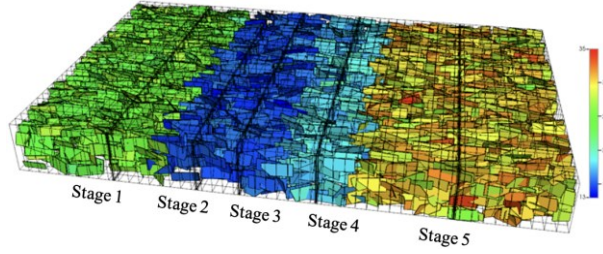
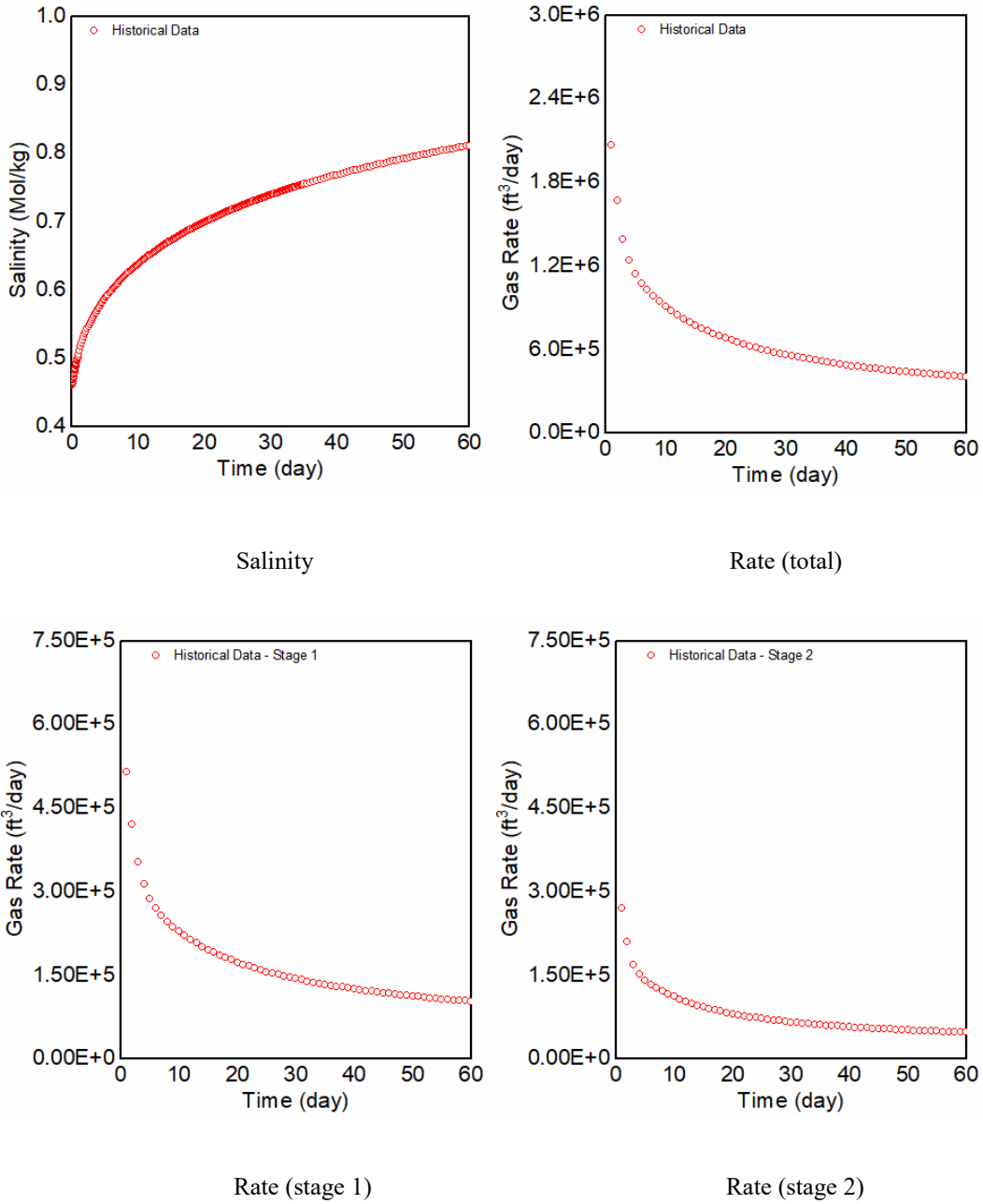
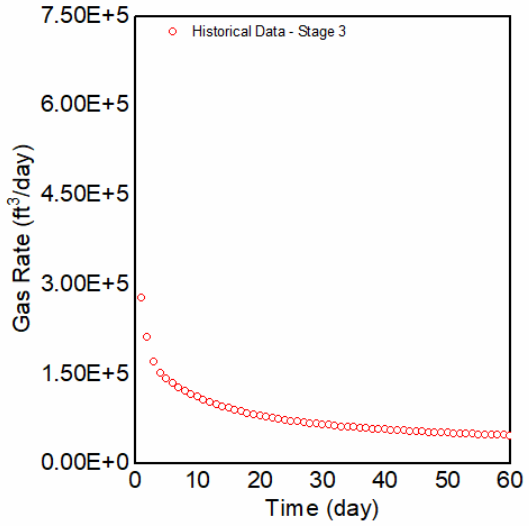
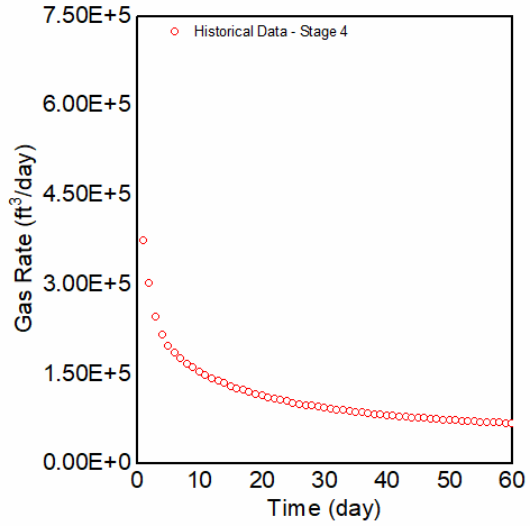


Figure 5-23. True case for unequal primary fracture length and uneven primary fracture spacing model.

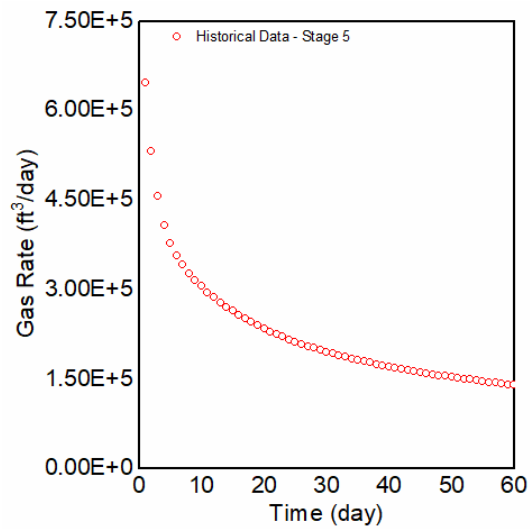




Rate (stage 3)



Rate (stage 4)

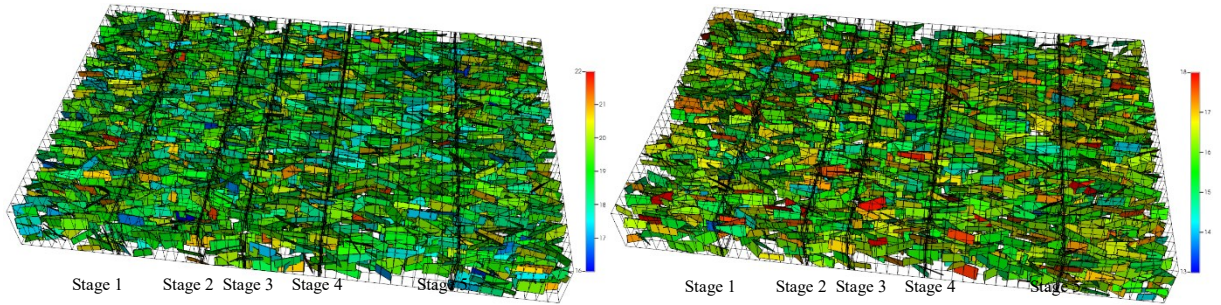


Rate (stage 5)

Figure 5-24. Salinity and rate histories for multi-stage horizontal well with

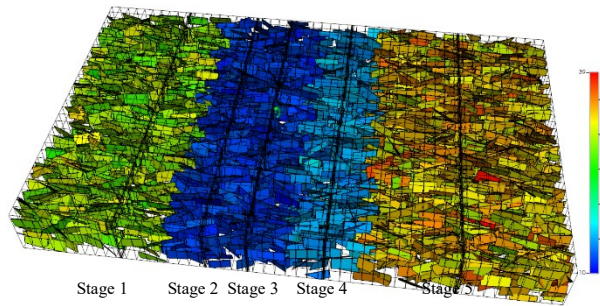
Table 5-5 Fracture parameters predicted by RSM for multi-stage horizontal well with unequal primary fracture length and uneven primary fracture spacing.

Parameter	PF Length (ft)	PF Permeability (mD)	SF Coverage (ft ²)	SF P32 (ft ² /ft ³)	SF Aperture (Average) (ft)	SF Permeability (Average) (mD)
RSM-Salinity	341	10553	54159	0.0545	0.00046864	19
RSM-Rate (total)	321	10584	58239	0.0512	0.00060025	16
RSM-Rate (stage 1)	372	12826	76654	0.0655	0.00057107	29
RSM-Rate (stage 2)	252	6791	24605	0.0397	0.00027957	12
RSM-Rate (stage 3)	253	6753	34981	0.0381	0.00025862	11
RSM-Rate (stage 4)	346	7971	62605	0.0403	0.00053458	15
RSM-Rate (stage 5)	417	17262	77542	0.0812	0.00077258	33



RSM-Salinity

RSM-Rate (total)



RSM-Rate (stage)

Figure 5-25. The secondary fracture permeability distribution of the Multi-stage horizontal well with unequal primary fracture length and uneven primary fracture spacing constructed by RSM-Salinity, RSM-Rate (total), RSM (stage); the colour scale represents secondary fracture permeability distribution.

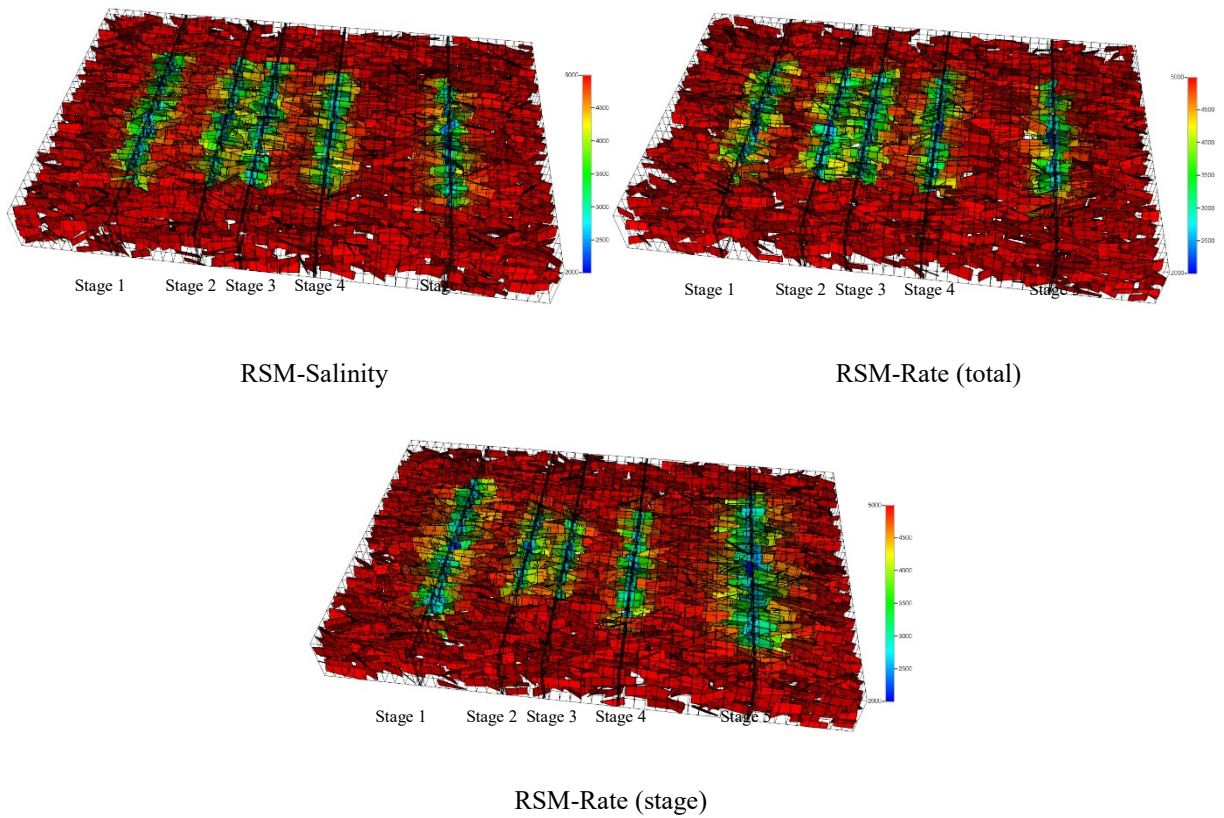


Figure 5-26. Multi-stage horizontal well with unequal primary fracture length and uneven primary fracture spacing; the colour scale represents pressure distribution (psi) after 60 days.

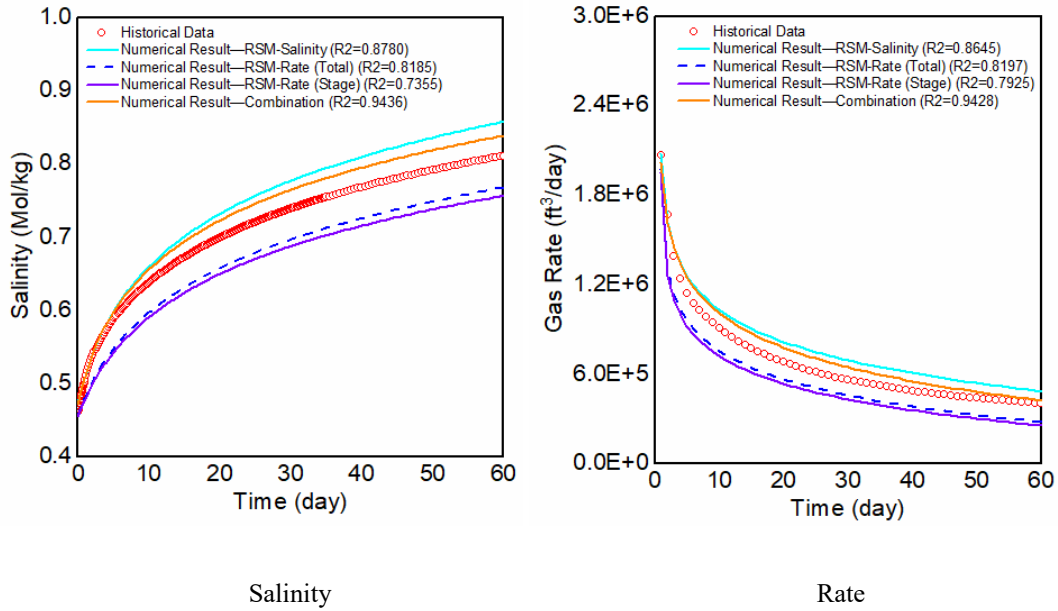


Figure 5-27. The comparison between true production profile and predicted curve for multi-stage horizontal well with unequal primary fracture length and uneven primary fracture spacing: (a) Salinity profile, and (b) Gas rate curve.

When unequal primary fracture lengths are introduced into a multi-stage horizontal well with uneven primary fracture spacing, as seen in section 5.4.2, stages in closer proximity (stages 2-4) continue to display interdependence, with relatively isolated behaviour in other stages like stage 5 (as seen in Figure 5-26). Figure 5-27 compares histories and numerically simulated outputs based on predicted fracture parameters (RSM-Salinity, RSM-Rate (total), and RSM-Rate (stage)). It is found that similar to the conclusion in section 5.4.2, the numerical model from RSM-Salinity is closer to the historical production data than RSM-Rate (total) and RSM-Rate (stage). A notable observation is the reduced R2 error compared to the previous section, a deviation attributed to the equal primary fracture length in section 5.4.2.

Due to unequal primary fracture length, the primary fracture parameters, PF length and PF permeability, predicted by RSM-Rate (total) and RSM-Salinity, will be the average across all primary fractures. In contrast, RSM-Rate (stage) may reflect the characteristics of the primary fracture. Furthermore, a hypothesis emerges given that the numerical model from RSM-Salinity is closer to the historical production data than RSM-Rate (total) and RSM-Rate (stage). Combining the secondary fracture parameters from RSM-Salinity with the primary fracture parameters from RSM-Rate (stage) for model construction could enhance the history matching. Fortunately, the production curve from this combined approach is closer to the histories, as shown by the orange line in Figure 5-27.

Table 5-6 Comparison of the total computing time with and without proxy models.

Steps	Proxy	Without Proxy
Time for training cases (min)	41 individuals * 30 min = 1230 min	-
Time for construction the proxy model (min)	1 day * 1440 min/day = 1440 min	-
Time for proxy model (min)	15 min	-
Time for numerical model (min)	-	14 day * 1440 min/day * 50 individuals = 1008000 min
Total time (min)	2685 min	1008000 min

In addition, the significant difference in simulation run-time between a full-scale numerical model and the RSM proxy method is a crucial aspect that justifies the latter's use in this research. Table 5-6 summarizes the computational assessment requirements for fracture characterization with and without proxy models. Building the proxy model involved running 41 single-stage well model cases, with each case requiring 30 minutes on an i7-8700 CPU @ 3.2 GHz computer. The entire process of building the proxy using single-stage well model results takes about one day. Using the

proxy (RSM-GA) to estimate fracture properties requires only 15 minutes. In contrast, simulating a five-stage horizontal well without the proxy models could take about 14 days for a single simulation, potentially extending to 700 days for 50 iterations to achieve optimal fracture characterization. This highlights the significant computational efficiency and practicality offered by employing proxy models for extensive fracture characterization.

In summary, a combination of predictive tools seems most effective when addressing multi-stage horizontal wells with unequal primary fracture length and uneven primary fracture spacing or working with completion heterogeneity models. RSM-Rate (stage) is adept at predicting primary fracture parameters for each stage. Meanwhile, RSM-Salinity remains a reliable tool for predicting secondary fracture parameters for the entire reservoir. Utilizing fracture parameters from RSM-Salinity for secondary fractures and from RSM-Rate (stage) for primary fractures provides a more accurate representation of the reservoir's behaviour. Combining these parameter sets for model initialization yields simulation results that closely match historical production data.

5.6 Summary

In Chapter 5, an effective workflow has been proposed, synergizing the power of RSM and GA, to utilize the salinity profile of flowback fluid and gas rate for fracture characterization. A comprehensive range of scenarios was examined, stretching from Single-Stage Wells to Multi-Stage Horizontal Wells and from homogeneous to heterogeneous fracture models.

Firstly, start by exploring uniform and non-uniform single-stage wells, observing a good agreement between the simulated profiles using the fracture parameters estimated using the RSM-GA workflow and the introduction of variability through Gaussian noise and the production history

of the true cases. However, the agreement will produce some sensitivities as the fracture pattern becomes more complex and heterogeneous. The main reason may be the assumptions in the RSM model step: all secondary fractures are interconnected with the primary fractures, leading to an underestimation of secondary fractures P32.

Then, the study was extended to multi-stage horizontal wells, focusing on various sub-categories, including equal primary fracture length and even primary fracture spacing, uneven primary fracture spacing, unequal primary fracture length and uneven primary fracture spacing. Finally, it is found that under the condition of multi-stage horizontal wells with unequal primary fracture length and variable primary fracture spacing or working with completion heterogeneity models, utilizing fracture parameters from RSM-Salinity for secondary fractures and from RSM-Rate (stage) for primary fractures provides a more accurate representation of the reservoir's behaviour. Combining these parameter sets for model initialization yields simulation results that closely match historical production data.

Chapter 6: Conclusions and Future Work

6.1 Key Conclusions

This research develops a coupled flow and geochemical model incorporating various geochemical mechanisms in commercial GEM software. An experimental core flood data set is used to validate the coupled model and other physical processes.

The primary objective of this coupled model is to simulate the impact of complex mechanisms and interactions on oil recovery and the composition of effluent fluids. The study found that ion exchange and mineral dissolution/precipitation reactions are the main mechanisms affecting oil recovery. For low-salinity water flooding, mineral dissolution/precipitation reaction plays a major role in the recovery factor. For high-salinity water flooding, ion exchange is more important, while mineral dissolution/precipitation reactions do not significantly impact the recovery factor.

Results from a sensitivity analysis are used to establish the RSM-Salinity and RSM-Rate regression models or proxies for predicting flowback fluid salinity and gas rate profiles for a single-stage hydraulically fractured reservoirs with uniform and homogeneous fracture properties. The models reveal the complex temporal relationships between the salinity of flowback fluid and production time.

Based on the validated RSM model, synergizing the power GA, and utilizing the salinity profile of flowback fluid and gas rate establishes a new fracture characterization workflow. A comprehensive range of scenarios was examined, stretching from Single-Stage Wells to Multi-Stage Horizontal Wells and from homogeneous to heterogeneous fracture models. The results indicate that RSM is highly effective in characterizing fracture parameters in single-stage wells,

whether uniform and non-uniform, or complexly heterogeneous. Further analysis reveals that in multi-stage horizontal wells, especially those with unequal primary fracture length and uneven primary fracture spacing or working with completion heterogeneity, combining secondary fracture parameters from RSM-Salinity and primary fracture parameters from RSM-Rate (stage) offers a comprehensive representation of the reservoir's fracturing characteristics.

6.2 Contributions

The primary contributions are summarized as follows:

Develop a framework for correlating fracture properties with the salinity of flowback fluid and gas rate and using these correlations and combine genetic algorithms to develop an effective workflow integrating the salinity of flowback fluid and gas rate for inferring fracture properties.

The proposed modelling schemes can be applied to that chemical compositional data that have applications in other parts, especially in subsurface fractured porous media. For instance, use the same idea to look at carbon storage because carbon dioxide interacts with the rock in the carbon storage process, also called mineralization, which is one of the most safety-trapping mechanisms. If they interact with the rock, then they will be mineralized.

6.3 Limitations and Recommendations for Future Work

The limitations of this research stem from its specific focus on a narrow set of cases and assumptions, which may not apply to a larger range or different reservoir properties. Although the current workflow has proven effective for the case studied, its application to other areas would

require repeating the entire process: selecting some new operational parameters for new reservoir modelling, and developing new RSM models to optimize fracture properties using GA. While potentially scalable, this approach would necessitate tailored adjustments to suit the unique characteristics of each new field or reservoir under study.

Based on the limitations of this work, I provide recommendations for future work from two perspectives: (1) scale-up; (2) coupling with Geomechanics:

(1) The current model incorporates specific geochemical reactions sourced from literature and lab studies for targeting areas. There exists an opportunity to expand upon this by including a wider range of reactions. This can offer a more comprehensive picture of the dynamics and implications of these reactions in reservoir environments. For example, collecting as much geochemical data on shale reservoirs as possible and developing a set of analytical models that can represent shale reservoirs to characterize fractures. Expanding the application of the model to various reservoir types, such as carbonates or tight formations, can provide insights into how these geochemical reactions manifest differently across varied geologies.

(2) The current numerical model ignores the dynamic behaviour of fracture closure, fracture properties are generally treated as static parameters. In fact, this will be one of the most important factors affecting the geochemical reaction. Because the opening and growth of fractures will increase reservoir contact per well, favoring geochemical reactions; conversely, the closure of fractures will hinder or inhibit geochemical reactions. This simplistic approach therefore often renders the modelling of interactions and/or interferences between geomechanics and geochemistry incomplete. Therefore, try to couple flow and geochemistry and geomechanics models to investigate the impact of geomechanics on geochemistry, and the impact on the RSM

prediction model. For instance, coupling the Bardon Bandies model, one of the most population geomechanics models, captures the fracture closure to provide a more realistic simulation result.

Bibliography

- Adegbite, J.O., Al-Shalabi, E.W., Ghosh, B., 2018. Geochemical modeling of engineered water injection effect on oil recovery from carbonate cores. *J. Petrol. Sci. Eng.* 170, 696–711. <https://doi.org/10.1016/j.petrol.2018.06.079>.
- Afram, A., Janabi-Sharifi, F., Fung, A.S. and Raahemifar, K., 2017. Artificial neural network (ANN) based model predictive control (MPC) and optimization of HVAC systems: A state of the art review and case study of a residential HVAC system. *Energy and Buildings*, 141, pp.96-113. <https://doi.org/10.1016/j.enbuild.2017.02.012>.
- Ahn, J.H., Kim, Y.P., Lee, Y.M., Seo, E.M., Lee, K.W. and Kim, H.S., 2008. Optimization of microencapsulation of seed oil by response surface methodology. *Food Chemistry*, 107(1), pp.98-105. <https://doi.org/10.1016/j.foodchem.2007.07.067>.
- Aksulu, H., Hamsø, D., Strand, S., Puntervold, T., Austad, T., 2012. Evaluation of low salinity enhanced oil recovery effects in sandstone: effects of the temperature and pH gradient. *Energy Fuel*. 26 (6), 3497–3503.
- Al-Ahmadi, H.A., 2010. A Triple-Porosity Model for Fractured Horizontal Wells (M.Sc. thesis), Texas A&M University, College Station, Texas.
- Alba, E., & Troya, J. M. (2002). Improving flexibility and efficiency by adding parallelism to genetic algorithms. *Statistics and Computing*, 12(2), 91-114.
- Ali, A., Siddiqui, S., and Dehghanpour, H. (2013). Analyzing the Production Data of Fractured Horizontal Wells by a Linear Triple Porosity Model: Development of Analysis Equations.

- Journal of Petroleum Science and Engineering, 112, 117-128.
<https://doi.org/10.1016/j.petrol.2013.10.016>.
- Almeida da Costa, A., Costa, G., Embiruçu, M., Soares, J.B., Trivedi, J.J., Rocha, P.S., Souza, A., Jaeger, P., 2021. The influence of rock composition and pH on reservoir wettability for low-salinity water-CO₂ enhanced oil recovery applications in Brazilian reservoirs. *SPE Reservoir Eval. Eng.* 24, 45–65. <https://doi.org/10.2118/195982-PA>.
- Alpers, C.N. and Nordstrom, D.K., 1999. Geochemical modeling of water-rock interactions in mining environments. *Reviews in economic geology*, 6, pp.289-324.
- Al-Qattan, A., Sanaseeri, A., Al-Saleh, Z., Singh, B.B., Al-Kaaoud, H., Delshad, M., et al., 2018. Low salinity waterflood and low salinity polymer injection in the Wara Reservoir of the Greater Burgan Field. March. SPE EOR Conference at Oil and Gas West Asia. <https://doi.org/10.2118/190481-MS>.
- Al-Saedi, H.N., Alhuraishawy, A.K., Flori, R., Brady, P.V., 2019. Sequential injection mode of high-salinity/low-salinity water in sandstone reservoirs: oil recovery and surface reactivity tests. *J. Pet. Explor. Prod. Technol.* 9 (1), 261–270. <https://doi.org/10.1007/s13202-018-0466-z>.
- Al-Shalabi, E.W., Sepehrnoori, K., 2016. A comprehensive review of low salinity/ engineered water injections and their applications in sandstone and carbonate rocks. *J. Petrol. Sci. Eng.* 139, 137–161. <https://doi.org/10.1016/j.petrol.2015.11.027>.
- Alvarez, M.J., Ilzarbe, L., Viles, E. and Tanco, M., 2009. The use of genetic algorithms in response surface methodology. *Quality Technology & Quantitative Management*, 6(3), pp.295-307. <https://doi.org/10.1080/16843703.2009.11673201>.

- Amini, M., Younesi, H., Bahramifar, N., Lorestani, A.A.Z., Ghorbani, F., Daneshi, A. and Sharifzadeh, M., 2008. Application of response surface methodology for optimization of lead biosorption in an aqueous solution by *Aspergillus niger*. *Journal of hazardous materials*, 154(1-3), pp.694-702. <https://doi.org/10.1016/j.jhazmat.2007.10.114>.
- Aminian, A., ZareNezhad, B., 2019. Oil-detachment from the calcium carbonate surfaces via the actions of surfactant, nanoparticle and low salinity brine: an insight from molecular dynamic simulation. *Chem. Eng. Sci.* 202, 373–382. <https://doi.org/10.1016/j.ces.2019.03.031>.
- Amirian, T., Haghghi, M., Mostaghimi, P., 2017. Pore scale visualization of low salinity water flooding as an enhanced oil recovery method. *Energy Fuel*. 31 (12), 13133–13143.
- Amirjanov, A., 2006. The development of a changing range genetic algorithm. *Computer methods in applied mechanics and engineering*, 195(19-22), pp.2495-2508. <https://doi.org/10.1016/j.cma.2005.05.014>.
- Anderson, M.J. and Whitcomb, P.J., 2016. RSM simplified: optimizing processes using response surface methods for design of experiments. Productivity press. <https://doi.org/10.1201/9781315382326>.
- Appelo, C.A.J., Postma, D., 2005. *Geochemistry, Groundwater and Pollution*, second ed. Balkema, Rotterdam. <https://doi.org/10.1201/9781439833544>.
- Arief, H.A.A., Wiktorski, T. and Thomas, P.J., 2021. A survey on distributed fibre optic sensor data modelling techniques and machine learning algorithms for multiphase fluid flow estimation. *Sensors*, 21(8), p.2801.

- Arps, J., 1945. Analysis of decline curves. *Trans. AIME* 160 (1), 228–247. <https://doi.org/10.2118/945228-G>. ARMA.
- Asadi, M., Woodroof, R.A. and Himes, R.E., 2008. Comparative study of flowback analysis using polymer concentrations and fracturing-fluid tracer methods: a field study. *SPE Production & Operations*, 23(02), pp.147-157. <https://doi.org/10.2118/101614-PA>.
- Aslan, N. E. V. Z. A. T. (2008). Application of response surface methodology and central composite rotatable design for modeling and optimization of a multi-gravity separator for chromite concentration. *Powder Technology*, 185(1), 80-86.
- Austad, T., RezaeiDoust, A., Puntervold, T., 2010. Chemical mechanism of low salinity water flooding in sandstone reservoirs. In: *SPE Improved Oil Recovery Symposium*, Tulsa, Oklahoma, USA. <https://doi.org/10.2118/129767-MS>.
- Awolayo, A.N., Sarma, H.K., Nghiem, L.X., 2018. Brine-dependent recovery processes in carbonate and sandstone petroleum reservoirs: review of laboratory-field studies, interfacial mechanisms and modeling attempts. *Energies* 11 (11), 3020. <https://doi.org/10.3390/en11113020>.
- Baptist, O.C., Sweeney, S.A., 1954. The effect of clays on the permeability of reservoir sands to waters of different saline contents. *Clay Clay Miner.* 3 (1), 505–515. <https://doi.org/10.1346/CCMN.1954.0030141>.
- Barati, R. and Liang, J.T., 2014. A review of fracturing fluid systems used for hydraulic fracturing of oil and gas wells. *Journal of Applied Polymer Science*, 131(16). <https://doi.org/10.1002/app.40735>.

- Baş, D. and Boyacı, İ.H., 2007. Modeling and optimization I: Usability of response surface methodology. *Journal of food engineering*, 78(3), pp.836-845. <https://doi.org/10.1016/j.jfoodeng.2005.11.024>.
- Baskerville, G.L., 1972. Use of logarithmic regression in the estimation of plant biomass. *Canadian Journal of Forest Research*, 2(1), pp.49-53. <https://doi.org/10.1139/x72-009>.
- Bearinger, D., 2013. August. Message in a Bottle. SPE/AAPG/SEG Unconventional Resources Technology Conference. <https://doi.org/10.1190/urtec2013-148>.
- Bedrikovetsky, P., Zeinijahromi, A., Siqueira, F.D., Furtado, C.A., de Souza, A.L.S., 2012. Particle detachment under velocity alternation during suspension transport in porous media. *Transport Porous Media* 91 (1), 173–197. <https://doi.org/10.1007/s11242-011-9839-1>.
- Behrang, M., Hosseini, S., Akhlaghi, N., 2021. Effect of pH on interfacial tension reduction of oil (Heavy acidic crude oil, resinous and asphaltenic synthetic oil)/low salinity solution prepared by chloride-based salts. *J. Petrol. Sci. Eng.* 205, 108840.
- Bello, R. O. (2009). Rate Transient Analysis in Shale Gas Reservoirs With Transient Linear Behavior. PhD dissertation, Texas A & M University, College Station, Texas (May 2009).
- Bernard, G.G., 1967. Effect of Floodwater Salinity on Recovery of Oil from Cores Containing Clays. SPE California Regional Meeting, Los Angeles, California. <https://doi.org/10.2118/1725-MS>.
- Bertoni, A., & Dorigo, M. (1993). Implicit parallelism in genetic algorithms. *Artificial Intelligence*, 61(2), 307-314.

- Bethke, C.M., 1996. *Geochemical Reaction Modelling*. Oxford University Press, New York.
- Bezerra, M.A., Santelli, R.E., Oliveira, E.P., Villar, L.S. and Escaleira, L.A., 2008. Response surface methodology (RSM) as a tool for optimization in analytical chemistry. *Talanta*, 76(5), pp.965-977. <https://doi.org/10.1016/j.talanta.2008.05.019>.
- Bhattacharya, S., Ghahfarokhi, P.K., Carr, T.R. and Pantaleone, S., 2019. Application of predictive data analytics to model daily hydrocarbon production using petrophysical, geomechanical, fiber-optic, completions, and surface data: A case study from the Marcellus Shale, North America. *Journal of Petroleum Science and Engineering*, 176, pp.702-715.
- Bhuvankar, P., Cihan, A., Birkholzer, J., 2022. Pore-scale CFD simulations of clay mobilization in natural porous media due to fresh water injection. *Chem. Eng. Sci.* 247, 117046 <https://doi.org/10.1016/j.ces.2021.117046>.
- Birkle, P., & Makechnie, G. K. (2022). Geochemical cycle of hydraulic fracturing fluids: Implications for fracture functionality and frac job efficiency in tight sandstone. *Journal of Petroleum Science and Engineering*, 208, 109596. <https://doi.org/10.1016/j.petrol.2021.109596>.
- Birkle, P., & MaKechnie, G. K. 2020. Geochemical Interpretation of Flowback Fluids To Assess Fracking Efficiency and Reservoir Compartmentalization. *Asia Pacific Unconventional Resources Technology Conference*, Brisbane, Australia, 18-19 November 2019 (pp. 1236-1248). <https://doi.org/10.15530/AP-URTEC-2019-198206>
- Blauch, M.E., Myers, R.R., Moore, T.R., Lipinski, B.A. and Houston, N.A., 2009, September. Marcellus shale post-frac flowback waters—Where is all the salt coming from and what are the

- implications?. In SPE Eastern Regional Meeting (pp. SPE-125740). SPE.
<https://doi.org/10.2118/125740-MS>.
- Bocora, J., 2012. Global prospects for the development of unconventional gas. *Procedia-Social and Behavioral Sciences*, 65, pp.436-442.
- Bodenhofer, U. (2004). *Genetic algorithms: theory and applications*.
- Boning, D. S., & Mozumder, P. K. (1994). DOE/Opt: A system for design of experiments, response surface modeling, and optimization using process and device simulation. *IEEE Transactions on Semiconductor Manufacturing*, 7(2), 233-244.
- Box, G.E., 1951. P and Wilson KB On the experimental attainment of optimum conditions. *Journal of the Royal Statistical Society*, 13, pp.1-45.
- Brady, P.V., Krumhansl, J.L., 2012. A surface complexation model of oil–brine–sandstone interfaces at 100 C: Low salinity waterflooding. *J. Petrol. Sci. Eng.* 81, 171–176.
<https://doi.org/10.1016/j.petrol.2011.12.020>.
- Brady, P.V., Thyne, G., 2016. Functional wettability in carbonate reservoirs. *Energy Fuel*. 30 (11), 9217–9225.
- Brookfield, A.E., Hansen, A.T., Sullivan, P.L., Czuba, J.A., Kirk, M.F., Li, L., Newcomer, M.E. and Wilkinson, G., 2021. Predicting algal blooms: Are we overlooking groundwater?. *Science of the Total Environment*, 769, p.144442. <https://doi.org/10.1016/j.scitotenv.2020.144442>.
- BuKhamseen, N.Y. and Ertekin, T., 2017, April. Validating hydraulic fracturing properties in reservoir simulation using artificial neural networks. In SPE Kingdom of Saudi Arabia annual technical symposium and exhibition. OnePetro. <https://doi.org/10.2118/188093-MS>.

- Callegaro, C., Bartosek, M., Nobili, M., Masserano, F., Pollero, M., Baz, D.M., Kortam, M. M., 2015. Design and implementation of low salinity waterflood in a north African brown field. November. Abu Dhabi International Petroleum Exhibition and Conference. <https://doi.org/10.2118/177590-MS>.
- Carpenter, C., 2016. Distributed acoustic sensing for downhole production and injection profiling. *Journal of Petroleum Technology*, 68(03), pp.78-79. <https://doi.org/10.2118/0316-0078-JPT>.
- Chaturvedi, K.R., Ravilla, D., Kaleem, W., Jadhawar, P., Sharma, T., 2021. Impact of low salinity water injection on CO₂ storage and oil recovery for improved CO₂ utilization. *Chem. Eng. Sci.* 229, 116127 <https://doi.org/10.1016/j.ces.2020.116127>.
- Chen, P. and Rahman, M.M., 2015, October. A novel approach to predict interaction between hydraulic fracture and natural fracture using artificial neural networks. SPE Asia Pacific Oil and Gas Conference and Exhibition. <https://doi.org/10.2118/176143-MS>.
- Cheng, H. C., Chen, W. H., & Chung, I. C. (2004). Integration of simulation and response surface methods for thermal design of multichip modules. *IEEE transactions on components and packaging technologies*, 27(2), 359-372.
- Cheng, Y. (2012). Impact of Water Dynamics in Fractures on the Performance of Hydraulically Fractured Wells in Gas-Shale Reservoirs. *J. Can Pet Technol* 51 (2): 143–151. SPE-127863-PA. <https://doi.org/10.2118/127863-PA>.
- Cheng, Y., Lee, W. J., and MacVay, D. A. (2009). A New Approach for Reliable Estimation of Hydraulic Fracture Properties Using Elliptical Flow Data in Tight Gas Wells. *SPE Res. Eval & Eng.* 12 (2): 254–262. SPE-105767-PA. <https://doi.org/10.2118/105767-PA>.

- Cissokho, M., Bertin, H., Boussour, S., Cordier, P., Hamon, G., 2010. Low salinity oil recovery on clayey sandstone: experimental study. *Petrophysics* 51 (5).
- Clarkson, C.R., 2021. Unconventional Reservoir Rate-Transient Analysis.
- CMG, 2022a. CMG GEM User's Guide. Computer Modelling Group Ltd, Calgary, Alberta, Canada.
- CMG, 2022b. CMG CMOST User's Guide. Computer Modelling Group Ltd, Calgary, Alberta, Canada.
- Collins, D.A., Nghiem, L.X., Li, Y.K., Grabonstotter, J.E., 1992. An efficient approach to adaptive-implicit compositional simulation with an equation of state. *SPE Reservoir Eng.* 7 (2), 259–264. <https://doi.org/10.2118/15133-PA>.
- Dang, C., Nghiem, L., Nguyen, N., Chen, Z., Nguyen, Q., 2015. Modeling and Optimization of Low Salinity Waterflood. SPE-173194-MS. SPE Reservoir Simulation Symposium, Houston, Texas, USA.
- De Jong, K. A. (1993). Genetic algorithms are NOT function optimizers. In *Foundations of genetic algorithms* (Vol. 2, pp. 5-17). Elsevier.
- Delaihdem, D. K. (2013). Decline curve analysis and enhanced shale oil recovery based on Eagle Ford Shale data. University of Alaska Fairbanks.
- Deng, L. and Cai, C.S., 2010. Bridge model updating using response surface method and genetic algorithm. *Journal of Bridge Engineering*, 15(5), pp.553-564.

- Ding, S., Su, C. and Yu, J., 2011. An optimizing BP neural network algorithm based on genetic algorithm. *Artificial intelligence review*, 36, pp.153-162. <https://doi.org/10.1007/s10462-011-9208-z>.
- Dong, X., Li, W., Liu, Q. and Wang, H., 2022. Research on convection-reaction-diffusion model of contaminants in fracturing flowback fluid in non-equidistant fractures with arbitrary inclination of shale gas development. *Journal of Petroleum Science and Engineering*, 208, p.109479. <https://doi.org/10.1016/j.petrol.2021.109479>.
- Dorie, V., Harada, M., Carnegie, N. B., & Hill, J. (2016). A flexible, interpretable framework for assessing sensitivity to unmeasured confounding. *Statistics in medicine*, 35(20), 3453-3470.
- Ehrlich, Robert, Wygal, Robert J., 1977. Interrelation of crude oil and rock properties with the recovery of oil by caustic waterflooding. *SPE J.* 17, 263–270. <https://doi.org/10.2118/5830-PA>.
- El-Mihoub, T. A., Hopgood, A. A., Nolle, L., & Battersby, A. (2006). Hybrid Genetic Algorithms: A Review. *Eng. Lett.*, 13(2), 124-137.
- Esene, C., Onalo, D., Zendehboudi, S., James, L., Aborig, A., Butt, S., (2018). Modeling investigation of low salinity water injection in sandstones and carbonates: effect of Na⁺ and SO₄²⁻. *Fuel* 232, 362–373. <https://doi.org/10.1016/j.fuel.2018.05.161>.
- Espósito, R. O., Tavares, F. W., & Castier, M. (2005). Phase equilibrium calculations for confined fluids, including surface tension prediction models. *Brazilian Journal of Chemical Engineering*, 22, 93-104.

- Evje, S., Hiorth, A., 2010. A mathematical model for dynamic wettability alteration controlled by water-rock chemistry. *Netw. Heterogeneous Media* 5 (2), 217.
- Evje, S., Hiorth, A., 2011. A model for interpretation of brine-dependent spontaneous imbibition experiments. *Adv. Water Resour.* 34 (12), 1627–1642. <https://doi.org/10.1016/j.advwatres.2011.09.003>.
- Fakcharoenphol, Perapon , Kurtoglu, Basak , Kazemi, Hossein , Charoenwongsa, Sarinya , and Yu-Shu Wu. "The Effect of Osmotic Pressure on Improve Oil Recovery from Fractured Shale Formations." *SPE/AAPG/SEG Unconventional Resources Technology Conference*, Woodlands, Texas, USA, April 2014. doi: <https://doi.org/10.2118/168998-MS>.
- Fisher, M. K., Wright, C. A., Davidson, B. M., Steinsberger, N. P., Buckler, W. S., Goodwin, A., & Fielder, E. O. (2005). Integrating fracture mapping technologies to improve stimulations in the Barnett shale. *SPE Production & Facilities*, 20(02), 85-93. <https://doi.org/10.2118/77441-PA>.
- Fjelde, I., Asen, S.M., Omekeh, A., 2012. Low salinity water flooding experiments and interpretation by simulations. In: *SPE Improved Oil Recovery Symposium*, Tulsa, Oklahoma, USA. <https://doi.org/10.2118/154142-MS>.
- Fogden, A., Kumar, M., Morrow, N.R., Buckley, J.S., 2011. Mobilization of fine particles during flooding of sandstones and possible relations to enhanced oil recovery. *Energy Fuel*. 25 (4), 1605–1616.
- Fu, Y., Jiang, Y., Hu, Q., Luo, T., Li, Y., Zhian, L., Wang, Z. and Yin, X., 2021. Fracturing flowback fluids from shale gas wells in western chongqing: Geochemical analyses and

- relevance for exploration & development. *Journal of Natural Gas Science and Engineering*, 88, p.103821. <https://doi.org/10.1016/j.jngse.2021.103821>.
- Gaudlip, A.W., Paugh, L.O. and Hayes, T.D., 2008, November. Marcellus shale water management challenges in Pennsylvania. SPE Shale Gas Production Conference. SPE. <https://doi.org/10.2118/119898-MS>.
- Gdanski, R., Weaver, J. and Slabaugh, B., 2007, January. A new model for matching fracturing fluid flowback composition. SPE Hydraulic Fracturing Technology Conference and Exhibition. SPE. <https://doi.org/10.2118/106040-MS>.
- Ghahfarokhi, P.K., Carr, T., Bhattacharya, S., Elliott, J., Shahkarami, A. and Martin, K., 2018, September. A fiber-optic assisted multilayer perceptron reservoir production modeling: A machine learning approach in prediction of gas production from the Marcellus shale. Unconventional Resources Technology Conference, Houston, Texas, 23-25 July 2018 (pp. 3291-3300). Society of Exploration Geophysicists, American Association of Petroleum Geologists, Society of Petroleum Engineers. <https://doi.org/10.15530/urtec-2018-2902641>.
- Ghahfarokhi, P.K., Carr, T.R., Wilson, C. and Martin, K., 2021. Production Distributed Temperature Sensing versus Stimulation Distributed Acoustic Sensing for the Marcellus Shale. *Distributed Acoustic Sensing in Geophysics: Methods and Applications*, pp.149-160. <https://doi.org/10.1002/9781119521808.ch11>.
- Ghanbari, E., Abbasi, M.A., Dehghanpour, H. and Bearinger, D., 2013, November. Flowback volumetric and chemical analysis for evaluating load recovery and its impact on early-time production. SPE Canada Unconventional Resources Conference. <https://doi.org/10.2118/167165-MS>.

- Ghorbani, M., Rashidi, F. and Mousavi-Dehghani, A., 2022. Investigation of crude oil properties impact on wettability alteration during low salinity water flooding using an improved geochemical model. *Scientific Reports*, 12(1), p.6600. <https://doi.org/10.1038/s41598-022-10506-3>.
- Goldberg, D.E. and Holland, J.H., 1988. Genetic algorithms and machine learning. 3 (2): 95-99.
- Golder Associates, 2018. FRACMAN 7.9 User Documentation.
- Gorges-Schleuter, M. (1990, October). Explicit parallelism of genetic algorithms through population structures. In *International Conference on Parallel Problem Solving from Nature* (pp. 150-159). Berlin, Heidelberg: Springer Berlin Heidelberg.
- Guo, J., Zhou, S., Chen, J. and Chen, Q., 2021. How information technology capability and knowledge integration capability interact to affect business model design: A polynomial regression with response surface analysis. *Technological Forecasting and Social Change*, 170, p.120935. <https://doi.org/10.1016/j.techfore.2021.120935>.
- Hanrahan, G. and Lu, K., 2006. Application of factorial and response surface methodology in modern experimental design and optimization. *Critical Reviews in Analytical Chemistry*, 36(3-4), pp.141-151. <https://doi.org/10.1080/10408340600969478>.
- He, X., Li, P., Shi, H., Xiao, Y., Guo, Y. and Zhao, H., 2022. Identifying strontium sources of flowback fluid and groundwater pollution using $^{87}\text{Sr}/^{86}\text{Sr}$ and geochemical model in Sulige gasfield, China. *Chemosphere*, 306, p.135594. <https://doi.org/10.1016/j.chemosphere.2022.135594>.

- He, X., Zhu, W., AlSinan, M., Kwak, H. and Hoteit, H., 2022, February. CO2 Storage Capacity Prediction In Deep Saline Aquifers: Uncertainty and Global Sensitivity Analysis. International Petroleum Technology Conference. <https://doi.org/10.2523/IPTC-22463-MS>.
- Hiorth, A., Cathles, L.M., Madland, M.V., 2010. The impact of pore water chemistry on carbonate surface charge and oil wettability. *Transport Porous Media* 85 (1), 1–21. <https://doi.org/10.1007/s11242-010-9543-6>.
- Hoffman, B.T. and Chang, W.M., 2009. Modeling hydraulic fractures in finite difference simulators: application to tight gas sands in Montana. *Journal of Petroleum Science and Engineering*, 69(1-2), pp.107-116. <https://doi.org/10.1016/j.petrol.2009.08.007>.
- Holland, J. H. (1975). *Adaptation in neural and artificial system*. Ann Arbor, Univeristy of Michigan Press.
- Holland, J.H., 1992. Genetic algorithms. *Scientific american*, 267(1), pp.66-73.
- Hongjun, W. A. N. G., Feng, M. A., Xiaoguang, T. O. N. G., Zuodong, L., Zhang, X., Zhenzhen, W. U., ... & Liuyan, Y. A. N. G., 2016. Assessment of global unconventional oil and gas resources. *Petroleum Exploration and Development*, 43(6), 925-940. [https://doi.org/10.1016/S1876-3804\(16\)30111-2](https://doi.org/10.1016/S1876-3804(16)30111-2).
- Horn, J., & Goldberg, D. E. (1995). Genetic algorithm difficulty and the modality of fitness landscapes. In *Foundations of genetic algorithms* (Vol. 3, pp. 243-269). Elsevier.
- Hubbert, M.K. and Willis, D.G., 1957. Mechanics of hydraulic fracturing. *Transactions of the AIME*, 210(01), pp.153-168. <https://doi.org/10.2118/686-G>.

- Jadhunandan, P.P., Morrow, N.R., 1991. Spontaneous imbibition of water by crude oil/ brine/rock systems. *Situ* 15 (4).
- Januardi, J. and Widodo, E., 2021, January. Response surface methodology of dual-channel green supply-chain pricing model by considering uncertainty. In *Supply Chain Forum: An International Journal* (Vol. 22, No. 1, pp. 16-27). Taylor & Francis. <https://doi.org/10.1080/16258312.2020.1788904>.
- Jerauld, Gary R., Lin, C.Y., Webb, Kevin J., Secombe, Jim C., 2008. Modeling lowsalinity waterflooding. *SPE Reservoir Eval. Eng.* 11, 1000–1012. <https://doi.org/10.2118/102239-PA>.
- Jia, C., Huang, Z., Sepehrnoori, K., Yao, J., 2021a. Modification of two-scale continuum model and numerical studies for carbonate matrix acidizing. *J. Petrol. Sci. Eng.* 197, 107972 <https://doi.org/10.1016/j.petrol.2020.107972>.
- Jia, Cunqi, Sepehrnoori, Kamy, Huang, Zhaoqin, Yao, Jun, 2021b. Modeling and analysis of carbonate matrix acidizing using a new two-scale continuum model. *SPE J.* 26, 2570–2599. <https://doi.org/10.2118/205012-PA>.
- Jossi, J.A., Stiel, L.I., Thodos, G., 1962. The viscosity of pure substances in the dense gaseous and liquid phases. *AIChE J.* 8 (1), 59–63.
- Karimi-Fard, M., Durlofsky, L.J. and Aziz, K., 2004. An efficient discrete-fracture model applicable for general-purpose reservoir simulators. *SPE journal*, 9(02), pp.227-236. <https://doi.org/10.2118/88812-PA>.

- Kestin, J., Khalifa, H.E., Correia, R.J., 1981. Tables of the dynamic and kinematic viscosity of aqueous NaCl solutions in the temperature range 20–150 C and the pressure range 0.1–35 MPa. *J. Phys. Chem. Ref. Data* 10 (1), 71–88. <https://doi.org/10.1063/1.555641>.
- Kharaka, Y.K., Gunter, W.D., Aggarwal, P.K., Perkins, E. and DeBraal, J.D.: “SOLMINEQ.88: A Computer Program for Geochemical Modeling of Water-Rock Reactions,” U.S. Geological Survey Water-Resources Investigations Report 88- 4227, Menlo Park, California, 1989.
- Khoo, L. P., & Chen, C. H. (2001). Integration of response surface methodology with genetic algorithms. *The International Journal of Advanced Manufacturing Technology*, 18, 483-489.
- King, G. E., 2014. 60 Years of Multi-Fractured Vertical, Deviated and Horizontal Wells: What Have We Learned?. SPE Annual Technical Conference and Exhibition. <https://doi.org/10.2118/170952-MS>.
- King, G.E., 2012, February. Hydraulic fracturing 101: What every representative, environmentalist, regulator, reporter, investor, university researcher, neighbor and engineer should know about estimating frac risk and improving frac performance in unconventional gas and oil wells. SPE Hydraulic Fracturing Technology Conference and Exhibition. <https://doi.org/10.2118/152596-MS>.
- Kinnear, K. E. (1994, June). Fitness landscapes and difficulty in genetic programming. In *Proceedings of the First IEEE Conference on Evolutionary Computation. IEEE World Congress on Computational Intelligence* (pp. 142-147). IEEE.
- Kjetil, J., Brian, D. and Mahmoud, F., 2012. Distributed Acoustic Sensing-A New Way of Listening to Your Well/Reservoir. Paper SPE 149602 presented at the SPE Intelligent Energy International. <https://doi.org/10.2118/149602-MS>.

- Kondash, A. J., Albright, E., & Vengosh, A. (2017). Quantity of flowback and produced waters from unconventional oil and gas exploration. *Science of the Total Environment*, 574, 314-321.
- Lager, A., Webb, K., Black, C., et al., 2006. Low salinity oil recovery – an experimental investigation. In: Norway International Symposium of core Analysts, Trondhiem, 12–16 September. SCA-2006-36.
- Lager, A., Webb, K.J., Black, C.J.J., Singleton, M., Sorbie, K.S., 2008. Low salinity oil recovery-an experimental investigation1. *Petrophysics* 49 (1).
- Lan, X., Zhang, Y. and Kang, Z., 2020. Application of Neural Network Method Based on Sample Optimization in Reservoir Fracture Identification. *Science Technology and Engineering*, 20(21), pp.8530-8536.
- Law, B. E., Spencer, C. W., & Howell, D. G., 1993. Gas in tight reservoirs-an emerging major source of energy. *The future of energy gases: US Geological Survey Professional Paper*, 1570, 233-252.
- Lester, Y., Ferrer, I., Thurman, E. M., Sitterley, K. A., Korak, J. A., Aiken, G., & Linden, K. G. (2015). Characterization of hydraulic fracturing flowback water in Colorado: implications for water treatment. *Science of the Total Environment*, 512, 637-644.
- Li, Y.K., Nghiem, L.X., 1986. Phase equilibria of oil, gas and water/brine mixtures from a cubic equation of state and Henry's law. *Can. J. Chem. Eng.* 64 (3), 486–496. <https://doi.org/10.1002/cjce.5450640319>.
- Ligthelm, D.J., Gronsveld, J., Hofman, J., Brussee, N., Marcelis, F., van der Linde, H., 2009. Novel Waterflooding Strategy by Manipulation of Injection Brine Composition. June.

EUROPEC/EAGE Conference and Exhibition, Amsterdam, The Netherlands.
<https://doi.org/10.2118/119835-MS>.

Liu, J., Sheng, J.J., Emadibaladehi, H. and Tu, J., 2021. Experimental study of the stimulating mechanism of shut-in after hydraulic fracturing in unconventional oil reservoirs. *Fuel*, 300, p.120982. <https://doi.org/10.1016/j.fuel.2021.120982>.

Liu, Y., Liu, L., Leung, J.Y., Moridis, G.J., 2020. Sequentially coupled flow and geomechanical simulation with a discrete fracture model for analyzing fracturing fluid recovery and distribution in fractured ultra-low permeability gas reservoirs. *J. Petrol. Sci. Eng.* 189, 107042 <https://doi.org/10.1016/j.petrol.2020.107042>.

Liu, Y., Liu, L., Leung, J.Y., Wu, K., Moridis, G., 2021. Coupled flow/geomechanics modeling of interfracture water injection to enhance oil recovery in tight reservoirs. *SPE J.* 26, 1–21. <https://doi.org/10.2118/199983-PA>.

MacPhail, W., Lisoway, B. and Banks, K., 2012, February. Fiber optic distributed acoustic sensing of multiple fractures in a horizontal well. In *SPE Hydraulic Fracturing Technology Conference and Exhibition* (pp. SPE-152422). SPE.

Martin, J.C., 1959. The effects of clay on the displacement of heavy oil by water. In: *Venezuelan Annual Meeting*, Caracas, Venezuela. <https://doi.org/10.2118/1411-G>.

MathWorks, 2022a. MATLAB Documentation. <https://www.mathworks.com/help/matlab/index.html>.

- McGuire, P.L., Chatham, J.R., Paskvan, F.K., Sommer, D.M., Carini, F.H., 2005. Low Salinity Oil Recovery: an Exciting New EOR Opportunity for Alaska's North Slope. SPE Western Regional Meeting, Irvine, California. <https://doi.org/10.2118/93903-MS>.
- Medeiros, F., Kurtoglu, B., Ozkan, E. et al. (2010). Analysis of Production Data From Hydraulically Fractured Horizontal Wells in Shale Reservoirs. SPE Res Eval & Eng13 (3): 559–568. SPE-110848-PA.
- Medeiros, F., Ozkan, E., and Kazemi, H. (2008). Productivity and Drainage Area of Fractured Horizontal Wells in Tight Gas Reservoirs. SPE Res Eval & Eng11 (5): 902–911. SPE-108110-PA. <https://doi.org/10.2118/108110-PA>
- Mehana, M. and Fahes, M., 2016, April. The Impact of the Geochemical Coupling on the Fate of Fracturing Fluid, Reservoir Characteristics and Early Well Performance in Shale Reservoirs. In SPE Kingdom of Saudi Arabia Annual Technical Symposium and Exhibition (pp. SPE-182744). SPE. <https://doi.org/10.2118/182744-MS>.
- Meyer, B.R., Bazan, L.W., Jacot, R.H. and Lattibeaudiere, M.G., 2010, February. Optimization of multiple transverse hydraulic fractures in horizontal wellbores. SPE Unconventional Resources Conference/Gas Technology Symposium. <https://doi.org/10.2118/131732-MS>.
- Miller, G.F., Todd, P.M. and Hegde, S.U., 1989, June. Designing Neural Networks Using Genetic Algorithms. In ICGA (Vol. 89, pp. 379-384).
- Mirjalili, S., 2019. Evolutionary algorithms and neural networks. In Studies in computational intelligence (Vol. 780). Berlin/Heidelberg, Germany: Springer.
- Mitchell, M., 1998. An introduction to genetic algorithms. MIT press.

- Molenaar, M.M. and Cox, B.E., 2013, January. Field cases of hydraulic fracture stimulation diagnostics using fiber optic distributed acoustic sensing (DAS) measurements and Analyses. In SPE Middle East Unconventional Resources Conference and Exhibition (pp. SPE-164030). SPE.
- Morrow, N., Buckley, J., 2011. Improved oil recovery by low-salinity waterflooding. *J. Petrol. Technol.* 63 (5), 106–112. <https://doi.org/10.2118/129421-JPT>.
- Morrow, N.R., Tang, G.Q., Valat, M., Xie, X., 1998. Prospects of improved oil recovery related to wettability and brine composition. *J. Petrol. Sci. Eng.* 20 (3–4), 267–276. [https://doi.org/10.1016/S0920-4105\(98\)00030-8](https://doi.org/10.1016/S0920-4105(98)00030-8).
- Muecke, T.W., 1979. Formation fines and factors controlling their movement in porous media. *J. Petrol. Technol.* 31 (2), 144–150. <https://doi.org/10.2118/7007-PA>.
- Muniruzzaman, M. and Rolle, M., 2016. Modeling multicomponent ionic transport in groundwater with IPhreeqc coupling: Electrostatic interactions and geochemical reactions in homogeneous and heterogeneous domains. *Advances in Water Resources*, 98, pp.1-15. <https://doi.org/10.1016/j.advwatres.2016.10.013>.
- Myers, R., 2008. Marcellus shale update. Independent Oil & Gas Association of West Virginia.
- Myers, R.H., Montgomery, D.C. and Anderson-Cook, C.M., 2016. Response surface methodology: process and product optimization using designed experiments. John Wiley & Sons.
- Nghiem, L., Sammon, P., Grabenstetter, J., Ohkuma, H., 2004. Modeling CO₂ Storage in Aquifers with a Fully-Coupled Geochemical EOS Compositional Simulator. April 2004. SPE/DOE Symposium on Improved Oil Recovery, Tulsa, Oklahoma. <https://doi.org/10.2118/89474-MS>.

- Nghiem, L., Shrivastava, V., Kohse, B., 2011. Modeling aqueous phase behavior and chemical reactions in compositional simulation. In: SPE Reservoir Simulation Symposium, The Woodlands, Texas, USA. <https://doi.org/10.2118/141417-MS>.
- Nghiem, L.X., Rozon, B.J., 1989. A Unified Approach for Handling and Solving Large Systems of Equations in Reservoir Simulation. In Proceedings of the First and Second International Forum on Reservoir Simulation, Alpbach, Austria.
- Nwabia, F.N. and Leung, J.Y., 2021a. Probabilistic history matching of multi-scale fractured reservoirs: Integration of a novel localization scheme based on rate transient analysis. *Journal of Natural Gas Science and Engineering*, 94, p.104067. <https://doi.org/10.1016/j.jngse.2021.104067>.
- Nwabia, F.N. and Leung, J.Y., 2021b. Inference of hydraulically fractured reservoir properties from production data using the indicator-based probability perturbation assisted history-matching method. *Journal of Petroleum Science and Engineering*, 198, p.108240. <https://doi.org/10.1016/j.petrol.2020.108240>.
- Pal, N., Saxena, N., Laxmi, K.D., Mandal, A., 2018. Interfacial behaviour, wettability alteration and emulsification characteristics of a novel surfactant: implications for enhanced oil recovery. *Chem. Eng. Sci.* 187, 200–212. <https://doi.org/10.1016/j.ces.2018.04.062>.
- Patterson, J.R., Cardiff, M., Coleman, T., Wang, H., Feigl, K.L., Akerley, J. and Spielman, P., 2017. Geothermal reservoir characterization using distributed temperature sensing at Brady Geothermal Field, Nevada. *The Leading Edge*, 36(12), pp.1024a1-1024a7.
- Peng, D.Y., Robinson, D.B., 1976. A new two-constant equation of state. *Ind. Eng. Chem. Fundam.* 15 (1), 59–64.

- Poirier, J.P. and Tarantola, A., 1998. A logarithmic equation of state. *Physics of the Earth and Planetary Interiors*, 109(1-2), pp.1-8.
- Rawlins, G.J. ed., 2014. *Foundations of Genetic Algorithms 1991 (FOGA 1)*. Elsevier.
- RezaeiDoust, A., Puntervold, T., Strand, S., Austad, T., 2009. Smart water as wettability modifier in carbonate and sandstone: a discussion of similarities/differences in the chemical mechanisms. *Energy Fuel*. 23 (9), 4479–4485.
- Rosenblum, J., Nelson, A.W., Ruyle, B., Schultz, M.K., Ryan, J.N. and Linden, K.G., 2017. Temporal characterization of flowback and produced water quality from a hydraulically fractured oil and gas well. *Science of the Total Environment*, 596, pp.369-377. <https://doi.org/10.1016/j.scitotenv.2017.03.294>.
- Rowe Jr., A.M., Chou, J.C., 1970. Pressure-volume-temperature-concentration relation of aqueous sodium chloride solutions. *J. Chem. Eng. Data* 15 (1), 61–66.
- Rubin, B., 2010, May. Accurate simulation of non-Darcy flow in stimulated fractured shale reservoirs. In *SPE Western regional meeting* (pp. SPE-132093). SPE. <https://doi.org/10.2118/132093-MS>.
- Samandarli, O., Valbuena, E., and Ehlig-Economides, C. (2012). *Production Data Analysis in Unconventional Reservoirs With Rate-Normalized Pressure (RNP): Theory, Methodology, and Applications*. Presented at the *SPE Americas Unconventional Resources Conference*, Pittsburgh, Pennsylvania, USA, 5–7 June. SPE-155614-MS. <https://doi.org/10.2118/155614-MS>.

- Seccombe, J.C., Lager, A., Webb, K., Jerauld, G., Fueg, E., 2008. Improving waterflood recovery: LoSal™ EOR field evaluation. April. In: SPE Symposium on Improved Oil Recovery. <https://doi.org/10.2118/113480-MS>.
- Sen, R. and Swaminathan, T., 2004. Response surface modeling and optimization to elucidate and analyze the effects of inoculum age and size on surfactin production. *Biochemical Engineering Journal*, 21(2), pp.141-148. <https://doi.org/10.1016/j.bej.2004.06.006>.
- Shabani, A., Zivar, D., 2020. Detailed analysis of the brine-rock interactions during low salinity water injection by a coupled geochemical-transport model. *Chem. Geol.* 537, 119484 <https://doi.org/10.1016/j.chemgeo.2020.119484>.
- Shang, J.S., Li, S. and Tadikamalla*, P., 2004. Operational design of a supply chain system using the Taguchi method, response surface methodology, simulation, and optimization. *International Journal of Production Research*, 42(18), pp.3823-3849. <https://doi.org/10.1080/00207540410001704050>.
- Sharak, A. Z. (2018). Analysis of Shale-Water Interactions and Flowback Water Chemistry for Fracture Characterization.
- Sharma, M.M., Filoco, P.R., 2000. Effect of brine salinity and crude-oil properties on oil recovery and residual saturations. *SPE J.* 5 (3), 293–300. <https://doi.org/10.2118/65402-PA>.
- Siddiqui, S.K., Ali, A. and Dehghanpour, H., 2012, October. New advances in production data analysis of hydraulically fractured tight reservoirs. SPE Canadian Unconventional Resources Conference. <https://doi.org/10.2118/162830-MS>.

- Sierra, J., Kaura, J., Gualtieri, D., Glasbergen, G., Sarker, D. and Johnson, D., 2008, September. DTS monitoring of hydraulic fracturing: Experiences and lessons learned. In SPE Annual Technical Conference and Exhibition? (pp. SPE-116182). SPE.
- Silva, E. M., Rogez, H., & Larondelle, Y. (2007). Optimization of extraction of phenolics from *Inga edulis* leaves using response surface methodology. *Separation and Purification Technology*, 55(3), 381-387.
- Singh, K.P., Gupta, S., Singh, A.K. and Sinha, S., 2010. Experimental design and response surface modeling for optimization of Rhodamine B removal from water by magnetic nanocomposite. *Chemical engineering journal*, 165(1), pp.151-160. <https://doi.org/10.1016/j.cej.2010.09.010>.
- Sivanandam, S.N., Deepa, S.N., Sivanandam, S.N. and Deepa, S.N., 2008. Genetic algorithms (pp. 15-37). Springer Berlin Heidelberg.
- Smith, M. L., Scales, J. A., & Fischer, T. L. (1992). Global search and genetic algorithms. *The Leading Edge*, 11(1), 22-26.
- Soave, G., 1972. Equilibrium constants from a modified Redlich-Kwong equation of state. *Chem. Eng. Sci.* 27 (6), 1197–1203.
- Soliman, M.Y., Daal, J. and East, L., 2012. Fracturing unconventional formations to enhance productivity. *Journal of Natural Gas Science and Engineering*, 8, pp.52-67. <https://doi.org/10.1016/j.jngse.2012.01.007>.

- Soliman, M.Y., East, L. and Augustine, J., 2010, June. Fracturing design aimed at enhancing fracture complexity. SPE EUROPEC/EAGE Annual Conference and Exhibition. <https://doi.org/10.2118/130043-MS>.
- Song, B. and Ehlig-Economides, C. (2011). Rate-Normalized Pressure Analysis for Determination of Shale Gas Performance. Presented at the North American Unconventional Gas Conference, The Woodlands, Texas, USA, 14–16 June. SPE-144031-MS. <https://doi.org/10.2118/144031-MS>.
- Song, S.J., Zhao, X.G., Zhang, N. and Zhao, L., 2014. Numerical Simulation and Analysis of Sand-Shale Ratio of Bedrock Impacting Mining Subsidence. *Advanced Materials Research*, 962, pp.1195-1200. <https://doi.org/10.4028/www.scientific.net/AMR.962-965.1195>.
- Sookprasong, P.A., Hurt, R.S. and Gill, C.C., 2014, December. Downhole monitoring of multicluster, multistage horizontal well fracturing with fiber optic distributed acoustic sensing (DAS) and distributed temperature sensing (DTS). In *International Petroleum Technology Conference* (pp. IPTC-17972). IPTC. <https://doi.org/10.2523/IPTC-17972-MS>
- Srinivas, M., & Patnaik, L. M. (1994). Genetic algorithms: A survey. *computer*, 27(6), 17-26.
- Srinivasan, S. and Leung, J.Y., 2022. *Petroleum Reservoir Modeling and Simulation: Geology, Geostatistics, and Performance Prediction*. 1st ed. New York: McGraw Hill.
- Sullivan, R., Woodroof, R., Steinberger-Glaser, A., Fielder, R. and Asadi, M., 2004, September. Optimizing fracturing fluid cleanup in the bossier sand using chemical frac tracers and aggressive gel breaker deployment. SPE Annual Technical Conference and Exhibition. <https://doi.org/10.2118/90030-MS>.

- Sun, M., 2020. Concentration and cavitation phenomena of Riemann solutions for the isentropic Euler system with the logarithmic equation of state. *Nonlinear Analysis: Real World Applications*, 53, p.103068. <https://doi.org/10.1016/j.nonrwa.2019.103068>.
- Tang, G.Q. and Morrow, N.R., 1997. Salinity, temperature, oil composition, and oil recovery by waterflooding. *SPE Reservoir Engineering*, 12(04), pp.269-276. <https://doi.org/10.2118/36680-PA>.
- Tang, G.Q., Morrow, N.R., 1999. Influence of brine composition and fines migration on crude oil/brine/rock interactions and oil recovery. *J. Petrol. Sci. Eng.* 24 (2–4), 99–111. [https://doi.org/10.1016/S0920-4105\(99\)00034-0](https://doi.org/10.1016/S0920-4105(99)00034-0).
- Tang, L., Zhang, Y., Li, C., Zhou, Z., Nie, X., Chen, Y., Cao, H., Liu, B., Zhang, N., Said, Z. and Debnath, S., 2022. Biological stability of water-based cutting fluids: progress and application. *Chinese Journal of Mechanical Engineering*, 35, pp.1-24. <https://doi.org/10.1186/s10033-021-00667-z>.
- Thede, S. M. (2004). An introduction to genetic algorithms. *Journal of Computing Sciences in Colleges*, 20(1), 115-123.
- Vazquez, O., Young, C., Demyanov, V., Arnold, D., Fisher, A., MacMillan, A. and Christie, M., 2014. Estimating scale deposition through reservoir history matching in the Janice field. *SPE Production & Operations*, 29(01), pp.21-28. <https://doi.org/10.2118/164112-PA>.
- Venkatesh, V. and Goyal, S., 2010. Expectation disconfirmation and technology adoption: polynomial modeling and response surface analysis. *MIS quarterly*, pp.281-303. <https://www.jstor.org/stable/20721428>.

- Vesterstrom, J. and Thomsen, R., 2004, June. A comparative study of differential evolution, particle swarm optimization, and evolutionary algorithms on numerical benchmark problems. In Proceedings of the 2004 congress on evolutionary computation (IEEE Cat. No. 04TH8753) (Vol. 2, pp. 1980-1987). IEEE. [https://doi: 10.1109/CEC.2004.1331139](https://doi.org/10.1109/CEC.2004.1331139).
- Vladislavleva, E. J., Smits, G. F., & Den Hertog, D. (2008). Order of nonlinearity as a complexity measure for models generated by symbolic regression via pareto genetic programming. *IEEE Transactions on Evolutionary Computation*, 13(2), 333-349.
- Wang, M., Leung, J.Y., 2015. Numerical investigation of fluid-loss mechanisms during hydraulic fracturing flow-back operations in tight reservoirs. *J. Petrol. Sci. Eng.* 133, 85–102. <https://doi.org/10.1016/j.petrol.2015.05.013>.
- Wang, M., Leung, J.Y., 2016. Numerical investigation of coupling multiphase flow and geomechanical effects on water loss during hydraulic-fracturing flowback operation. *SPE Reservoir Eval. Eng.* 19 (2016), 520–537. <https://doi.org/10.2118/178618-PA>.
- Wanniarachchi, W.A.M., Ranjith, P.G. and Perera, M.S.A., 2017. Shale gas fracturing using foam-based fracturing fluid: a review. *Environmental Earth Sciences*, 76, pp.1-15. <https://doi.org/10.1007/s12665-017-6399-x>.
- Webb, K.J., Black, C.J.J., Al-Ajeel, H., 2004. Low Salinity Oil Recovery – Log-Inject-Log. SPE/DOE Symposium on Improved Oil Recovery, Tulsa, Oklahoma. <https://doi.org/10.2118/89379-MS>.
- Wei, G., Ding, S., Yang, H., Liu, W., Yin, M. and Li, L., 2022. A Novel Localization Method of Wireless Covert Communication Entity for Post-Steganalysis. *Applied Sciences*, 12(23), p.12224. <https://doi.org/10.3390/app122312224>.

- Willberg, D.M., Steinsberger, N., Hoover, R., Card, R.J. and Queen, J., 1998, April. Optimization of fracture cleanup using flowback analysis. SPE Rocky Mountain Petroleum Technology Conference/Low-Permeability Reservoirs Symposium. <https://doi.org/10.2118/39920-MS>.
- Woodroof, R.A., Asadi, M. and Warren, M.N., 2003, May. Monitoring fracturing fluid flowback and optimizing fracturing fluid cleanup using chemical frac tracers. SPE European Formation Damage Conference. <https://doi.org/10.2118/82221-MS>.
- Xiong, H., Davidson, B., Saunders, B. and Holditch, S.A., 1996, October. A comprehensive approach to select fracturing fluids and additives for fracture treatments. SPE Annual Technical Conference and Exhibition. <https://doi.org/10.2118/36603-MS>.
- Xu, Z., Leung, J.Y., 2022. Analyzing the impacts of meshing and grid alignment in dualporosity dual-permeability upscaling. SPE Reservoir Eval. Eng. 25, 61–80. <https://doi.org/10.2118/208573-PA>.
- Xue, Y.Z., Lou, B. and Qian, W., 2016, December. The research of model on the apparent viscosity of sludge. In International Symposium on Mechanical Engineering and Material Science (ismems-16) (pp. 371-379). Atlantis Press.
- Yang, Tianyi , and Xingru Wu. "Water Flowback Analysis and Hydraulic Fracture Characterization in Marcellus Unconventional Reservoir." Paper presented at the SPE Oklahoma City Oil and Gas Symposium, Oklahoma City, Oklahoma, USA, March 2017. doi: <https://doi.org/10.2118/185090-MS>.
- Yildiz, H.O., Morrow, N.R., 1996. Effect of brine composition on recovery of Moutray crude oil by waterflooding. J. Petrol. Sci. Eng. 14 (3–4), 159–168. [https://doi.org/10.1016/0920-4105\(95\)00041-0](https://doi.org/10.1016/0920-4105(95)00041-0).

- Yousef, A.A., Al-Saleh, S., Al-Kaabi, A., Al-Jawfi, M., 2010. Laboratory Investigation of Novel Oil Recovery Method for Carbonate Reservoirs. Canadian Unconventional Resources and International Petroleum Conference. Canada, Calgary, Alberta. <https://doi.org/10.2118/137634-MS>.
- Yousef, A.A., Al-Saleh, S., Al-Kaabi, A., Al-Jawfi, M., 2011. Laboratory investigation of the impact of injection-water salinity and ionic content on oil recovery from carbonate reservoirs. SPE Reservoir Eval. Eng. 14, 578–593. <https://doi.org/10.2118/137634-PA>.
- Yousef, A.A., Liu, J., Blanchard, G., Al-Saleh, S., Al-Zahrani, T., Al-Zahrani, R., et al., 2012. Smartwater flooding: industry’s first field test in carbonate reservoirs. October. SPE Annual Technical Conference and Exhibition. <https://doi.org/10.2118/159526-MS>.
- Zhang, G. and Leung, J.Y., 2023. Design of injected water salinity for enhanced oil recovery applications in sandstone reservoirs using coupled flow-geochemical simulation. Geoenergy Science and Engineering, 224, p.211614. <https://doi.org/10.1016/j.geoen.2023.211614>.
- Zhang, G., Leung, J.Y., 2022. Numerical Simulation of Geochemical Effects on Flowback Analysis and Enhanced Oil Recovery Strategies. SPE/AAPG/SEG Unconventional Resources Technology Conference, Houston, Texas, USA. <https://doi.org/10.15530/urtec-2022-3721536>.
- Zhang, X., 2019. Use of Mathematical Models to Simulate Fracture Propagation, Radial Fracture Verification, and Productivity of Multi-Fractured Horizontal Wells in Unconventional Oil Reservoirs. University of Louisiana at Lafayette.
- Zhao, J., Liu, C., Yang, H., & Li, Y., 2015. Strategic questions about China’s shale gas development. Environmental Earth Sciences, 73, 6059-6068. <https://doi.org/10.1007/s12665-015-4092-5>.

- Zhong, C., Leung, J.Y., 2020a. Numerical analysis of the effects of apparent-permeability modeling and secondary-fracture distribution for hydraulic-fractured shale-gas production analysis. *SPE Reservoir Eval. Eng.* 23, 1233–1250. <https://doi.org/10.2118/201201-PA>.
- Zhong, C., Leung, J.Y., 2020b. Numerical investigation of water retention in secondary fractures and apparent permeability modeling in shale gas production. *J. Petrol. Sci. Eng.* 192, 107294 <https://doi.org/10.1016/j.petrol.2020.107294>.
- Zolfaghari, A., Dehghanpour, H., Ghanbari, E., & Bearinger, D. (2016). Fracture characterization using flowback salt-concentration transient. *Spe Journal*, 21(01), 233-244. <https://doi.org/10.2118/168598-PA>.
- Zolfaghari, A., Noel, M., Dehghanpour, H. and Bearinger, D., 2014. Understanding the origin of flowback salts: A laboratory and field study. *SPE/CSUR Unconventional Resources Technology Conference*, Canada. <https://doi.org/10.2118/171647-MS>.

Appendix A

Table A-1 Fracture parameters estimated using RSM-GA workflow and its percentage error for the non-uniform secondary fracture model.

Parameter	PF Length (ft)	PE (%)	PF Permeability (mD)	PE (%)	SF Coverage (ft ²)	PE (%)	SF P32 (ft ² /ft ³)	PE (%)	SF Aperture (Average) (ft)	PE (%)	SF Permeability (Average) (mD)	PE (%)
True value	420	-	7000	-	75600	-	0.0619	-	0.00043744	-	35	-
RSM-Salinity	417	0.71	7233	3.33	74495	1.46	0.0639	3.23	0.00042947	1.82	33	5.71
RSM-Rate	425	1.19	6797	2.90	73886	2.27	0.0641	3.55	0.00044885	2.61	39	11.43

Table A-2 Fracture parameters estimated using RSM-GA workflow and its percentage error for heterogeneous secondary fracture DFN model.

Parameter	PF Length (ft)	PE (%)	PF Permeability (mD)	PE (%)	SF Coverage (ft ²)	PE (%)	SF P32 (ft ² /ft ³)	PE (%)	SF Aperture (Average) (ft)	PE (%)	SF Permeability (Average) (mD)	PE (%)
True value	420	-	7000	-	75600	-	0.0619	-	0.00043744	-	35	-
RSM-Salinity	414	1.43	7336	4.80	80034	5.87	0.0585	5.49	0.00041578	4.95	38	8.57
RSM-Rate	429	2.14	7346	4.94	80131	5.99	0.0588	5.01	0.00046167	5.54	30	14.29

Table A-3 Fracture parameters estimated using RSM-GA workflow and its percentage error for multi-stage horizontal well with equal primary fracture length and even primary fracture spacing.

Parameter	PF Length (ft)	PE (%)	PF Permeability (mD)	PE (%)	SF Coverage (ft ²)	PE (%)	SF P32 (ft ² /ft ³)	PE (%)	SF Aperture (Average) (ft)	PE (%)	SF Permeability (Average) (mD)	PE (%)
True Value	420	-	7000	-	75600	-	0.0619	-	0.00043744	-	35	-
RSM-Salinity	426	1.43	7268	3.83	69963	7.46	0.0574	7.27	0.00047001	7.45	31	11.43
RSM-Rate	428	1.90	7324	4.63	79953	5.76	0.0578	6.62	0.00040942	6.41	30	14.29
RSM-Rate Stage 1	426	1.43	7316	4.51	70381	6.90	0.0575	7.11	0.00045611	4.27	33	5.71
RSM-Rate Stage 2	407	3.10	7284	4.06	70354	6.94	0.0572	7.59	0.00041126	5.98	39	11.43
RSM-Rate Stage 3	432	2.86	6685	4.50	78598	3.97	0.0586	5.33	0.00046237	5.70	32	8.57
RSM-Rate Stage 4	414	1.43	7258	3.69	70141	7.22	0.0575	7.11	0.00047015	7.48	30	14.29
RSM-Rate Stage 5	408	2.86	6689	4.44	70579	6.64	0.0578	6.62	0.00040468	7.49	39	11.43

Table A-4 Fracture parameters estimated using RSM-GA workflow and its percentage error for multi-stage horizontal well with equal primary fracture length and uneven primary fracture spacing

Parameter	PF Length (ft)	PE (%)	PF Permeability (mD)	PE (%)	SF Coverage (Average) (ft ²)	PE (%)	SF P32 (Average) (ft ² /ft ³)	PE (%)	SF Aperture (Average) (ft)	PE (%)	SF Permeability (Average) (mD)	PE (%)	
True Value	420	-	12000	-	62160	-	0.0743	-	0.00063231	-	23	-	
RSM-Salinity	426	1.43	11547	3.78	57841	6.95	0.0685	7.81	0.00057768	8.64	25	8.70	
RSM-Rate	413	1.67	12519	4.33	55135	11.30	0.0627	15.61	0.00052523	16.93	18	21.74	
Stage 1	True Value	420	-	12000	-	75600	-	0.0667	-	0.00051237	-	21	-
	RSM-Rate	424	0.95	11461	4.49	82218	8.75	0.0611	8.40	0.00046192	9.85	17	19.05
Stage 2	True Value	420	-	12000	-	46200	-	0.0857	-	0.00084268	-	26	-
	RSM-Rate	432	2.86	11590	3.42	41590	9.98	0.0764	10.85	0.00074882	11.14	20	23.08
Stage 3	True Value	420	-	12000	-	46200	-	0.0857	-	0.00084268	-	26	-
	RSM-Rate	415	1.19	11444	4.63	52906	14.52	0.0724	15.52	0.00071238	15.46	19	26.92
Stage 4	True Value	420	-	12000	-	67200	-	0.0762	-	0.00064891	-	24	-
	RSM-Rate	417	0.71	12544	4.53	58268	13.29	0.0664	12.86	0.00056019	13.67	28	16.67
Stage 5	True Value	420	-	12000	-	75600	-	0.0571	-	0.00031492	-	16	-
	RSM-Rate	413	1.67	12312	2.60	78462	3.79	0.0535	6.30	0.00033929	7.74	18	12.50

Table A-5 Fracture parameters estimated using RSM-GA workflow and its percentage error for multi-stage horizontal well with unequal primary fracture length and uneven primary fracture spacing

Parameter	PF Length (Average) (ft)	PE (%)	PF Permeability (Average) (mD)	PE (%)	SF Coverage (Average) (ft ²)	PE (%)	SF P32 (Average) (ft ² /ft ³)	PE (%)	SF Aperture (Average) (ft)	PE (%)	SF Permeability (Average) (mD)	PE (%)	
True Value (Average)	332	-	10100	-	51120	-	0.0598	-	0.00051446	-	21	-	
RSM-Salinity (Average)	341	2.71	10553	4.49	54159	5.94	0.0545	8.86	0.00046864	8.91	19	9.52	
RSM-Rate (Average)	321	3.31	10584	4.79	58239	13.93	0.0512	14.38	0.00060025	16.68	16	23.81	
Stage 1	True Value	380	-	12500	-	68400	-	0.0737	-	0.00063486	-	25	-
	RSM-Rate	372	2.11	12826	2.61	76654	12.07	0.0655	11.13	0.00057107	10.05	29	16.00
Stage 2	True Value	260	-	6500	-	28600	-	0.0462	-	0.00032781	-	15	-
	RSM-Rate	252	3.08	6791	4.48	24605	13.97	0.03979	13.87	0.00027957	14.72	12	20.00
Stage 3	True Value	260	-	6500	-	28600	-	0.0462	-	0.00032781	-	15	-
	RSM-Rate	253	2.69	6753	3.89	34981	22.31	0.0381	17.53	0.00025862	21.11	11	26.67
Stage 4	True Value	340	-	8200	-	54400	-	0.0471	-	0.00045813	-	18	-
	RSM-Rate	346	1.76	7971	2.79	62605	15.08	0.0403	14.44	0.00053458	16.69	15	16.67
Stage 5	True Value	420	-	16800	-	75600	-	0.0857	-	0.00082367	-	30	-
	RSM-Rate	417	0.71	17262	2.75	77542	2.57	0.0812	5.25	0.00077258	6.20	33	10.00